This is to certify that the

thesis entitled

Characterisation of the barrier properties of styrene butadiene copolymer (KR-10) film.

presented by

Derek McDowell

has been accepted towards fulfillment
of the requirements for

M.S. degree in Packaging

Major professor

Date 19 nov. 1997

Characterisation of the barrier properties of styrene butadiene copolymer (KR-10) film.

by

Derek McDowell

A thesis

Submitted to
Michigan State University
in partial fulfilment of the requirements
for the degree of

Master of Science

School of Packaging

1997

ABSTRACT

Characterisation of the gas and vapour barrier properties of KR-10 (styrene butadiene copolymer) film.

by

Derek McDowell

The solubility and diffusion coefficients of ethyl acetate and d-limonene vapour as single permeants were determined by a gravimetric method using a Cahn electrobalance. Solubility and diffusion coefficients of ethyl acetate were also determined by an isostatic method using a MOCON Aromatran. The transmission rates of water vapour, oxygen and carbon dioxide gases were determined by isostatic procedures.

Studies considered the concentration and temperature dependencies of the mass transfer processes for the organic permeants and water vapour. The temperature dependency of the oxygen transmission rate was also studied. The Arrhenius relationship described the mass transfer processes over the temperature range studied. Vapour concentration had no effect on the diffusion coefficient of the organic permeants when determined by the gravimetric method over the vapor activity range studied. Concentration had no significant effect on the water vapour permeability coefficient over the relative humidity range studied.

Solubility coefficient and diffusion coefficient values of ethyl acetate determined by the isostatic procedure were approximately three to four times higher than values obtained by the gravimetric method.

To my dear wife and our two wonderful daughters.

Acknowledgements

I would like to thank Dr Hernandez for his valuable advice while acting as my advisor. Appreciation is also expressed to Dr Giacin and Dr Beaudry for serving on my guidance committee.

A special thank you is extended to the Department of Agriculture for Northern Ireland without whom this would not be possible. Thanks also, to Biometrics Division for assisting in the statistical analysis.

Many thanks to faculty, staff and students in the School of Packaging for their help, advice and friendship.

Table of contents

Appendices

List of Tables

List of Figures

Introduction

Consumer demands in the US and Europe shape the range and type of food products on the supermarket shelves. Increasing demand for fresh, high quality, convenience, value for money foods has encouraged retailers to seek innovative products and packaging to maintain consumer loyalty in a highly competitive retail market. Retailers want year-round availability of products packaged to maximise shelf life, provide good appearance and consumer appeal and to ensure high returns on shelf space allocation. The package plays a key role in marketing and distributing the food product from its point of manufacture to its desired point of consumption. The ideal package will adequately protect the product for its intended shelf life, and no longer. Over packaging is unnecessary, expensive and wasteful.

Plastics are now used extensively in packaging of food and beverage products. Light weight, clarity, good processing and heat sealing attributes, strength, barrier properties and low cost relative to performance, are some of the desirable characteristics of plastics which make them suitable as packaging materials. Advances in polymer processing has enabled development of plastics which are better suited to particular food packaging applications. Coextrusion

and lamination of plastics can produce a package which utilises the desired properties of each component material to best match product and distribution requirements.

The U.S. packaging market was worth $78 billion in 1995, with food and beverages valued at $50 billion (Fishman, 1995). The plastic-based packaging market continues to show growth in both rigid and flexible applications and accounts for over 30% of the total packaging market. The use of plastics is expected to grow by more than four percent between 1993 and 1998 in the US and Europe (Hernandez, 1996).

Plastic packaging can interact with components in the food and with gases and vapours in the package headspace and in the surrounding environment. Food packaging interactions impact significantly on product quality, safety and shelf life. An understanding of the properties of polymeric packaging materials and their behaviour in packaging applications leads to improved packaging design by matching packaging material to product requirements. Unsympathetic matching of polymer and product can lead to a number of undesirable outcomes, including flavour scalping by the package, migration of undesirable components from the packaging material into the product and permeation of gases and vapours from the external environment into the pack headspace and subsequently into the product itself.

Offering protection from gas and vapour exchange between the package and its environment is dependent upon integrity of the seals and closures and the mass transfer characteristics of the packaging materials (Karel, 1975).

New polymeric packaging materials are being produced and introduced to the market place, as general packaging materials or, due to special properties, with specific applications in mind. KR-10 resin is a styrene butadiene copolymer produced by Phillips.

The objectives of this study are to characterise the barrier properties of Phillips KR-10 film by:

1. Determining the sorption and diffusion coefficients of ethyl acetate and d-limonene vapour, as single permeants, in Phillips KR-10 (styrene butadiene copolymer) film by the gravimetric procedure,
2. Determining the sorption and diffusion coefficients of ethyl acetate in KR-10 film by the isostatic procedure, using the MOCON Aromatran 1A,
3. Determining the oxygen, carbon dioxide and water vapour permeabilities for styrene butadiene film using the Ox-tran twin, Permatran-W and Permatran-C respectively,
4. Evaluating the concentration and temperature dependencies of organic permeants and gases in styrene butadiene film.

Literature review

Mass transfer in a package

Mass transfer refers to the sorption and diffusion processes of gases, vapours and liquids within or through polymeric plastic materials. This includes the sorption, desorption and diffusion of compounds by polymeric materials. Diffusion is an activated process and should not be confused with porosity, which describes the flow of gases flow through macrovoids such as small pores, cracks and imperfections in the material.

Mass transfer of molecular species through a polymeric material can be described in terms of the solubility coefficient (*S*), the diffusion coefficient (*D*) and the permeability coefficient (*P*). The diffusion and solubility coefficients of organic compounds in polymer films can be determined by gravimetric methods - monitoring weight increase of the polymer sample during the sorption process. Permeability and diffusion coefficients of gases and organic vapours are obtained from permeability studies by monitoring transport of a permeant through a polymer film using methods based on isostatic or quasi-isostatic procedures.

The difference in partial pressure across each side of the film provides the driving force for mass transfer processes. In the absence of imperfections, such as pinholes and cracks (which are only found in very thin polymer films), the

partial pressure difference will generally control the rate and extent of permeation of a particular gas or vapour.

Sorption

The solubility coefficient (*S*) is a thermodynamic term which describes how many permeant molecules will dissolve into a polymer at equilibrium conditions per unit of sorbate concentration. It is an equilibrium partition coefficient which is dependent on the activity of the sorbate within the polymer at equilibrium (Neilsen, 1994). A large value of *S* implies a tendency for the penetrant molecules to dissolve and be retained in the polymer.

Sorption relates to the condensation, penetration and dispersion of penetrant molecules into the polymer matrix and includes adsorption, (surface attachment), absorption (access to the polymer matrix), incorporation into microvoids, cluster formation and other modes of mixing (Rogers, 1985).

Braunauer (1944) explains the tendency for gas molecules to adsorb to the surface of solids on the basis of reducing the free surface energy. The surface of a polymer is in a constant state of tension as a result of the unbalanced forces - the inward pull being greater than the outward forces. Any process which tends to decrease the free surface energy (the product of surface area and surface tension) will occur spontaneously. All adsorption phenomena result in a decrease in the free energy of the system and therefore will be accompanied by a decrease in the enthalpy and release of energy. The rate of sorption is often very fast - granular Darco G (adsorbant activated charcoal)

adsorbs three hundred times its own volume of nitrogen gas at -183°C in under one minute. However the fast adsorption stage is often followed by a slow absorption process.

The molecular chains of polymeric materials are held together by secondary forces which are much weaker than the strong primary covalent bonds holding the monomer units of the polymer chain together. The molecular chains can be separated when the secondary forces are weakened and the attraction between neighbouring chains is reduced. Gases and vapours dissolve into polymers by weakening the interchain forces. A diffusant vapour will dissolve in a polymer if the dissolved state exhibits a lower free energy. If the forces between vapour and polymer molecules are stronger than those between polymer molecules then solubility is favoured. Polymers are readily dissolved by compounds of similar solubility parameter. Polar solvents dissolve polar polymers and non-polar solvents dissolve low polarity hydrocarbon-based polymers. Therefore compounds of similar polarity to the polymer will be readily sorbed (Lau and Wang, 1995).

The concentration of penetrant in the polymer is difficult to measure. However, the Nernst equation describes the partition of penetrant between the ambient and polymer phases:

$$K = \frac{c_p}{c_f} \qquad (1)$$

where c_p is the sorbed penetrant concentration; c_f is the ambient penetrant concentration in contact with the polymer surface and K is a constant.

Sorption behaviour is described on the basis of the relative strengths of the interactions between the permeant molecules and the polymer, or between the permeant molecules themselves within the polymer structure. Polymer structure, free volume, segmental mobility, site availability and the physiochemical properties of the penetrant will determine the mechanism of sorption and transport of penetrant within the polymer. Several models have been proposed to describe sorption behaviour, the main models are Henry's law sorption, Langmuir-type sorption, Type III sorption, Type IV sorption and Dual-mode sorption.

Henry's law sorption

For gases and vapours c_f is proportional to pressure (p) and therefore the equilibrium concentration of a penetrant in a polymer is described by Henry's law:

$$c_p = S\ p \qquad (2)$$

where S is the Henry's law solubility coefficient (Rogers, 1985).

Henry's law sorption describes the simplest case of ideal solution behaviour and occurs when interactions between permeant/permeant and polymer/permeant are weak compared to the stronger interactions between polymer chains. This results in low solubility of permeant gases in the polymer and follows ideal solution behaviour with penetrant randomly dispersed

throughout the polymer. Penetrant molecules do not interact with each other and one molecule has no effect on the distribution of other molecules in the polymer matrix. Ideal solution behaviour occurs in gas/polymer systems when gas pressure is less than one atmosphere. The solubility coefficient is a constant independent of sorbed permeant concentration and the sorption isotherm shows a linear relationship between concentration and partial pressure at a given temperature (Rogers, 1985), Refer to Figure 1 a.

In practice this relationship does not accurately describe permeant solubility in plastics due to the presence of microvoids and sorption sites within the polymer into which permeant molecules can adsorb. The presence of crystalline regions in the polymer reduce the degree of solubility, as microvoids or 'holes' into which permeant molecules solubilise, are only associated with amorphous regions. Tight, regular packaging of polymer chains, associated with crystalline regions, offer a barrier to sorption and diffusion. Further models have therefore been developed to explain non-ideal behaviour. The various types of sorption can occur concurrently, depending on the particular penetrant/polymer system and the concentration of the penetrant.

Langmuir sorption isotherm

Langmuir-type sorption is characterised by high levels of sorption at low partial pressures and low levels of sorption at higher pressures. This is indicative of permeant molecules sorbing on specific sites or in microvoids in the polymer structure at low pressures. Upon saturation of the active sites, a small amount of

penetrant dissolves randomly in the polymer, following ideal solution behaviour. Figure 1 b.

A form of the Langmuir equation, (for derivation refer to Braunauer, 1944), describes the concentration (c_H) of permeant molecules sorbed by active sites within a polymer:

$$c_H = \frac{s_H . b. p}{1 + b. p} \qquad (3)$$

where s_H is a site, or hole, saturation constant, p is the gas or vapour pressure, b is a site, or hole constant representing the ratio of rate constants for adsorption and desorption and is therefore an indication of the affinity of a permeant molecule for an active site.

Sorption of gases into glassy polymers which contain microvoids can follow this sorption pattern. Solubility of carbon dioxide into polyethylene terephthalate is described by this model (Hernandez, 1996).

Flory-Huggins

Flory-Huggins sorption describes systems where the penetrant-penetrant forces are much stronger than penetrant-polymer interactions. Penetrant molecules form clusters within the polymer matrix. Rogers (1985) has reported examples where clustering has resulted in a decreasing diffusion coefficient with increasing penetrant concentration, due to the reduced mobilities of clustered molecules compared with single penetrant molecules. This behaviour is in

contrast to the plasticising effect of certain organic penetrants which swell and open up the polymer matrix facilitating diffusion and resulting in an increasing diffusion coefficient as penetrant concentration increases. At low penetrant concentrations, Flory-Huggins sorption approximates Henry's law sorption. The Flory-Huggins model is illustrated in Figure 1 c.

Dual-mode sorption

Dual-mode sorption in glassy polymers proposes the existence of two sorbed penetrant populations in the polymer. A population of the permeant molecules dissolves into the polymer by a mode which obeys Henry's law, while a population binds to active sites or pre-existing cavities within the polymer following a Langmuir-type sorption behaviour (Stern and Trohalaki, 1990), Figure 1 d. Barrie et al. (1980), suggested that the permeant molecules within micro-cavities are not totally immobile, but can contribute to the flux. As temperature increases to Tg, the contribution by penetrant obeying Langmuir sorption decreases and my be absent above Tg, where penetrant sorption obeys Henry's law.

A form of the dual-mode sorption equation takes into account the negative contribution to sorption by the crystalline regions of the polymer and is shown in Equation 4:

$$c^* = S_{max} \cdot (1 - V_x) \cdot p + c^*_H \frac{bP}{1 + bP} \qquad (4)$$

where S_{max} is Henry's law solubility constant for the amorphous matrix; V_x is the fraction of crystallinity; c^*_H is the hole saturation constant and b is a constant representing the affinity for permeant molecules to sorb into microvoids (Birley et al. 1992). This model has been useful in explaining the permeation of low hydrocarbon vapours (C_1 to C_5) and carbon dioxide gas through glassy polymers (Robertson 1993).

Figure 1. Sorption models: a) Henry's law; b) Langmuir sorption isotherm

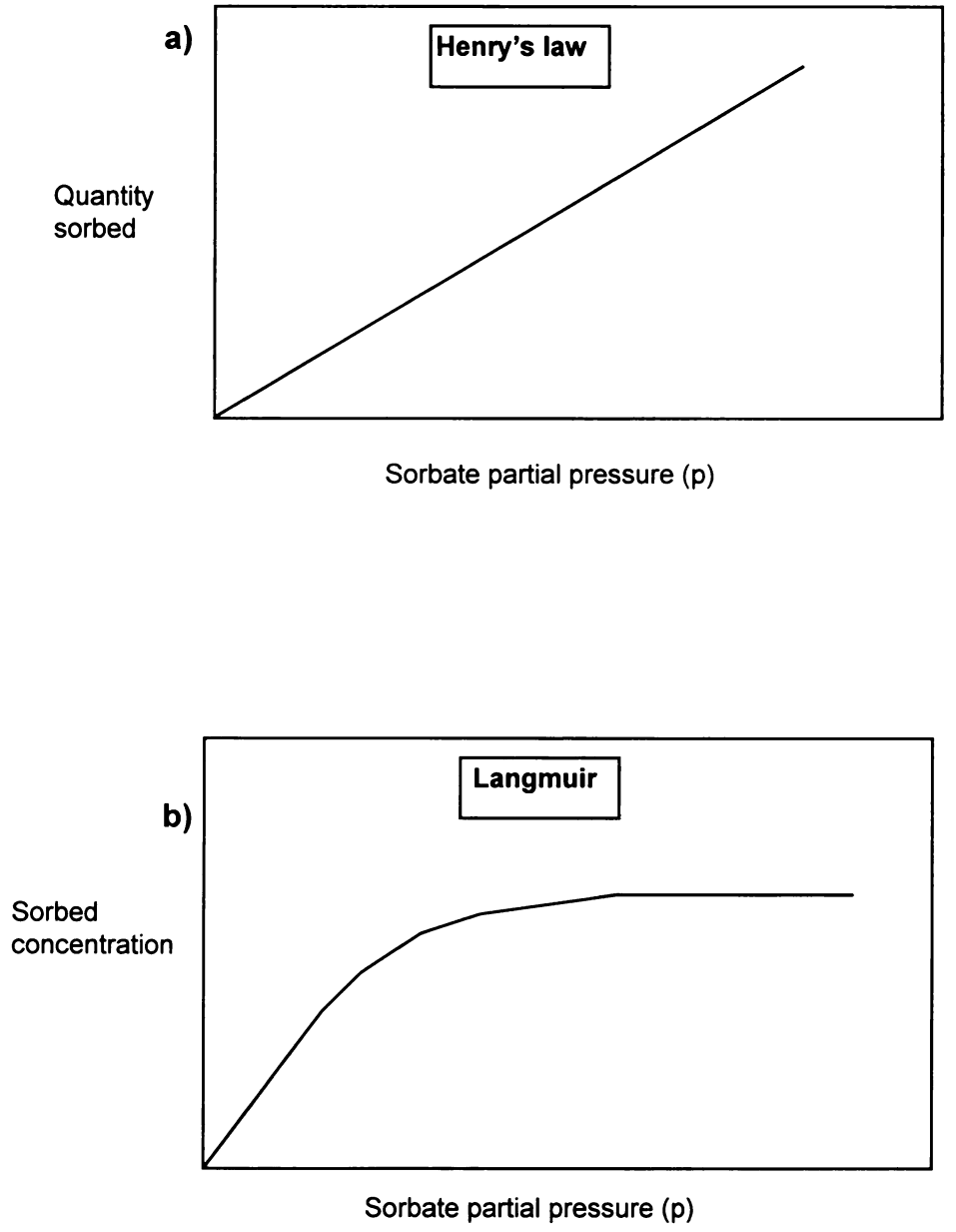

Figure 1. Sorption models (cont.): c) Flory-Huggins; e) Dual mode.

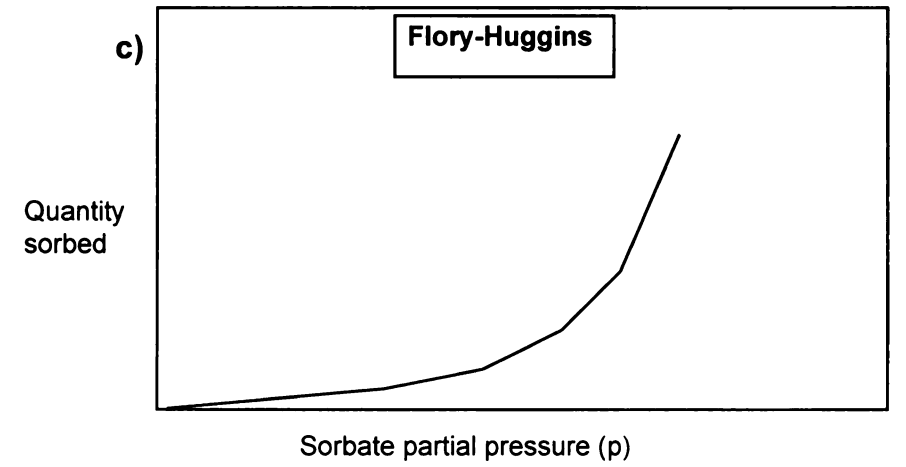

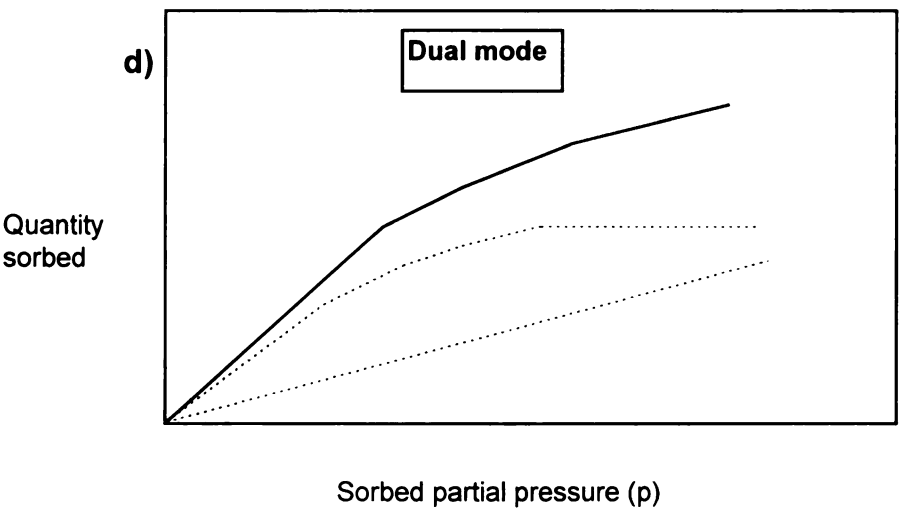

Diffusion and diffusion coefficient

Diffusion describes the process where a permeant molecule advances within the polymer structure from an area of high to an area of low concentration or partial pressure. It is also a measure of the length of time required for a permeant/polymer combination to reach a steady state condition. Permeant size, shape and interaction with the polymer influences the diffusion rate.The ideal diffusion process is described by Fick's first law (Equation 5):

$$F = -D \frac{\delta c}{\delta x} \qquad (5)$$

where, F is the flow, or flux, of penetrant per unit area, expressed as the mass of diffusing species per unit area of polymer film per time (t); c is the concentration of the penetrant in the film, expressed in the same unit of mass of diffusing species per unit of volume or mass of the polymer; D is the diffusion coefficient, in (length)^2/time; x is the distance in the direction of penetrant transport (Crank, 1975). The diffusion coefficient (D), is a proportionality constant, however for many penetrant/polymer systems, D is not a constant but a function of concentration, or time. Low-molecular weight permeants in solid polymers exhibit diffusion coefficient values ranging from 1×10^{-12} to 1×10^{-18} m^2s^{-1} (Hernandez, 1996).

Fick's first law states that for diffusion in one direction, the flow of permeant through a plane perpendicular to the direction of flow, is directly proportional to the rate with which the concentration changes with distance. This

law can only be applied when the permeant concentration in the polymer does not change with time, ie. under steady state conditions where the permeant concentration gradient across the polymer reaches and maintains a constant level (Cromyn, 1985).

Non-steady state conditions are described by Fick's second law, which has several forms. A simplified form of Fick's second law applies under circumstances where diffusion is limited to the *x* direction and *D* is independent of concentration (Equation 6):

$$\frac{\delta c}{\delta t} = \frac{\delta}{\delta x}\left(D \frac{\delta c}{\delta x}\right) \qquad (6)$$

Diffusion is an activated process and therefore follows an Arrhenius-type relationship described by Equation 7:

$$D = D_0 e^{-\frac{E_D}{RT}} \qquad (7)$$

where D_0 is a pre-exponential factor related to the frequency and magnitude of pre-existing holes in the polymer matrix in the absence of permeant; E_D is the activation energy for diffusion (kJ.mol^{-1}); R is the universal gas constant (8.314 kJ.mol^{-1}); T is the temperature in degrees Kelvin. Sorbed permeant can decrease the activation energy for diffusion by increasing polymer chain mobility, therefore increasing the permeant's rate of diffusion through the polymer. Temperature

increases the segmental mobility of the polymer chains and therefore increases the rate of permeant diffusion through the polymer.

The diffusion coefficient can be independent of, or a function of, the penetrant concentration in the polymer. and in both cases the diffusion process is described as Fickian or Case I. If the diffusion coefficient is time dependent then the diffusion process is described as non-Fickian.

Rubbery polymers (above Tg), generally exhibit Fickian diffusion to gases and vapours at low pressures due to attainment of a fast sorption equilibrium, obeying Henry's law, and the ability of the polymer matrix to achieve a rapid homogeneity to the relatively slower diffusing penetrant. If sorption equilibrium cannot be attained at the gas/polymer interface, due to significant surface evaporation, departure from Fickian behaviour may occur.

Glassy polymers (below Tg) exhibit complicated behaviour to penetrants. Comparatively slower segmental motion in the polymer matrix has the effect of yielding cavities which can be occupied by penetrant molecules. As discussed, this results in a dual-mode type of sorption behaviour with two distinct penetrant populations and an anomalous or non-Fickian diffusion coefficient. Other penetrant/polymer systems below Tg and at temperatures at, or above, the critical temperature of the vapour, can experience Case II diffusion. This is characterised by a rapid diffusion process compared to slow relaxation processes with swelling and distortion of the polymer structure behind an advancing penetrant boundary (Frisch, 1980). Organic permeants in glassy

polymers can exhibit time-dependent diffusion, if there is strong interaction with the polymer. Water can show time dependence diffusion in hydrophilic polymers below glass transition temperatures (Rogers and Machin, 1992).

Diffusion models for rubbery polymers

In order to explain the diffusion process and its dependence on temperature and, in certain cases, concentration, two main types of diffusion models have developed. Theses are the 'molecular' models and the 'free volume' models.

Molecular models of diffusion suggest that penetrant molecules advance through the polymer matrix by jumping through microcavities or voids which exist between polymer chains. Each jump involves a rearrangement of the penetrant molecule and neighbouring polymer chain segments. This may temporarily result in breaking a number of Van der Waals type interactions between the chain segments. As the size and shape of the penetrant molecule increases then the amount of energy required to disrupt the interactions to form a void of sufficient volume to accommodate a diffusing molecule will also increase (Rogers, 1985). At equilibrium, a definite size distribution of voids is established on a time-average basis. A void of sufficient size can contain a dissolved penetrant molecule which 'jumps' into a vacant void once it acquires sufficient energy. Penetrant flow occurs in response to a driving force which results in molecules moving from an area of high concentration to one of low concentration. The flow magnitude is dependent on the availability of suitable

microcavities at a sufficient concentration and of sufficient size to accommodate penetrant molecules (Stern and Trohalaki, 1990). A number of molecular models have been proposed including those of Meares (1954), Brandt, (1985) and DiBenedetto and Paul (1963).

The value of the diffusion coefficient for a permeant/polymer combination is described by Equation 8:

$$D = K \exp(A\beta c) f_o^{-2} \qquad (8)$$

where K is a jumping frequency factor; A is a factor related to the minimum hole size for a jump to occur; f_o is the polymer free volume fraction in the absence of the organic permeant; β is a measure of the permeant compound to increase the free volume of the polymer; c is the concentration of the permeant compound in the polymer. Chen and Edin (1980) using a series of alkanes in glassy polycarbonate calculated an average jump distance of 12Å (one Ansgstrom = 10 nm).

Free volume models are based on the assumption that diffusing molecules move from one void to another void which has a volume above a certain critical value. Total free volume is the combined effect of molecular vibrations and discontinuous voids. Diffusion is as a result of redistribution of free-volume voids in the polymer matrix caused by random fluctuations in local density (Lau and Wong, 1995). The thermodynamic diffusion coefficient (D_T) according to Fujita (1961) is calculated from Equation 9:

$$D_T = R\ T\ A_d\ e^{-\frac{Bd}{Vf}} \qquad (9)$$

where A_d is a parameter related to the shape and size of the permeant; B_d is a parameter describing the amount of free volume required; V_f is the fractional free volume. D_T increases with increasing temperature and permeant concentration, and with decreasing permeant size and T_g (Neilsen, 1994).

Diffusion models for glassy polymers

In contrast to rubbery polymers that have very short relaxation times, glassy polymers exhibit slow reaction to changes in stresses brought about for, example, by temperature changes or the presence of sorbed penetrant molecules. Structural microcavities found in the glassy state act as active sorption sites and provide a population of permeant molecules whose sorption characteristics follow the Langmuir isotherm.

Permeation and permeability coefficient

Permeation is the diffusional molecular exchange of gases, vapours or liquid permeants across a plastic material which is devoid of imperfections such as cracks and perforations (Hernandez, 1996). Permeability is the product of the thermodynamic parameter of solubility and the kinetic parameter of diffusion. The diffusion coefficient describes how quickly the molecular species moves in the

film and the solubility coefficient is a measure of the quantity of a substance that will be sorbed by a polymer.

The permeability coefficient describes the transport rate at steady state. Therefore the degree to which the molecular species is soluble in the polymer and the rate of diffusion through the polymer structure, prior to desorption on the exterior surface, are important determinants of the film's permeability to the permeant species. The permeability coefficient will therefore depend on the temperature and physio-chemical properties of the polymer and permeant.

The driving force for permeation of gases or vapours through a polymer film is the difference in concentration or partial pressure of the test gas or vapour between each side of the film. (The partial pressure, as defined by Dalton's law, is the pressure exerted by a constituent gas in a mixture of gases where the total pressure exerted is the sum of the partial pressure for each constituent gas). Therefore the rate of permeation of a constituent gas through a polymer film is a function of its partial pressure difference and not the total pressure difference across the film. The resultant concentration gradient drives a flow of permeant molecules from the high concentration side to the low concentration side of the film. If the low concentration side is significantly lower, then a constant concentration gradient will be established and the permeation rate will reach steady state where the permeant flow is constant per unit time. Figure 2 illustrates a model for gas or vapour permeability through a plastic packaging film. The permeability coefficient, diffusion coefficient and solubility coefficient are related by Equation 10:

$$P = D \times S \qquad (10)$$

This relationship is valid when the diffusion coefficient is concentration independent and the solubility coefficient follows Henry's law. The permeability coefficient is a function of the penetrant molecules solubility in the polymer and their diffusion rate across the polymer and is defined in the following terms:

$$P = \frac{Q \; l}{A \; t \; \Delta_p} \qquad (11)$$

where Q is the amount of penetrant under stated conditions permeating through a material of thickness l and area A, in time t, and under a partial pressure difference of Δ_p. There is no convention for units to be used for the permeability coefficient and over 30 appear in the literature. The preferred units in this study are based on the SI system, which for P are: $m^3 \; m \; m^{-2} \; s^{-1} \; Pa^{-1}$. Figure 2. illustrates a permeability model for gas or vapour in a plastic film.

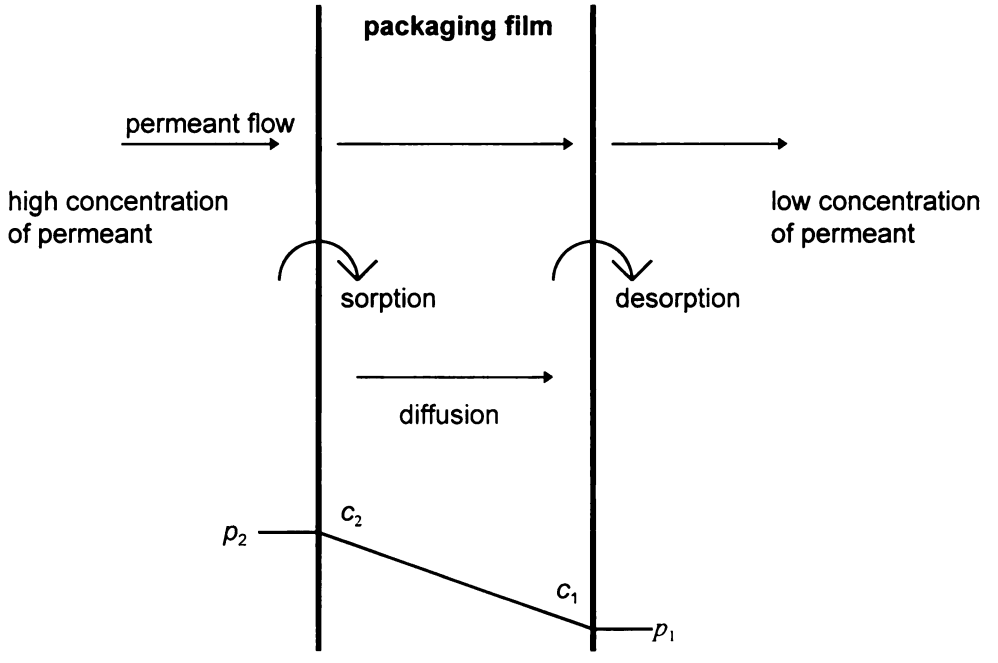

Figure 2. Permeability model for gas or vapour transfer through a plastic packaging film, (Giacin, Hernandez, 1996).

Flavour scalping

Flavour scalping is a sorption process, which results when a major flavour component of a food product has a high solubility in the packaging material. The volatile component dissolves into the polymer, leaving a considerably lower concentration in the pack headspace. An imbalance in the flavour profile results in a detectable reduction in the organoleptic quality of the product. The sorption of d-limonene from orange juice by polymeric packaging materials, is a notable example of flavour scalping. Several authors have reported a significant reduction in sensory quality of fruit juices stored in cartons with an inner polyethylene (PE) layer compared to juice stored in glass containers (Moshonas and Shaw, 1989; Marshall et al., 1986; Mannhiem et al., 1987).

Yamada and co-workers (1992), reported 50 per cent sorption by a low density polyethylene (LDPE) contact layer of the d-limonene content of orange juice and 94 per cent of the d-limonene content of a model citrus mix. The lower scalping effect with the juice sample was attributed to the stabilising effect of the citrus pulp. Increasing the film thickness also increased the extent of sorption (Peiper et al., 1992).

Flavour scalping is not limited to fruit-based beverages. Hansen and Arora (1990), reported significant losses of high molecular weight flavour compounds from ultra-high temperature (UHT) dairy products in contact with LDPE following 12 weeks of storage. After 24 weeks storage low molecular weight components were also sorbed, resulting in a reduction in sensory quality.

In addition to flavour loss, scalping can indirectly reduce product quality by plasticising and swelling the polymer causing modified gas and aroma permeabilities. This can promote scalping of other volatile components. Sorption of organic volatiles can also lead to delamination of the package layers by a mechanism of adhesive or cohesive failure (Peiper and Petersén, 1995; Olafsson et al., 1993). Both conditions can potentially result in loss of package integrity and subsequent product quality loss.

Migration

In addition to loosing aroma compounds by scalping, food may also gain compounds from the packaging material in a process called migration. Components (migrants) in the package diffuse to the package/product interface from where they may, under suitable conditions, diffuse into the food. The rate of migration (mass / area. time) is determined by the initial concentration of the migrant in the package, the partition coefficient (the ratio of the concentration of migrant in the polymer to that in the food), the diffusion coefficient in the food to that in the polymer and the solubility of migrant in the polymer and food.

Potential migrants include processing additives such as plasticisers, antioxidants, lubricants, residual monomers (e.g. vinyl chloride, styrene), solvents (e.g. pentanol), remaining catalysts and catalyst residues. The use of recycled and regrinded resins are a potential source of migrant compounds if insufficiently treated prior to package manufacture. (Hernandez, 1996).

Table 1. summarises some of the food product/packaging interactions of importance.

Table 1. Effects of food product/package interactions.

Product/package interaction	**Transient components**	**Deleterious effect to food or package**
sorption by package (scalping)	aroma volatiles	flavour scalping, loss of package integrity due to plasticising effect and/or delamination
permeation into package	aroma volatiles moisture oxygen	tainting, textural changes, eg caking growth of aerobic microbes, lipid oxidation, rancidity, colour changes
permeation out of package	aroma volatiles moisture carbon dioxide	flavour loss, dehydration and textural changes, decarbonation
migration from package to product	residual monomer additives	health concerns, tainting

Polymer properties affecting mass transfer

Chemical composition

Mass transfer in plastics is affected by several polymer properties including structural regularity, conformational flexibility and intermolecular forces of attraction.

Crystallinity, crosslinking and orientation will tend to decrease permeability. Crystalline polymers have high melting points, high densities, high moduli of plasticity, resist dissolution and swelling and are virtually impenetrable

to diffusion of small molecules. Mass transfer is therefore restricted to the amorphous regions of the polymer where polymer chains are randomly orientated. If sufficient energy is available, the chains are free to move, resulting in an increase in the free volume which may accommodate the passage of transient molecules. Several authors have reported the effect of increasing polymer crystallinity on the reduction in sorption, diffusion and permeability of gases and organic compounds (Michaels et al., 1963; Shimoda et al., 1988; Vieth and Wuerth, 1969).

Polymer properties can be affected by certain compounds which facilitate the segmental mobility of the polymer chains at a particular temperature, by plasticising the polymer. For example, ethylene vinyl alcohol (EVOH) is a polymer with very low oxygen permeability under dry conditions. Interchain hydrogen bonding prevents gas diffusion by reducing the segmental mobility of the polymer chains in the amorphous regions. In the presence of water EVOH becomes plasticised, as the hydrogen bonds are disrupted and the free volume of the polymer increases. Above 80% relative humidity and at autoclave temperatures EVOH is plasticised to a point where oxygen permeability increases 50 to 100 fold (Axelson-Larsson 1992).

Crosslinking polymer chains restricts chain mobility and consequently reduces permeability. Rogers (1985), proposes this effect results from a decrease in molecular diffusion through the polymer structure, rather than its effect on the solubility coefficient.

Ashley (1985), discusses the effect of polymer functional groups and side groups on oxygen permeability. Functional groups such as benzene rings, methyl groups and hydrogen groups offer a relatively poor barrier to oxygen compared to the polar hydroxyl, cyanide and chlorine groups. Linear hydrocarbon chains with hydrogen side groups are a relatively good barrier to oxygen, provided they permit close packing of polymer chains, compared to ethyl or t-butyl groups which are bulky and have a poor packing ability. The presence of crystalline regions in the polymer will reduce oxygen permeability since crystallites are impermeable to gases and create a more tortuous path for diffusing molecules (Hernandez, 1996).

Glass transition temperature

The glass transition temperature (T_g) marks the temperature at which segmental motion of 20-40 carbon atom units in amorphous polymers becomes possible. Below T_g segmental motion is virtually absent and a non-crystalline polymer has properties characteristic of a glass; amorphous, hard and brittle. If the polymer contains some crystallinity then at temperatures below T_g it will be hard and tough with a high melting point. At T_g segmental motion increases in the amorphous regions transforming the polymer into a soft, plastic state.

Cohesive energy and solubility parameter

The cohesive energy (E_{coh}) is defined as the internal energy required per mole of substance to eliminate all the intermolecular forces. In effect, it is the

energy required to pull polymer chains apart so that non-covalent intermolecular forces equal zero. The cohesive energy density (δ_{coh}) is the cohesive energy per unit volume of substance. A polymer with weak intermolecular forces will have a lower E_{coh} than one with strong intermolecular attractions. For example, polyethylene (E_{coh} 260 J cm^{-3}), has weak dispersion forces, and therefore interchain attraction is weak. Polyhexamethylene adipamide (E_{coh} 775 J cm^{-3}), has intermolecular forces comprised of hydrogen bonds which result in stronger attraction between polymer chains.

Plasticisers reduce δ_{coh} and therefore increase the segmental motion in polymer chains. This opens up the polymer structure which facilitates diffusion of transient molecules between the molecular chains and therefore through the polymer material.

Compounds interact with polymers if they have similar functional groups and bond types. Polar compounds will tend to dissolve in polar solvents, and non-polar compounds will be soluble in non-polar solvents.The solubility parameter (ρ, which is related to the the cohesive energy density by: $\rho = [\delta_{coh}]^{0.5}$), provides a qualitative prediction of the solubility of a compound in a polymer. Similar ρ values for a compound and polymer indicate that sorption is likely. Solubility parameters for chemical compounds and polymers can be calculated from published data (Hoftyzer-Van Krevelen, 1976) on the group contributions from polar, dispersive and hydrogen bond elements of a molecule.

Other factors influencing mass transfer

Solute interaction

At low pressure transport of simple gases through a polymer film has a permeability coefficient independent of concentration. Permeability measurements at high concentrations can therefore be reliably extrapolated to predict rates at low permeant concentrations. In the case of many organic permeants, the rate of transport through polymer films is concentration dependent. In such cases permeant molecules may plasticise the polymer, resulting in greater segmental mobility, an increase in the concentration and size of microvoids and an increased permeant diffusion rate. Complex interactions can exist in co-permeant systems where one component may plasticise the polymer facilitating the diffusion of another permeant compound.

Nielsen and Giacin, (1996) reported the effect of ethyl acetate and d-limonene vapour co-permeants in biaxially orientated polypropylene (BOPP) film. Limonene plasticised the polymer structure, increasing the permeability of ethyl acetate some 500%, compared to the permeability of ethyl acetate as a single permeant.

Hydrophilic barriers can become plasticised in high relative humidity environments resulting in accelerated permeability to certain organic compounds. Liu et al. (1988) reported an increase in toluene vapour diffusion through nylon at high relative humidities. Johansson and Leufvén (1994) investigated the effect of relative humidity of organic permeants in several polymeric films. They found that relative humidity had a significant influence on

the permeability coefficient of aldehydes and alcohols in EVOH film. At 20% RH, permeability coefficients were 10 to 100 times less than in linear low density polyethylene (LLDPE) and high density polyethylene (HDPE) films. However at 80% RH the barrier properties of EVOH were significantly reduced and the order of magnitude of permeability was the same in all films.

Permeant structure

Shimoda et al. (1987) reported the effect of increasing carbon chain length on sorption, for homologous series of hydrocarbons, esters, aldehydes and alcohols in the vapour phase. Increasing molecular weight resulted in an increase in the solubility coefficient, due primarily to an increase in the boiling point. For fixed gases there is a linear relationship between the logarithm of the solubility coefficient and the boiling point of the gas. Zobel (1985), reported this relationship will generally hold for low organic vapour concentrations, when the permeant/polymer interaction is negligible.

Small permeant molecules have a higher probability of finding a microvoid of sufficient volume to occupy compared to larger molecules and therefore the diffusion coefficient increases with decreasing permeant volume. As chain length of the penetrant molecules in the vapour phase increases, the solubility coefficient and permeability coefficient increased two to five times with each additional methyl group. This phenomenon holds for molecules up to ten carbon atoms in length. For molecules containing more than ten carbon atoms the effect is less and with some functional groups produces a negative effect. Chen

and Edin (1980), found the logarithm of the diffusion coefficient of an alkane series in glassy polycarbonate films to be linearly related to the square of the pentrant diameter. Berens and Hopfenberg (1982), reported higher diffusivities (up to a factor of 10^3), for n-alkanes and other elongated or flattened molecules than for spherical molecules of similar molar volume. The authors suggested that permeant molecules move through the polymer matrix in a direction which minimises the displacement of polymer chains. This implies that diffusive motion occurs along the molecules long axis.

Permeant concentration will have an effect on permeability at levels where interaction occurs with the polymer. Zobel (1985), working with a range of homologous organic compounds, found that the rate of change of permeability coefficient in polypropylene film, was small provided the permeant concentration was under ≈10 per cent of saturated vapour pressure.

Temperature

Temperature has a varying effect on the solubility and diffusion coefficients and therefore can impact either way on the permeability coefficient depending on the overall effect on *S* and *D*. The effect of temperature on the solubility coefficient can be represented by an Arrhenius-type relationship:

$$S = S_0 \exp(-\Delta H_s/RT) \qquad (12)$$

where ΔH_s is the heat of solution for the permeant gas, R is the gas constant and T is the temperature (°K). ΔH_s is the sum of the molar heat of condensation ΔH_c and the molar heat of mixing ΔH_m:

$$\Delta H_s = \Delta H_c + \Delta H_m$$

For gases well above their critical point at room temperature (eg. hydrogen, oxygen and nitrogen), the heat of soluton is small and positive and therefore S increases slightly with temperature. For easily condensable organic vapours the heat of solution is always negative and therefore S decreases with increasing temperature (Braunauer, 1965).

The diffusion coefficient's effect with temperature, can also be represented by an Arrhenius-type equation:

$$D = D_0 \exp(-E_D/RT) \qquad (13)$$

where E_D (the activation energy for the diffusion process) is always positive and therefore D always increases with temperature.

The apparent activation energy for permeation (E_p), is the sum of the activation energy for the diffusion process and the heat of solution for the particular permeant-polymer system. It is related to the permeability coefficient by the following equation:

$$P = P_0 \exp(-E_p/RT) \qquad (14)$$

The permeability coefficient may increase or decrease depending on the relative values of E_D and ΔH. E_p, E_D and ΔH are related by the following equation:

$$E_p = \Delta H + E_D \qquad (15)$$

Measurement of permeant sorption and diffusion in polymers

Sorption measurement by gravimetry

Sorption experiments are frequently carried out using a gravimetric technique which continually records weight change of a film sample with time. A number of researchers have studied the sorption of organic vapours using apparatus utilising an electrobalance (Hernandez et al., 1986; Baner, 1987).

The electrobalance consists of a balance beam and highly sensitive weighing unit which converts torque to current. The greater the weight, the larger the torque and thus the larger the current required to maintain the balance beam in a horizontal position. The current is therefore indicative of the weight suspended from the balance beam. The high sensitivity of this instrument, which can measure weight changes down to 1×10^{-7} g, makes it ideal for measuring small weight increases in films sorbing organic vapours. The electrobalance output can be monitored by a chart recorder or alternatively by a computer via an analogue to digital converter to provide weight/time data.

The electrobalance is contained within a glass vessel, and the film sample is suspended from the balance beam wire enclosed in the hangdown tube. This isolates the instrument from the external environment, thus experiments can be

conducted under a controlled gaseous or vapour atmosphere. To avoid condensation of moisture on the weighing unit and to maintain an inert environment, the apparatus is never exposed to air but continuously flushed with dry nitrogen gas (Cahn, 1987). The instrument is highly sensitive to mechanical shocks and therefore should be isolated from external vibration, ideally wall mounted to provide a rigid and firm support.

Prior to testing, the electrobalance is calibrated using known weights and flushed with inert gas to remove residual organic vapours from the previous run. The polymer film sample is suspended from the balance arm of the instrument in the hangdown tube and the instrument is rezeroed. Upon initiation of the test, organic vapour of the desired partial pressure and at constant flow rate is introduced into the system. The apparatus is held at a constant temperature throughout the experiment.

The vapour generator system comprises an aeration flask containing the desired organic liquid. Nitrogen gas is bubbled through the liquid to produce the vapour stream which flows into the hangdown tube and surrounds the film sample. The vapour exists at the top of the hangdown tube and is directed into a fume cupboard.

After a short lag period, which corresponds to the time taken for organic test vapour to reach the film sample and to be sorbed in a quantity which is above the sensitivity of the electrobalance, the weight of the sample increases and will, with time, attain a steady state condition where the sample weight remains constant. A typical sorption curve is shown in Figure 3.

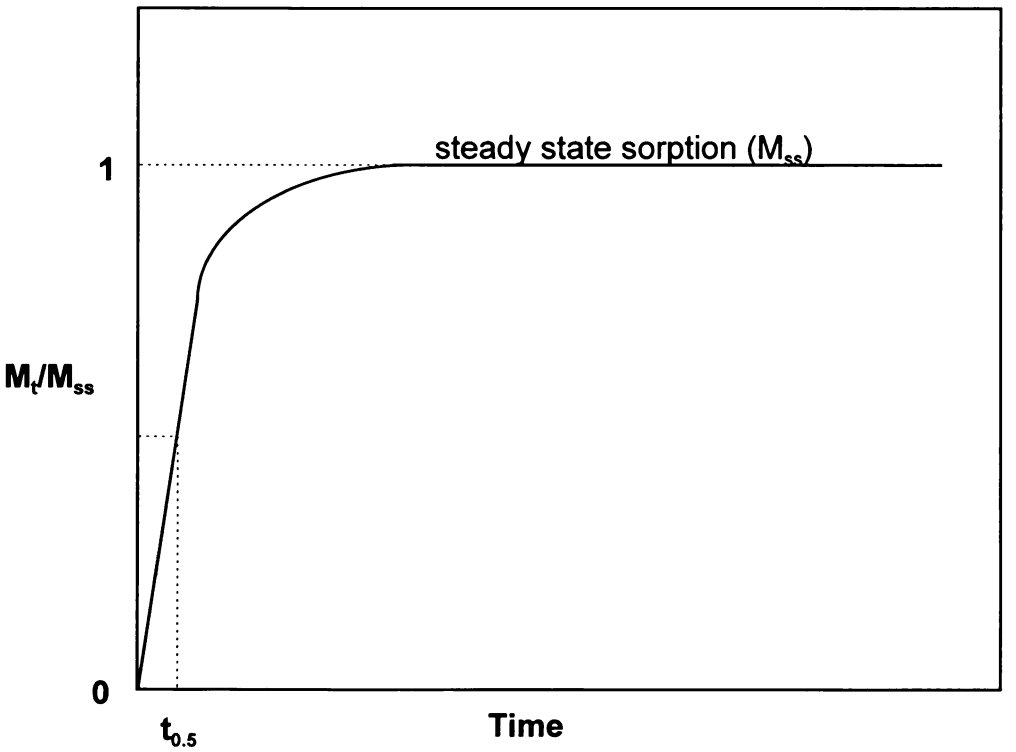

Figure 3. Generalised sorption profile curve illustrating determination of half-time sorption value ($t_{0.5}$) from steady state sorption value (M_{ss}).

The solubility coefficient (S) expressed as mass of vapour sorbed at equilibrium per mass of polymer per driving force is determined from steady state experimental sorption data using Equation 16.

$$S = \frac{M_{ss}}{w\ b} \qquad (16)$$

where M_{ss} is the total mass of vapour sorbed by the polymer at steady state conditions and at a particular temperature; w is the weight of the polymer sample tested and b is the penetrant driving force in units of pressure or concentration.Crank (1975) developed an expression for the sorption of a penetrant by a polymer, Equation 17.

$$\frac{M_t}{M_{ss}} = 1 - \frac{8}{\pi^2}\left[\exp\left(\frac{-D_s \times \pi^2 \times t}{l^2}\right) + \frac{1}{9}\exp\left(\frac{-9\,D_s \times \pi^2 \times t}{l^2}\right)\right] \quad (17)$$

where M_t is the quantity of permeant sorbed by the polymer film at time t; M_{ss} is the equilibrium sorption level at steady state, after infinite time; t is the time to reach M_{ss} ; l is the film thickness.

The sorption diffusion coefficient (D_s) is calculated from sorption data by setting M_t/M_{ss} = 0.5, and solving Equation 18 to find D_s:

$$D_s = \frac{0.049\, l^2}{t_{0.5}} \quad (18)$$

where $t_{0.5}$ is the time required to reach half the steady state sorption value when M_t/M_{ss} = 0.5, as shown in Figure 3.

Measurement of transmission rate and permeability

Several methods exist for measuring transmission rate and permeability of gases and vapours. The two main types of measurement are the 'isostatic' (Figure 4.), and the 'quasi-isostatic' (Figure 5.) methods.

Isostatic method

In the isostatic method both sides of the test film are maintained at the same total pressure but a partial pressure difference is maintained by passing test gas continuously on one side of the film while inert carrier gas continuously removes permeant from the other side of the film. This maintains a very low partial pressure of permeated test gas and establishes a constant partial pressure difference across the film. This is also referred to as the 'concentration increase' method. Since the total pressure is equal on both sides of the test sample, there is no requirement to support the film.

Quasi-isostatic method

In the quasi-isostatic method a test film separates two chambers where one side of the film is exposed to test gas, while initially the other is in contact with inert gas. The partial pressure difference between the two sides of the test film provides the driving force for permeation to occur. Gas samples are periodically withdrawn from the low pressure side of the film using a gas syringe and quantified by a suitable method. Since the permeant is not continuously removed from the low pressure side, the partial pressure increases until a constant rate value is attained. This method has also been referred to as the 'pressure increase' or 'accumulation' method.

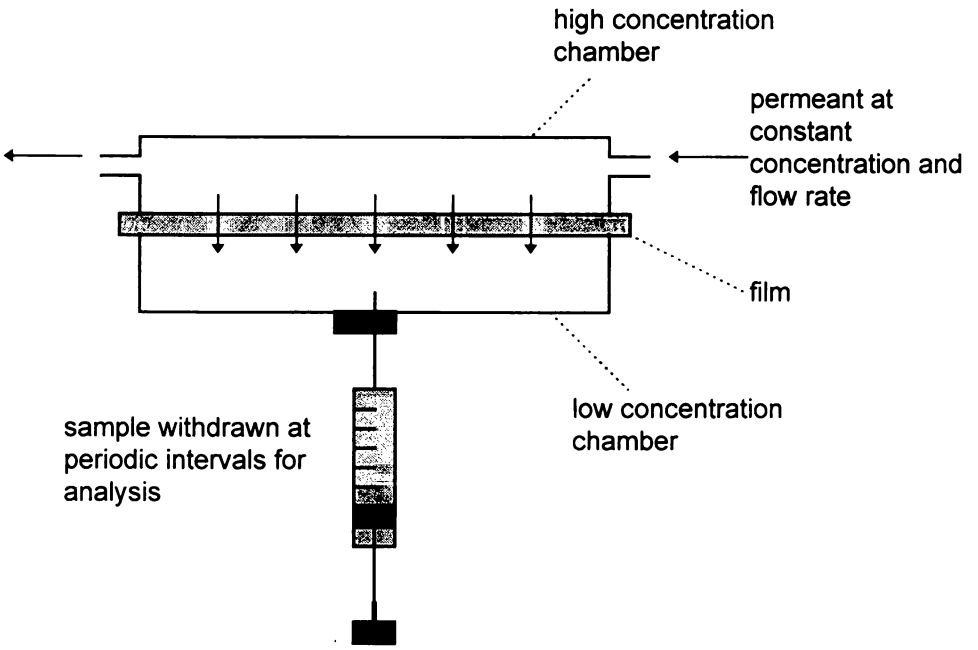

Figure 4 . Diagram illustrating the quasi-isostatic test procedure for determining the transmission rate of a permeant through a polymeric film.

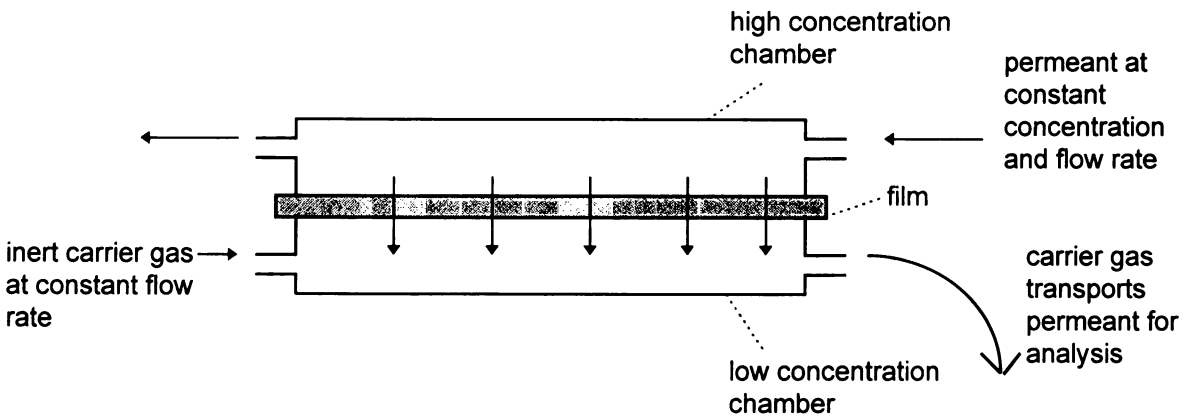

Figure 5. Diagram illustrating the isostatic test procedure for determining the transmission rate of a permeant through a polymeric film.

Baner et al. (1986) presented a method based on the quasi-isostatic procedure for determining the diffusion of organic solvents through plastic films. A constant vapour concentration in the high pressure chamber was achieved by passing a continuous flow of organic vapour through the chamber. Permeated vapour concentration was measured by employing a gas chromatography.

The quantity of penetrant (*Q*) permeating through the film, at steady state, can be determined from Equation 19:

$$Q = \frac{Dc}{l^2}\left(t - \frac{l^2}{6D}\right) \qquad (19)$$

where *D* is the diffusion coefficient; *C* is the permeant concentration in the high concentration face of the film of thickness *l* (Cromyn, 1985).

The diffusion coefficient can be obtained from the transmission rate profile by determining the lag time (θ) for the curve. The lag time is found by extrapolating the steady state portion of the transmission rate profile to the time axis where the quantity permeated is zero. This is illustrated in Figure 6. The intercept has the equation:

$$\theta = \frac{l^2}{6D} \qquad (20)$$

Therefore the diffusion coefficient (D) can be determined from the following expression which was presented by Barrer (1939):

$$D = \frac{l^2}{6\theta} \qquad (21)$$

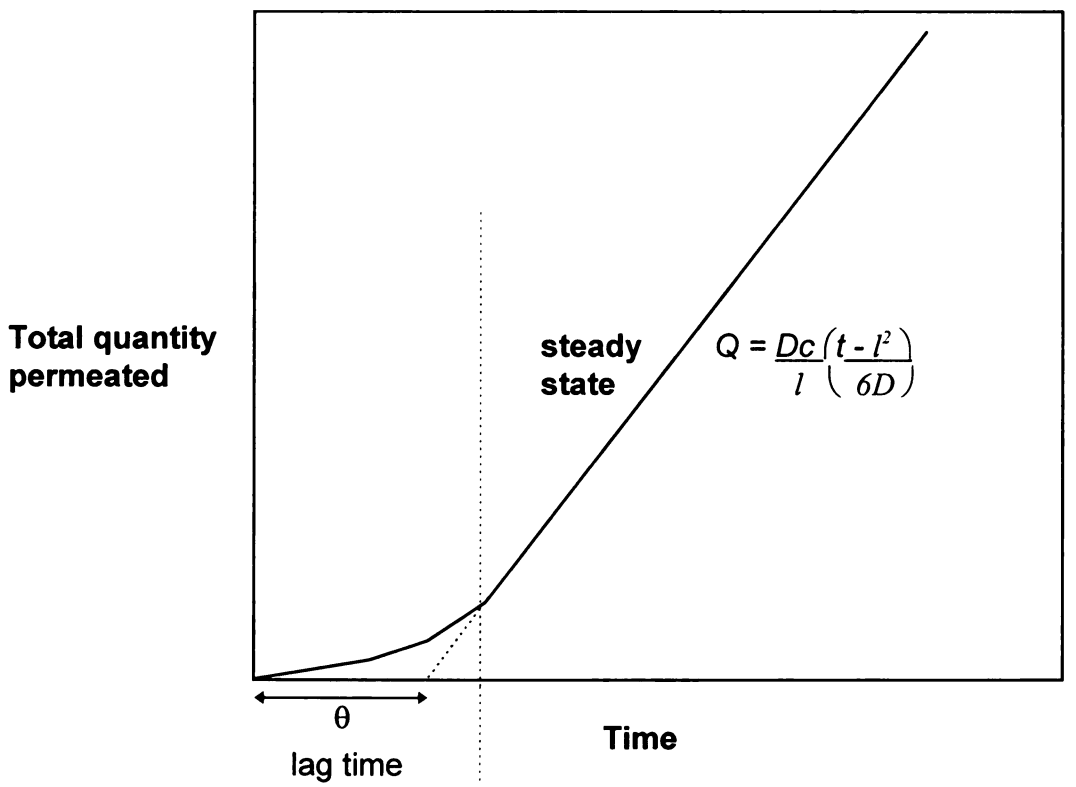

Figure 6. Generalised transmission rate curve for the quasi-isostatic procedure

The steady state permeability coefficient is obtained from quasi-isostatic data by the following expression:

$$P = \frac{\alpha\, l}{A\, \rho} \qquad (22)$$

where α is the slope of the steady state portion of the transmission rate profile curve; l is the film thickness; A is the area of film exposed to the permeant; ρ is the permeant driving force given by the concentration or partial pressure gradient.

Water vapour transmission rate and measurement

Water vapour transmission rate (WVTR) is defined as the time rate of water vapour flow (Q/t), normal to the two surfaces, under steady state conditions through unit area of a test film material:

$$\text{WVTR} = \frac{Q}{A\ t} \qquad (23)$$

The WVTR does not take into account the thickness of the test material or the driving force of permeant across the polymer. Therefore it is not a real constant for the test film, but is useful for comparative purposes. WVTR data are normally reported at 38°C for films tested at 95% relative humidity.

There are several methods for measuring WVTR and water vapour permeability. Earlier methods were based on gravimetric procedures and measured the weight increase by a dessicant sealed in an aluminium cup by the

test film. In 1990 ASTM introduced a new test standard (ASTM F 1249) based on the isostatic method and employing solid state electronics with pulse-modulated infra-red sensors which can detect down to one ppm water vapour.

MOCON® (Modern Controls Inc. Minneapolis, MN) manufactures and markets an instrument, the Permatran-W 3/31, which meets the requirements of ASTM F 1249. Test temperatures can be controlled from 10 to 40°C (± 0.5°C) and relative humidity can be controlled from 35% to 90% RH (± 3%). The instrument can test at 100% RH (± 3%) by inserting water saturated sponges in the test cell.

Relative humidity is controlled by exposing pressurised dry nitrogen gas to pure water (HPLC grade) is an enclosed chamber where the equilibrium relative humidity reaches 100%. The gas is then released to a lower pressure environment which results in a reduction in the percent relative humidity. This two-pressure method is used by the Permatran-W 3/31 to generate water vapour at the required percent relative humidity. Test gas relative humidity is measured by a solid state semi-conductor device which is located in the outer chamber of both test cells.

Water vapour permeating across the film is transported by dry nitrogen gas to a pressure modulated infrared detection system intended for operation over a 5 to 50°C temperature range. The detector consists of a pump, a sensing chamber, infrared source, 2.6 micrometer infrared filter, a lead sulphide photodetector and an amplifier. The pump varies the pressure and density of the

gas mixture in the sensing chamber, which consequently varies the absorption rate of infrared radiation by the water vapour present. The infrared photodetector produces a low-level electrical signal in response to the change in transmitted infrared radiation. The amplifier produces a filtered DC signal in direct proportion to the water vapour in the test cell and therefore proportional to the water vapour transmission of the test film.

Water vapour transmission rate by a relative, rather than an absolute, method of measurement. Therefore the instrument must be calibrated using reference films of known WVTR and at specific flow rates, generally at 10 cm^3min^{-1} and 100 cm^3min^{-1}. The system must be operated using the calibration flow rates, good barriers at the higher flow rate and poor barriers at the lower flow rate.

Measurement of oxygen transmission rate

Oxygen transmission rate is defined as the time rate of gaseous oxygen flow, normal to the two film surfaces, under steady state conditions through a unit area of a test film material.

The MOCON Ox-tran (Modern Controls Inc., Minneapolis, MN), measures the transmission rate of oxygen across flat films by a method based on the isostatic procedure, and use a coulometric sensor to detect permeated oxygen.

During testing a conditioned (dry) test specimen is clamped between the upper and lower chambers of the test cell. The chambers are flushed with dry nitrogen carrier gas (containing between 0.5 - 3.0% hydrogen and less than

100ppm oxygen) to outgas the film sample. The sensor is inserted and once a steady output is obtained oxygen gas (dry, containing more than 99.5% oxygen) is introduced into the diffusion cell. Oxygen gas permeates through the film sample and is transported to the sensor by the carrier gas. A steady state condition is denoted by a constant output from the sensor. The sensor can be damaged by excessive amounts of oxygen and therefore poor barriers (transmission rates in excess of 200 cm^3 (STP)/m^2.d), should be masked to reduce the test film area, or alternatively tested with gas containing a reduced and known level of oxygen, for example compressed air.

The coulometric sensor is an electro-chemical cell comprising a nickel/cadmium/graphite electrode. The sensor's output is a linear function of the mass flow rate of gaseous oxygen entering the cell. In principal, four electrons are produced by the sensor per molecule of oxygen gas that enters into it. (*ASTM D 3985, 1981*). More recent Ox-tran models use a patented coulometric sensor (COULOX) which provides parts per billion sensitivity even in the presence of water vapour. A computer installed with MOCON software is used to record and analyse information from the instrument.

The Oxtran-twin can be used to determine the oxygen diffusion coefficient by obtaining $t_{0.5}$ from transmission rate data and using the following equation:

$$D = \frac{l^2}{7.199\, t_{0.5}} \qquad (24)$$

Measurement of carbon dioxide transmission rate

The PERMATRAN C-IV manufactured and marketed by MOCON (Modern Controls Inc. Minneapolis, MN) is an instrument for measuring the rate at which gaseous carbon dioxide diffuses through a permeable barrier, including flat films and permeable containers. Test films are clamped between the upper and lower half of a diffusion cell, conditioned by flushing with nitrogen gas, then the upper half is flushed continuously with carbon dioxide gas. Permeated gas is carried to an infrared sensor by nitrogen gas where a response is generated proportional to the amount of carbon dioxide present.

The instrument can be used to determine the carbon dioxide loss from a plastic container by connecting a bottle test fixture to the lower half of the diffusion cell at one of the testing stations. Using this adaptor filled and unfilled containers can be tested (MOCON, 1983).

The PERMATRAN C-IV can operate in three testing modes for flat films and selection of a method is based on the barrier properties of the film:

Static accumulation - for high barrier films (less than 50 $cm^3m^{-2}day^{-1}$). Following purging of the test film, carbon dioxide gas is introduced into the upper half of the diffusion cell for a pre-determined duration (2 - 80 hours) depending on the barrier properties of the film. Permeated gas accumulates in the lower half of the cell and is transported by nitrogen carrier gas to the infrared sensor. The gas is measured and the resulting concentration is displayed by a strip chart recorder as a DC voltage value. The carbon dioxide concentration is determined by

comparison with the signal produced from a known concentration of carbon dioxide gas.

Dynamic accumulation - for testing medium barriers (between 50 - 300 $cm^3m^{-2}day^{-1}$). Test film is exposed to carbon dioxide gas on one side of the diffusion cell and a stream of nitrogen gas on the other side. The film is allowed to condition for a time which allows the carbon dioxide steady state transmission rate to be reached. Following conditioning the test cell is connected to the infrared sensor in a closed recirculating loop. As carbon dioxide permeates through the cell and its concentration increases, the sensor's output voltage increases to produce a sloping line across the chart paper. The transmission rate is calculated from the slope when compared to the signal produced when a known volume of carbon dioxide is injected into an identical volume.

Continuous flow - for testing medium to low barrier films (greater than 300 $cm^3m^{-2}day^{-1}$). Unlike the previous methods which are based on accumulation of permeated gas. In a closed loop system, the continuous flow method uses an open loop arrangement where nitrogen gas carries permeated carbon dioxide gas from the diffusion cell to the sensor and is then exhausted. The test film is compared to a reference film of known transmission rate which is similar to the expected value of the test film.

In cases where the test film offers a very low barrier to carbon dioxide gas, the test film may be mounted on an aluminium foil mask to reduce the test surface area from 50 cm^2 to 5 cm^2.

Measurement of organic vapour permeation

As noted above, sorption, diffusion and permeation of organic vapours can affect the quality of foods. The MOCON Aromatran 1A (Modern Controls Inc., Minneapolis, MN) is a recently developed and commercial instrument which measures the transmission rate of organic vapours across packages and packaging films. The instrument is designed to measure pure organic vapours and cannot differentiate multiple permeants.

The Aromatran is a modular, automated system consisting of a Master test module interfaced to a computer installed with system software, a dot matrix printer, an organic vapour generator system and gas supply (including nitrogen for carrying organic vapour to the instrument and also for transporting permeant to the sensor; air and hydrogen to produce the hydrogen flame in the flame ionisation detector). The Master module provides the environment in which films are tested, enabling control of test temperature (from 5 to 65°C, $\pm$ 5°C), and the relative humidity of the organic vapour (which can be set at 0% and 100 % and controlled from 35% to 90% RH, $\pm$ 3% RH). The computer controls test parameters and analyses data sent from the modules.

The system gases pass through a four-station filter assembly to remove impurities which could potentially damage the system plumbing and the flame ionisation detector and produce erroneous readings. An oxygen trap used with the carrier gas removes oxygen and traces of sulphur and chlorine. A moisture trap also used with the carrier gas removes water, oil and suspended solids such as dust. The compressed air and hydrogen pass through an activated charcoal filter which removes organic compounds.

The instrument uses a flame ionisation detector (FID) to sense the presence of organic vapour present in the carrier gas permeating a sample test film and quantifies the transmission rate of the particular organic vapour/test film combination. Nitrogen carrier gas transports the organic vapour which has permeated the test film to the FID. The vapour is burned at the tip of a hydrogen flame resulting in the formation of free electrons and charged particles which lower the electrical resistance across the gap between two electrodes. The resultant voltage drop is amplified and interpreted by an electrometer which generates an output reading in millivolts. The reading correlates with the transmission rate value for the vapour/film combination.

The FID measures only those substances which produce charged ions when burned in a hydrogen flame at 2100°C. The response is proportional to the number of oxidisable atoms reaching the FID. It does not respond to fully oxidised carbon atoms such as carbonyl groups and ethers, and the response diminishes with halogens, amines and hydroxyl groups. Its insensitivity to water

vapour and gases such as CO, CO_2, SO_2 and NH_3 is advantageous in permeation studies. The FID is first calibrated with permeant vapour of known concentration.

The Aromatran utilises Fick's first and second laws and Henry's law to calculate values of the permeability coefficient, diffusion coefficient and sorption coefficient for the test film or package. The assumption is that the permeability follows Fickian behaviour where no interaction occurs between the permeant and the test film. The permeability coefficient is calculated from transmission rate data for the permeant/material combination.

The diffusion coefficient (D) is calculated by the 'half-time' method, where the half-time ($t_{0.5}$) is the time at half the steady state transmission rate for the organic compound permeating through a test film of known thickness (l). The 'half-time' method utilises Equation (24) as for the Ox-tran twin to determine diffusion coefficient.

The film must be outgassed prior to testing to remove organic compounds which could interfere with the FID and produce inaccurate results. During testing one side of the film is continuously swept with the organic test vapour of known and constant concentration, while nitrogen carrier gas at a known and constant rate continuously flows past the opposite side transporting the permeated organic vapour to the detector for quantification. This is known as the 'void differential' method.

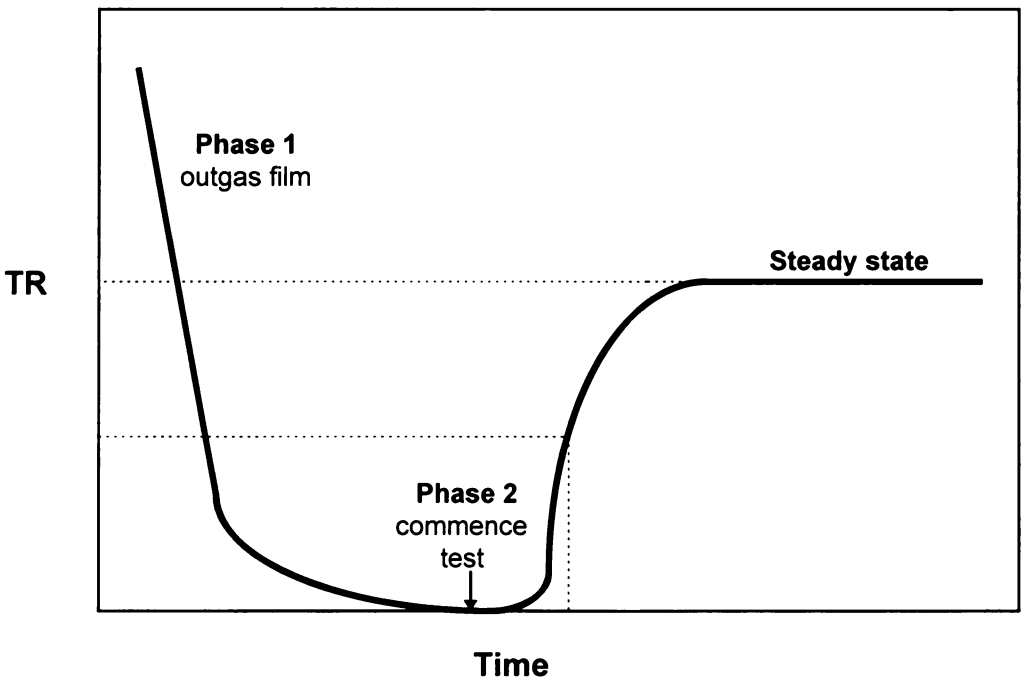

Figure 7. Profile of half-sorption time determination using the MOCON Aromatran 1A.

Organic vapour Is generated by passing nitrogen carrier gas through a sparging system containing pure organic compound.

Other methods of predicting polymer permeability

Salame (1986) deveoloped a method of predicting gas permeability of polymers based on their cohesive energy density and fractional free volume. The resultant value termed the 'Permachor value' (π), is related to permeability by the following expression:

$$P = A\, e^{-s\pi} \qquad (24)$$

where A and s are temperature dependent constants for the particular gases. To date this method has not been applied to organic vapours.

Wessling et al (1994), reported a method of determining carbon dioxide permeability based on the infra-red spectrum of a polymer film. The correlation is based on the assumption that 'hidden' information from the spectrum can forecast permeability. A neural network model was developed based on samples of 33 polymers which provided a performance correlation factor of 0.77. The workers suggest this method could be applied to mechanical and thermal properties of polymers.

Holland et al., (1980) report a spectrophotometric method for determining the permeability of polymeric film to gases. This employs an impregnated film which changes colour as the test gas or vapour is absorbed. Selection of reagents with high sensitivity results in rapid determination of the test gas in very low concentrations.

Styrene butadiene KR-10

K-Resin® is the trade mark for Phillips Chemical Company's (Phillips Petroleum Company, Bartlesville, Oklahoma) range of styrene-butadiene copolymers manufactured by incorporating polystyrene with less than 14% poly 1-4 butadiene. These plastics are recommended for a wide range of packaging applications due to their sparkling clarity, high gloss and impact resistance. The resins are versatile and can be processed by conventional methods including sheet extrusion, thermoforming, and injection blow moulding processes.

The polymer is produced by sequential anionic polymerisation of styrene and butadiene which produces star-shaped butadiene-styrene block co-polymers containing about 85% styrene (Brydson, 1991). The bulky nature of the benzene ring the polymer is amorphous and glassy. Differential scanning calorimetry analysis (DSC) of a KR-10 film sample (3.2 mg, scanned at a rate of 10°C min^{-1}, from -30° to 125°C) gave a Tg of 62.22°C. Sorption and permeation experiments were conducted below this temperature where the polymer is in the 'glassy' state.

The structure of the component monomer units for styrene butadiene are shown below:

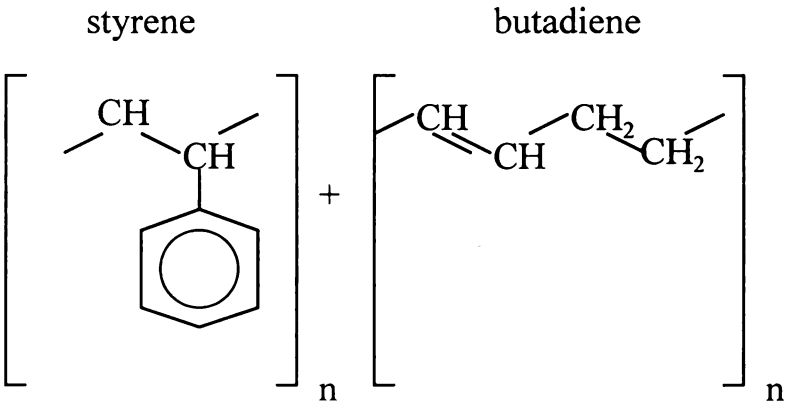

Suggested applications of KR-10 copolymers include produce packaging, medical packaging, twist wrap, overwrap, lidstock and labelling film (Phillips, 1996). KR-10 meets the Food and Drug Administration's (FDA) specifications of section 177.1640 of Title 21 of the Code of Federal Regulations (21 CFR 177.1640) for packaging of non-fatty foods.

D-Limonene

D-limonene, $C_{10}H_{16}$, (1-methyl-4-(1methylethenyl) cyclohexene), is an unsaturated terpene hydrocarbon with a molecular weight of 136.23 daltons, a boiling point of 175-176°C, a molar volume of 162.14 cm^3mol^{-1} and a solubility parameter of 26.4 $(J/cm^3)^{0.5}$. It is a clear, volatile, flammable liquid, insoluble in water but miscible with alcohol. It has a characteristic fruity odour, and is and important flavour component of citrus fruits, comprising 95 per cent of the oil

fraction of orange peel. Limonene is the most widely studied aroma compound in sorption studies which have shown it to interact with many polymeric packaging materials. The structure of d-limonene is shown below

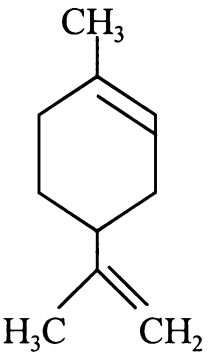

d-limonene

Ethyl acetate

Ethyl acetate belongs to the ester group, which forms one of the most important and widely occuring groups of natural organic compounds. They are important constituents of the flavour profiles of fruits and beverages. Esters are polar compounds, but lacking a hydrogen attached to oxygen, they cannot form strong hydrogen bonds to each other and therefore have boiling points lower than acids or alcohols of comparable molecular weight. Ethyl acetate has a molecular weight of 88.11 Daltons, a boiling point of 76 - 78°C, a molar volume of 97.8 cm^3mol^{-1} and a solubility parameter of 18.22 $(J/cm^3)^{0.5}$

ethyl acetate

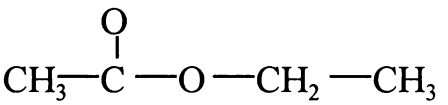

Materials and methods

Materials

Polymer film sample

The polymer used is KR-10 Resin®, a styrene butadiene copolymer, supplied by Phillips Chemical Co. (a Division of Phillips Petroleum Co., Bartsville, OK). The material was supplied in sheet form 11 inches x 8 inches x 1.0 mil (25.4μm) thick. Four sheets were selected at random and thickness measured on an automatic micrometer (TMI Machines Inc. Amityville, NY) at 50 points on each sheet. The average thickness was calculated as 1.0 mil.

Film handling and preparation

Film was outgassed overnight in a vacuum oven at room temperature. Samples were sealed in aluminium foil and stored in a dry environment at ambient temperature. Film was carefully handled with dedicated tweezers during preparation and cut to size using a dedicated template and scalple. Care was taken to avoid sample contamination by dust or grease during storage handling and testing.

Materials and methods

Materials

Polymer film sample

The polymer used is KR-10 Resin®, a styrene butadiene copolymer, supplied by Phillips Chemical Co. (a Division of Phillips Petroleum Co., Bartsville, OK). The material was supplied in sheet form 11 inches x 8 inches x 1.0 mil (25.4μm) thick. Four sheets were selected at random and thickness measured on an automatic micrometer (TMI Machines Inc. Amityville, NY) at 50 points on each sheet. The average thickness was calculated as 1.0 mil.

Film handling and preparation

Film was outgassed overnight in a vacuum oven at room temperature. Samples were sealed in aluminium foil and stored in a dry environment at ambient temperature. Film was carefully handled with dedicated tweezers during preparation and cut to size using a dedicated template and scalple. Care was taken to avoid sample contamination by dust or grease during storage handling and testing.

Chemicals

D-limonene ($C_{10}H_{16}$),
Aldrich Chemical Co. Inc. WI, USA,
Analytical reagent grade,
Molecular weight 136.23 Daltons,
Boiling point 177 +/- 1°C.

Ethyl acetate ($CH_3COOC_2H_5$),
J.T. Baker Chemical Company, Phillipsburg, NJ, USA,
Analytical reagent grade
Molecular weight: 88.11 Daltons
Boiling point: 77.2 +/- 0.5°C
Purity 99.9%

Acetonitrile
EM Science, Gibbstown, NJ, USA
HPLC grade
Molecular weight: 41.05 Daltons
Boiling point: 81.6°C
Purity: 99.8%

Water
J.T. Baker Chemical Company, Phillipsburg, NJ, USA),
HPLC reagent
Molecular weight: 18.00 Daltons
Boiling point: 100.0°C
Purity: residue after evapouration 2 ppm

Compressed gases

Nitrogen, oxygen, compressed air, carbon dioxide, helium and speciality gas(99%nitrogen, 1%hydrogen) from AGA Gas Inc. OH, USA).

Methods

Sorption Measurement

A Cahn D-200-02 Electrobalance (Cahn Instruments,Inc., Cerritos, CA, USA) was employed for the gravimetric sorption measurement in a method described by Hernandez et al., (1986), and illustrated in Figure 8. The electrobalance hangdown tube was placed in a temperature controlled chamber (Thermotron SM-8-SH, Thermotron Industries, Holland, MI, USA). Tests were conducted at 25, 35 and 42°C $\pm$ 1°C with film sample weights of 45 to 55 mg. The electrobalance sensitivity in this weight range is 0.0001mg (0.1μg). The electrobalance was connected to a Digital Interface (Cahn Instruments,Inc., Cerritos, CA, USA) which converts the analogue signal to a digital format enabling connection to a computer installed with software for recording, analysing and displaying weight data. Data was exported into Microsoft Excel for analysis.

In preparation for testing a film sample was hooked to one end of the nichrome wire and suspended freely in the hangdown tube. Prior to introducing the organic vapour, the initial sample weight was noted for solubility determination and thereafter monitored at pre-determined time intervals. The hangdown tube was exposed to test vapour at the desired vapour activity at constant temperature until steady state sorption was reached . Values were recorded and stored on Cahn instrument software. Following testing the sample film was removed and the system purged overnight with dry nitrogen gas to flush

out residual organic vapour and maintain the balance in a moisture free environment.

A constant concentration permeant vapour was produced by using a vapour generator system. Before actual testing was conducted, rotameter settings were determined to provide a range of vapour activities. Vapour activity was calculated by dividing the experimentally determined vapor pressure by the saturated vapour pressure. Saturated vapour pressures were obtained from published data (Marsh, Wilhoit and Yin, 1995). Rotameters (Cole Parmer, Chicago, IL) were used to provide an indication of the settings required for the desired vapour activities. The gas flows to the rotameters were regulated by Nupro 'M' series needle valves (Nupro Co., Willoughby, OH). For the calculation of vapour activity, standard calibration curves for d-limonene (from vapour standards), and ethyl acetate (from standard solutions of ethyl acetate in acetonitrile) were prepared. A procedure to measure the calibration factor is presented in Appendix B. Figures 36 and 37 show the standard calibration curves for d-limonene and ethyl acetate respectively.

Sorption profiles were obtained by continuous recording of weight-gain measurement at 25, 35 and 42°C until the system reached steady state. To ensure a true steady state had been attained, the tests were allowed to continue and the data examined for deviations from equilibrium values. Significant deviations from steady state values were not observed. To estimate the diffusion coefficient the 'half-sorption time' ($t_{0.5}$) was obtained by interpolating to $M_{ss} = 0.5$

from experimental data of M_t/M_{ss} versus time and substituting this value into Equation (17).

The theoretical sorption curve was found by substituting the experimental diffusion coefficient value into Equation (16), calculated values of weight increase were obtained. By using the minimum sum of square method (refer to Results and Discussion section), between calculated and experimental values, the best estimate for the calculated diffusion coefficient was found. This value was used find values for the theoretical weight increase due to sorbed organic vapour as a function of time. Calculated values were compared with the experimental values.

Analysis of permeant concentration was carried out by a gas chromatographic procedure with flame ionization detection.

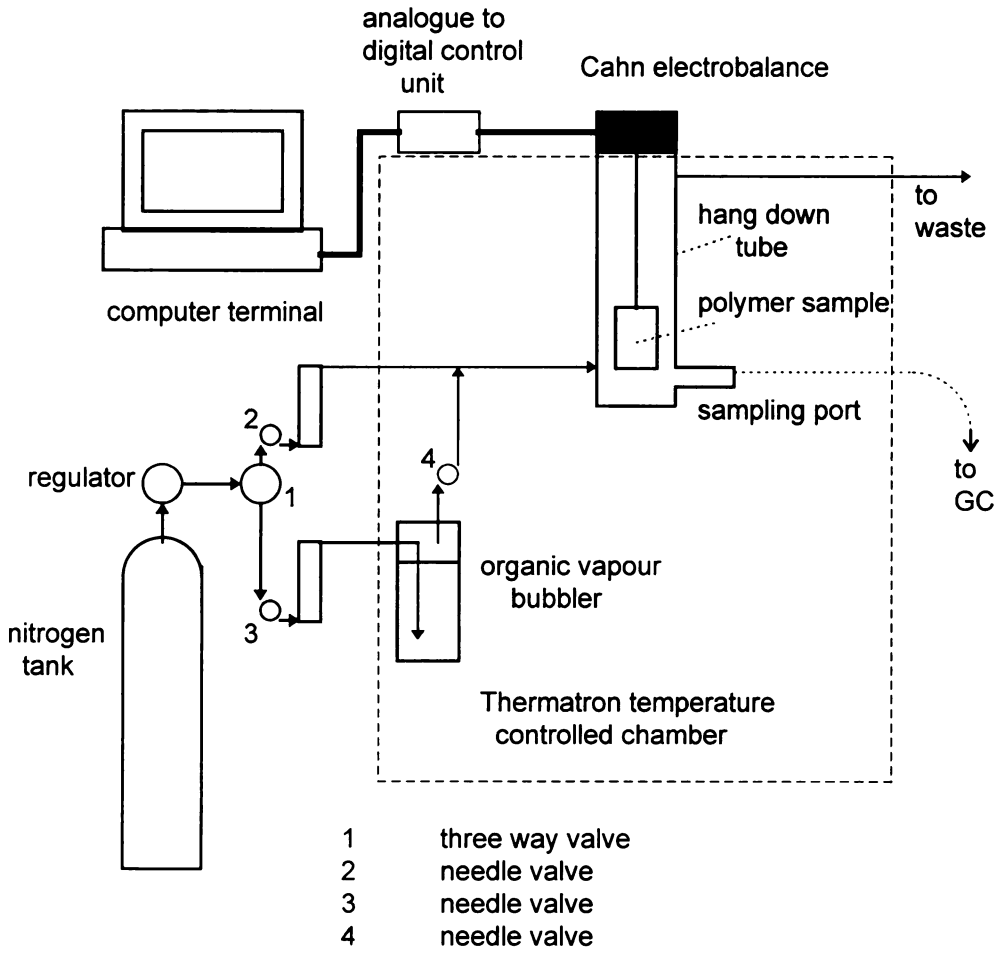

Figure 8. Schematic diagram of the Cahn electrobalance sorption apparatus

Gas Chromatographic Analysis

A Hewlett-Packard Model 5890A gas chromatograph equipped with flame ionization detector (FID) interfaced to a Hewlett-Packard Model 3392A integrator was employed for vapour pressure quantification. The gas chromatographic conditions are presented in Table 2. Standard curves of detector response versus quantity were constructed for ethyl acetate and d-limonene. Elution times for the organic vapours are shown in Table 2.

Vapour was injected into the chromatograph using a Gastight® #1750 syringe (Hamilton Co, Reno, NV). Liquid injections were made using a Microliter® #85 syringe (Hamilton Co, Reno, NV).

Conditions	Limonene	Ethyl acetate
Injection temperature (°C)	220	220
Detector temperature (°C)	250	250
Initial temperature (°C)	150	100
Final temperature (°C)	200	100
Heating rate ($°C\ min^{-1}$)	5.0	-
He carrier gas flow rate ($cc\ min^{-1}$)	7	7
Air flow rate ($cc\ min^{-1}$)	400	400
H gas flow rate ($cc\ min^{-1}$)	40	40
Elution time (min)	7.3	7.053
Column	Supelcowax™ 10 Fused silica capillary 30 m, 0.32 mm ID 0.25 film thickness	Supelcowax™ 10 Fused silica capillary 30 m, 0.32 mm ID 0.25 film thickness

Table 2. Setting conditions of gas chromatograph

Organic vapour permeability measurement

Organic vapour permeability coefficient (*P*), solubility coefficient (*S*) and diffusion coefficient (*D*) were determined for ethyl acetate in KR-10 on a MOCON Aromatran 1A Transmission Rate System (Modern Controls Inc., MN).

A film sample, prepared using a special die, was placed within the test cell. A 50cm^2 film surface separates an outer and inner cell which is clamped during testing to provide a gas tight seal. During individual zeroing (conditioning) carrier gas (dry nitrogen) flows through both cells to purge the film from organic compounds which may be present. During the testing cycle organic vapour flows through the outer cell at a pre-determined flow rate and carrier gas transports permeant vapour to an FID detector. A re-zeroing operation is conduced between testing to determine the zero baseline and provide a more accurate transmission rate result. The test cells are temperature controlled between 5 and 65°C. Film samples were tested at 25, 30 and 35°C. The test conditions are shown in Table 3.

Table 3. AROMATRAN 1A test conditions.

Test conditions	Ethyl acetate
Conditioning time (hour)	3
Test cycle duration (min)	10
Rezeroing cycle	3
Cell temperatures (°C)	25, 30, 35
Cell relative humidity (%)	0
Carrier gas flow rate(cc min^{-1})	15
Test gas flow rate (cc min^{-1})	15
Compressed air flow rate (cc min^{-1})	126
Hygrogen flow rate (cc min^{-1})	4
Film area (cm^2)	50
FID temperature (°C)	142
Sparging bath temperatures (°C)	0, 5, 10

Organic test vapour was generated by passing dry nitrogen carrier gas through a sparging system containing the organic liquid. The sparging system is placed in a temperature controlled bath containing 33% ethylene glycol and deionised water to enable temperatures down to -15°C to be reached. To avoid condensation of organic vapour in the supply pipelines, the vapour generation temperature was maintained at least 12°C below ambient.

It is necessary to calibrate the flame ionisation detector by exposing it to test vapour of known concentration. The calibration procedure is based on the two point method (Loebig, 1996). The relationship between the FID response and the organic vapour partial pressure is assumed to be linear between two points. If one point is assumed to be zero, then the second point is obtained experimentally by exposing the organic test vapour, of known partial pressure, directly to the FID. Calibration is complete when the FID output reaches a

constant value, thus providing a relationship between detector output and vapour partial pressure. This information is stored in the Aromatran calibration file and used in all subsequent permeability tests for that particular compound.

At a specific temperature the organic liquid generates a fixed and constant saturation pressure. As temperature increases saturation vapour pressure also increases. A table of saturation vapour pressures for d-limonene was used to obtain accurate values.

Water vapour permeability measurement

Water vapour permeability was determined from transmission rate values obtained from films tested on a MOCON Permatran-W 3/31 - Water Vapour Transmission Sysytem (Modern Controls, Inc. Mn, USA).

A film sample, prepared using a special die, was placed within the test cell. A 50cm^2 film surface separates an outer and inner cell which are clamped during testing to provide a gas tight seal. During the testing cycle water vapour flows through the outer cell at a pre-determined flow rate and nitrogen carrier gas transports water vapour to an infrared sensor which detects the amount of water vapour in the carrier stream. A re-zeroing operation is conduced at a predetermined interval between test runs to determine the zero baseline and provide a more accurate transmission rate result. The temperature controlled test cells can be operated between 5 and 65°C. Film samples were tested at 15, 25 and 35°C, at relative humidities of 40, 70, 90%. The test conditions are shown in Table 4.

Table 4. Test conditions for water vapour permeation determination by the MOCON PERMATRAN-W3/31.

Test parameters	Values
Conditioning time (min)	15
Test cycle duration (min)	5
Rezeroing cycle	3
Cell temperatures (°C)	15, 25, 35
Cell relative humidity (%)	40, 70, 90
Carrier gas flow rate(cm^3 min^{-1})	100

Oxygen permeability measurement

Oxygen permeability was determined from transmission rate values obtained by the Ox-tran Twin Oxygen Permeability Tester (Modern Controls Inc., Minneapolis, MN).

The diffusion cell has an effective surface area of 100cm^2, however due to the low gas barrier properties of the test film, samples were mounted onto a 5 cm^2 foil mask. In addition compressed air was used as the test gas in favour of oxygen to reduce the high oxygen flow which could damage the coulometric sensor. Transmission rate values were corrected to take these modifications into account.

The test film was clamped between the two halves of the test cell and outgassed with nitrogen/hygrogen mix. The sensor was inserted and a zero baseline established prior to the test. The test gas was introduced into the top half of the diffusion cell at the start of the test cycle and at two minute intervals

oxygen transmission rate is printed on a DL-200 data logger. The transmission rate is recorded in $cm^3m^2d^{-1}$. Films were tested at 30°C, 35°C and 42°C under dry conditions using compressed air as the test gas. The carrier gas is a mixture of hydrogen and nitrogen.

Carbon dioxide measurement

Carbon dioxide permeability was measured using a MOCON Permatran-CIV CO_2 Permeability Tester (Modern Controls Inc., MN). Test film was clamped between the upper and lower halves of the diffusion cell and flushed with nitrogen gas to remove residual carbon dioxide. Gaseous carbon dioxide was introduced into the top cell and permeant transferred to a fixed wavelength infrared sensor by nitrogen carrier gas. The sensor monitors the increasing carbon dioxide concentration and generates an electronic signal which drives a chart recorder. The carbon dioxide transmission rate is derived from the slope of the trace. Water absorbs at a similar wavelength to carbon dioxide and if present will result in a large detector reponse, therefore the the instrument must be run under dry conditions.

The instrument was calibrated by injecting a known quantity (0.0213 ml) of carbon dioxide gas into the sensor and noting the voltage change produced.

KR-10 film samples showed high permeability to carbon dioxide therefore film samples were tested using the continuous flow method and masked using adhesive aluminium foil blanks which reduced the test area from 50 cm^2 to 5 cm^2.

The test conditions are shown in Table 5. The test film was compared to a reference film of known transmission rate.

Table 5. Permatran-CIV test conditions for KR-10 film.

Carbon dioxide flow rate (cc min^{-1})	80
carrier gas flow rate (cc min^{-1})	3000
Temperature of test (°C)	24± 2
Purge time (min)	5
Accumulation time (min)	0
Chart speed (cm h^{-1})	60

Infrared analysis

A Perkin Elmer Spectrum 1000 (FTIR spectrometer) was used to determine the major peak frequencies of absorbance of the test film. The sample was scanned from a frequency of 4400 to 400 cm^{-1}. A table of major absobance peaks and their identification is attached in Appendix C.

Statistical analysis

All data was analysed by SPSS analysis of variance programme. Two way interaction, where appropriate, was examined by determining the common standard error for the mean (SEM), and the least significant difference (LSD). For 3 x 3 trials with three replicates, the least significant difference is found by:

$$LSD = t \times 2^{0.5} \times SEM$$

where t is the inverse of the student's t-test distribution and at the required probability and the necessary degrees of freedom. Treatment means were compared to the LSD and reported at the valid probability level (>5%, non-significant; 1 to 5%, significant; 0.1 to 1%, highly signficant; < 0.1% very highly significant.

Results and discussion

Solubility coefficient and diffusion coefficient values determined by the Cahn electrobalance gravimetric technique.

The equilibrium solubility is the ratio of the weight of permeant retained in a polymer sample at steady state, to the initial sample weight at the particular vapour pressure studied (expressed in kg per kg). The weight increase of polymer sample due to sorbed organic vapour was constantly monitored by the recording electrobalance. Sorption experiments were conducted at 25, 35 and 42°C, at vapour activities of 0.1, 0.2 and 0.3 for d-limonene and at 0.05, 0.1 and 0.2 for ethyl acetate. Each treatment was carried out in triplicate with film sample weights of between 45 to 55 mg. At this weight range the electrobalance has a sensitivity of 0.05μg.

Sorption curves for d-limonene and ethyl acetate in KR-10 film are attached in Appendix A. The sorption curves are plotted as M_t versus time, where M_t is the weight gain at time t. Superimposed on the experimental sorption curve is the theoretical curve calculated from Equation (17), using the best estimate diffusion coefficient (D_{cal}). Experimental curves generally fit the theoretical model and therefore it can be assumed that the diffusion process is Fickian. Half time steady state ($t_{0.5}$) was achieved within approximately 1,200

seconds (20 minutes) for ethyl acetate and within approximately 10,000 seconds (170 minutes) for d-limonene. As temperature increased and vapour activity decreased, an equilibrium state was reached more rapidly, therefore $t_{0.5}$ values decreased. For ethyl acetate at the lowest vapour activity/ highest temperature (Av, 0.05; temp., 42°C) combination, $t_{0.5}$ was approximately 400 seconds (7 minutes). For d-limonene, $t_{0.5}$ was approximately 1,200 seconds (20 minutes) at the lowest vapour activity/highest temperature combination (Av, 0.1; temp. 42°C). Ethyl acetate consistently showed lower $t_{0.5}$ values, compared with d-limonene under the same conditions of vapour activity and temperature and therefore had higher diffusion coefficients by approximately one order of magnitude.

Equilibrium solubility of d-limonene in KR-10 film

The equilibrium solubility values for d-limonene in KR-10 film as a function of vapour activity are shown in Table 6 and represented graphically in Figure 9. Values ranged from 0.019 to 0.150 kg kg^{-1} Pa^{-1}. From Table 6, it can be seen that there is a general trend for equilibrium solubility to increase as vapour activity increases and decrease as temperature increases.

Table 6. Equilibrium solubility of d-limonene (expressed as kg per kg) with standard deviation values in parenthesis and percent standard error (%SE).*

Vapour activity	Temperature (°C)					
	25	%SE	35	%SE	42	%SE
0.1	0.035± (0.002)	6	0.019± (0.002)	10	0.026± (0.003)	12
0.2	0.051± (0.004)	8	0.050± (0.003)	6	0.045± (0.006)	13
0.3	0.150± (0.025)	17	0.067± (0.018)	27	0.074± (0.015)	20

* Average values of triplicate runs.

Equilibrium solubility values for d-limonene are plotted as a function of vapour activity in Figure 9, and as can be seen, the data can be fitted by a linear model. The equilibrium solubility increases linearly with vapour activity, which suggests that the sorption process follows Henry's law over the activity range studied.

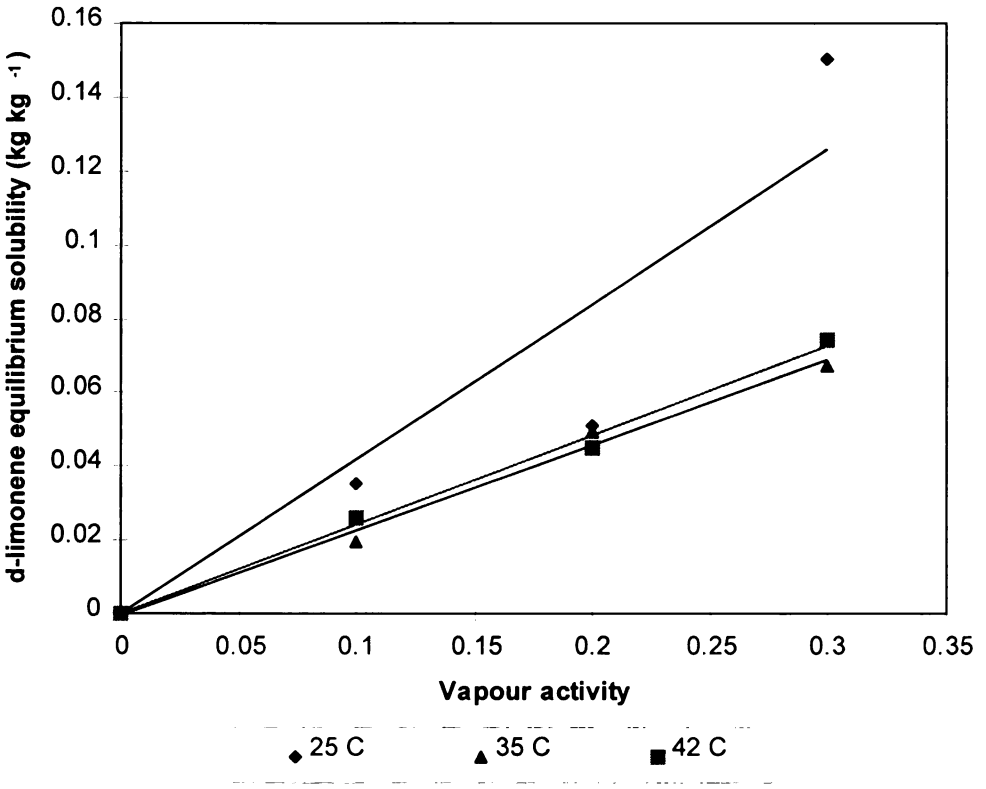

Figure 9. Equilibrium solubility of d-limonene in KR-10 film as a function of vapour activity at temperatures of 25°, 35° and 42°C.

Equilibrium solubility values for d-limonene are similar at temperatures of 35 and 42°C across the vapour activity range studied. At 25°C and vapour activity of 0.3, the equilibrium solubility value is solubility is almost twice the corresponding values for those at temperatures of 35 and 42°C. It is possible that permeant/polymer interactions are occuring at this temperature/vapour activity combination, resulting in significantly higher levels of d-limonene sorption. This behaviour would not be expected at low vapour activity levels, such as those employed in this study.

Solubility coefficient values for d-limonene in KR-10 film

Solubility coefficients for d-limonene, calculated from the slope of the curves in Figure 9, are summarised in Table 7, and plotted as a function of vapour activity at temperatures of 25, 35 and 42°C in Figure 10.

Table 7. Solubility coefficient values for d-limonene determined by the gravimetric method as a function of temperature.

Temperature (°C)	Solubility coefficient x10^4 (kg kg^{-1} Pa^{-1})
25	15.1
35	4.6
42	3.3

* average of triplicate runs.

Effect of temperature on the solubility coefficient of d-limonene in KR-10 film.

Temperature has a significant effect on the solubility coefficient of d-limonene vapour in KR-10 film. The solubility coefficient decreased as temperature increased within the temperature range studied. D-limonene is an organic compound with a negative heat of solution and therefore, according to the Arrhenius-type of relationship (Equation 12), the solubility coefficient will decrease with increasing temperature. Figure 11, an Arrhenius plot of the solubility coefficient againt the reciprocal of the absolute temperature for d-limonene, illustrates the linear temperature dependence of the d-limonene

solubility coefficient. The coefficient of simple determination (R^2), which describes the degree of linear relationship between the two variables has a value of 0.9641. The heat of solution, calculated from the slope of the line in Figure 11., has a value of 71 kJ mol^{-1} (17 kcal mol^{-1}).

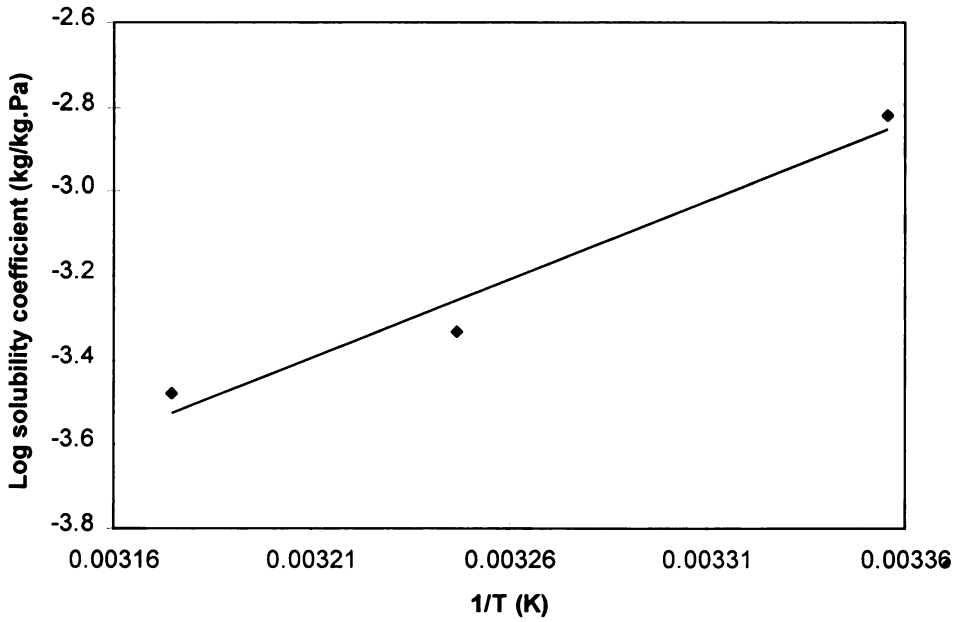

Figure 10. Temperature dependence of the solubility coefficient for d-limonene.

Diffusion coefficient values for d-limonene

The sorption diffusion coefficient (D_s) values for d-limonene in KR-10 film were determined from data obtained by the gravimetric procedure by using Equation (18) and setting $M_t/M_{ss} = 0.5$ to determine the half-time steady state sorption value ($t_{0.5}$). Sample thickness was assumed to be a uniform1.0 mil, the mean thickness of 200 random measurements from four randomly selected sheets. Theoretical sorption curves were obtained for each experimental run by using Equation (17) and superimposing this data on the experimental data. Sorption curves are attached in Appendix A. The sum of squares method was used to determine the best estimate for the diffusion coefficient (D_{cal}) for each experimental run. The sum of squares method selects the diffusion coefficient which gives the least differences between the experimental curve and the theoretical curve. Mathematically the method sums the squares of the differences between experimental and calculated sorption values at each point of the sorption curve. A plot of the corresponding sum of squares values versus diffusion coefficient can be used to determine the least sum of squares diffusion coefficient value. A sample plot for d-limonene is shown in figure 11. The best estimate diffusion coefficient value was used to obtain the theoretical sorption curve. The experimental and calculated diffusion coefficient values are shown in Table 8.

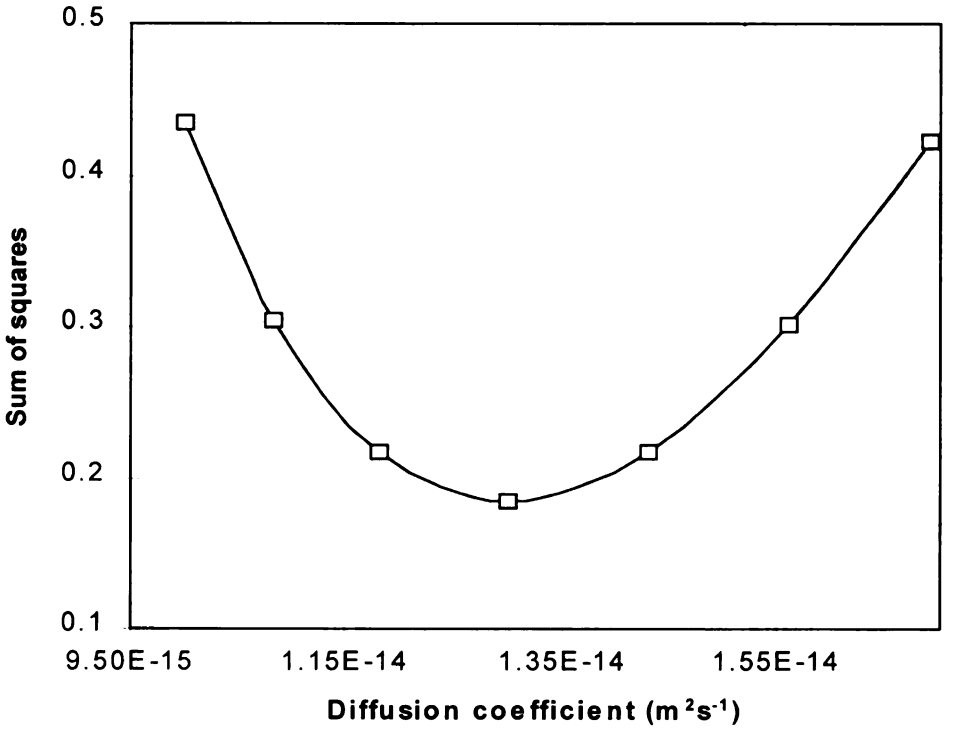

Figure 11. Sum of squares versus diffusion coefficient for for d-limonene in KR-10 film at Av = 0.1 and 42°C.

Table 8. Half-time (D_s) and calculated sorption diffusion coefficient (D_{cal}) values obtained by the gravimetric method for d-limonene.(*)

Temp. (°C)	Vapour activity	Diffusion coefficient x10^{15} (m^2sec^{-1})		
		D_{cal}	Std dev.	D_s
25	**0.1**	5.9	0.9	6.6
25	**0.2**	4.4	0.4	4.2
25	**0.3**	3.0	0.6	2.8
35	**0.1**	11.7	2.1	14.7
35	**0.2**	12.1	0.7	12.5
35	**0.3**	7.7	1.1	7.0
42	**0.1**	23.4	1.5	26.0
42	**0.2**	13.8	1.0	12.6
42	**0.3**	11.7	1.2	10.7

* average of triplicate runs.

Experimental diffusion coefficient values ranged determined by the gravimetric procedure ranged from 2.7 to 26.0 x10^{-15} m^2s^{-1}. The sum of squares best fit method had the effect of reducing the variability of the diffusion coefficients, resulting values ranging from 3.0 to 23.4 x10^{-15} m^2s^{-1}.

Neilsen and Giacin (1994) reported limonene diffusion coefficient values of between 1.9 - 3.7 x 10^{-15} m^2s^{-1} in orientated polypropylene film (OPP) at 22°C at vapour activities of 0.03 to 0.29. Theodorou and Paik (1991) reported a diffusion coefficient of 5.7 x 10^{-15} m^2s^{-1} in LDPE at 23°C. Franz (1993), reported values at 23°C of 2.1 to 570 x 10^{-16} m^2s^{-1} in BOPP, PP and HDPE , the latter film

giving the higher diffusion coefficient for limonene. These values are similar to the d-limonene diffusion coefficients found in the present study with KR-10 film.

Effect of vapour activity on the diffusion coefficient of d-limonene in KR-10 film

The diffusion coefficient values for d-limonene at 25, 35 and 42°C plotted as a function of vapour activity are shown in Figure 12. The diffusion coefficient appeared to decrease with increasing vapour activity over the range studied. This effect is opposite to the expected response when permeant molecules plasticise the polymer, lowering Tg and increasing the free volume of the polymer, facilitating permeant diffusion.

An 'antiplasticising' effect of the organic permeant on KR-10 film, where access through the polymer is reduced as vapour activity increases, would result in this type of behaviour. Alternatively, a 'clustering' effect of permeant molecules in the polymer matrix, (where molecules aggregate resulting in permeant immmobilisation), would result in a decreased diffusion coefficient.

Hernandez and Gavara (1994), describe the clustering effect of water molecules in nylon-6 above a water activity value of 0.5, at temperatures of 23 and 40°C.. An observed decrease in the diffusion coefficient of water is attributed to the formation of clusters, thought to be comprised of two to three molecules of water. Rogers and Machin, (1972) review the various modes of concentration dependent diffusion in polymers and the complex permeant/polymer interactions, including the effect of permeant clustering on the diffusion coefficient. Their

discussion is limited primarily to water, and to a lesser extent methanol, in hydrophobic polymers. Clustering occurs as a result of strong permeant-permeant hydrogen bonding compared to weak permeant-polymer interactions.

Clustering of d-limonene cannot be described by this mechanism, since it will not form hydrogen bonds. However there may be another type of mechanism which results in cluster formation of the molecules within the polymer matrix. The clusters, which would have a larger volume than single molecules, would have greater difficulty in diffusing through the polymer matrix and would therefore have lower diffusion coefficient values. However, with insufficient data in this study, the above theory is only speculation and therefore it is assumed that vapour activity has no effect on the d-limonene diffusion coefficient.

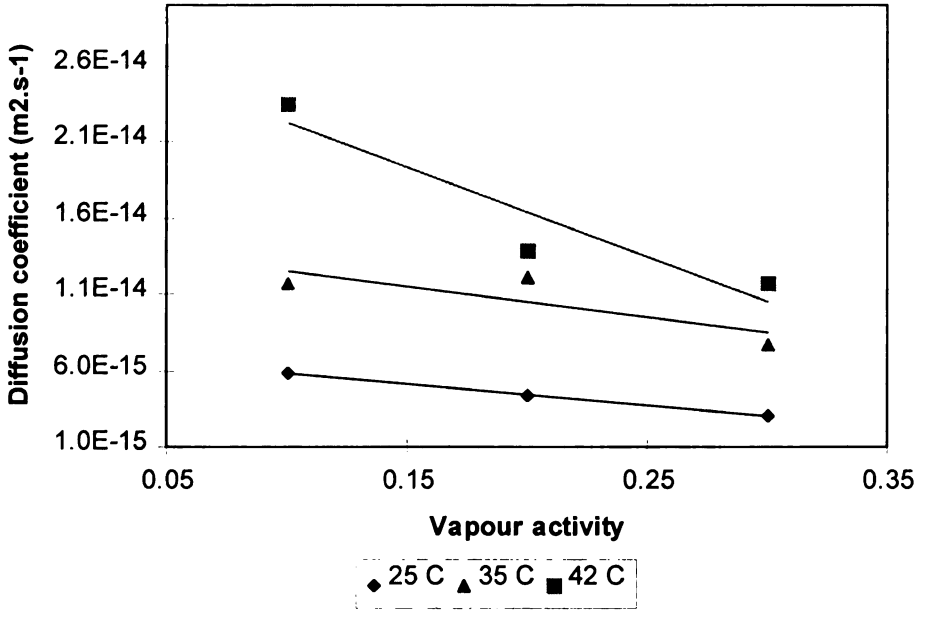

Figure 12. D-limonene diffusion coefficient as a function of vapour activity at temperatures of 25,35 and 42 C.

Temperature dependence of the diffusion coefficient for d-limonene

As temerature increased the diffusion coefficient increased at each of the three vapour activities studied. The total increase across the 17°C temperature range is approximately a factor of 4 (a general guide for the increase of the diffusion coefficient is a factor of 2 for each 10°C rise).

An Arrhenius plot of the diffusion coefficient of d-limonene through KR-10 film against the reciprocal of temperature (°K) is shown in Figure 13. The diffusion coefficient increases linearly as a function of temperature. Temperature was found statistically to have a very highly significant effect (0.1% level) on diffusion coefficient over the three vapour activity levels studied. Temperature provides the energy to increase the segmental mobility of the polymer chains, facilitating the passage of transient molecules through the polymer. The activation energy for diffusion (E_D) is a measure of the energy required to act against the cohesive forces of the polymer to form the holes of sufficient dimensions through which the permeant molecules can diffuse. The activation energy for diffusion is determined from the slope of the Arrhenius plot of the diffusion coefficient versus 1/T (°K).

The slope and R^2 values for each vapour activity plot in Figure 14 are:

vapour activity 0.1: $y = 3272.7x - 3.2658$; ($R^2 = 0.9855$)

0.2: $y = 2849.7x - 4.7569$; ($R^2 = 0.9127$)

0.3: $y = 3423.5x - 3.4235$; ($R^2 = 0.9896$)

The corresponding activation energies (E_D) for diffusion of d-limonene through KR-10 film are:

vapour activity 0.1: E_D = 63 kJ mol^{-1} (15 kcal mol^{-1})

0.2: E_D = 55 kJ mol^{-1} (13 kcal mol^{-1})

0.3: E_D = 63 kJ mol^{-1} (15 kcal mol^{-1})

The average activation energy for diffusion is 60 kJ mol^{-1} (14 kcal mol^{-1}).

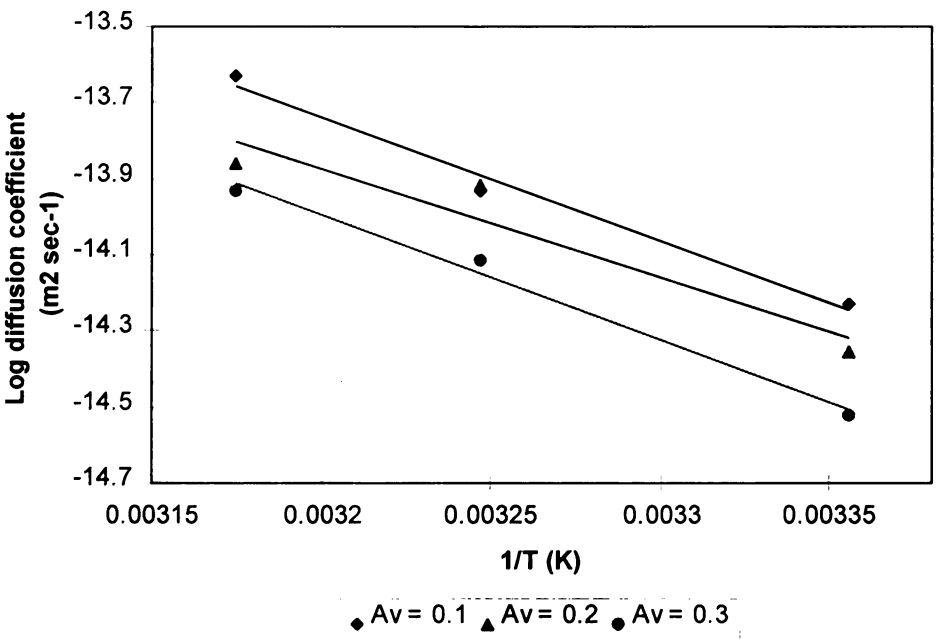

Figure 13. Temperature dependence of the diffusion coefficient for d-limonene in KR-10 film at vapour activities of 0.1, 0.2 and 0.3

Equilibrium solubility and solubility coefficient values of ethyl acetate in KR-10 film determined by the Cahn electrobalance gravimetric technique.

Equilibrium solubility was determined for ethyl acetate vapour in KR-10 film by the same procudure as for d-limonene. The equilibrium solubility values for ethyl acetate in KR-10 at vapour activities of 0.05, 0.1, 0.2 and at temperatures of 25, 35 and 42°C are shown in Table 9. Trial runs were conducted at a vapour activity of 0.3, however this resulted in swelling of the polymer. Experiments were therefore conducted at a lower vapour activity of 0.05. Each treatment was carried out in triplicate.

Solubility values ranged from 0.0096 to 0.0592 $kg.kg^{-1}$. Figure 14 shows a plot of equilibrium solubility against vapour activity at the three temperatures studied.

Table 9. Equilibrium solubility values ($kg\ kg^{-1}$) of ethyl acetate in KR-10 film at vapour activities of 0.05, 0.1 and 0.2 @ 25°, 35° and 42°C, with standard deviation values in parenthesis and percent standard error.

Vapour activity	Temperature (°C)								
	25		%SE	35		%SE	42		%SE
0.05	0.010	(0.002)	17	0.010	(0.001)	1	0.010	(0.001)	7
0.1	0.020	(0.001)	10	0.017	(0.006)	38	0.031	(0.003)	9
0.2	0.060	(0.025)	42	0.050	(0.006)	13	0.052	(0.008)	15

* Average values of triplicate runs.

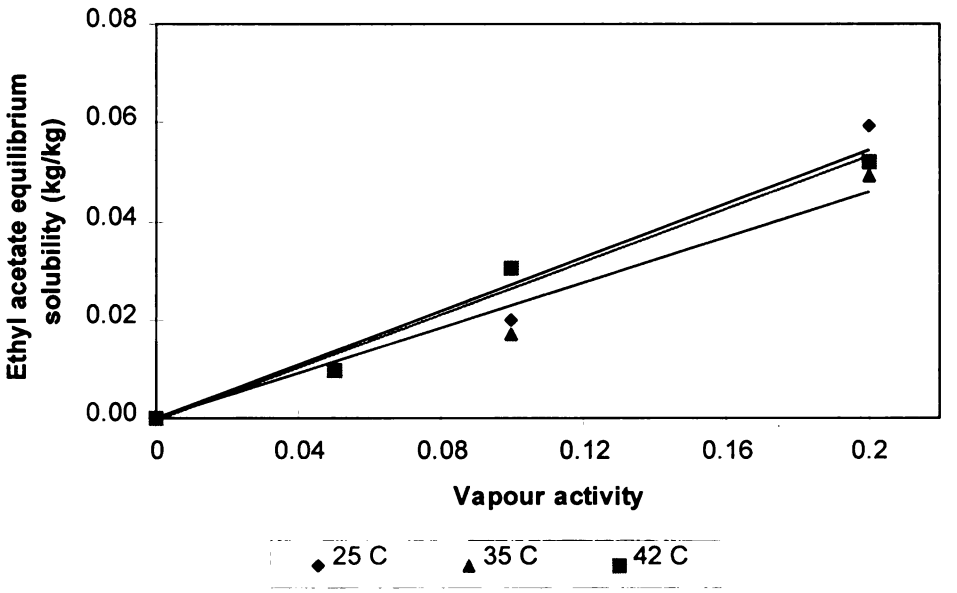

Figure 14. Equilibrium solubility of ethyl acetate in KR-10 film as a function of vapour activity @ 25°, 35° and 42°C.

Equilibrium solubility increased with increasing vapour activity in a linear relationship, suggesting Henry's law is obeyed over the concentration and temperature range studied, with sorption following ideal behaviour. The effect of vapour activity on equilibrium solubility is statistically very highly significant (0.1%) at all temperatures studied. The effect of temperature is not significant, except at a vapour activity of 0.1 which shows increasing equilibrium solubility values with increasing temperature.

The equilibrium solubility values of ethyl acetate and limonene are similar at equivalent vapour activities. The saturated vapour pressure of limonene is less than that for ethyl acetate at the same temperature. The higher boiling point (BP)of limonene (177°C) will contribute to a higher partition ratio between the

vapour phase and the polymer compared to ethyl acetate (BP 77°C). The solubility coefficient provides a better means of comparing solubility of different penetrants, since it takes into account the differing vapour pressures.

Solubility coefficient values for ethyl acetate in KR-10 film

Ethyl acetate solubility coefficent values are shown in Table 10 and plotted in Figure 16. Values ranged from 9.7 x10 $^{-6}$ kg kg^{-1} Pa^{-1} at 42°C to 21.6 x10 $^{-6}$ kg kg^{-1} Pa^{-1} at 25°C. Barr (1997), reported solubility coefficients for ethyl acetate in LDPE, LLDPE and ionomer film at 22°C of 2.3, 2.3 and 4.1 x 10^{-6} kg kg^{-1} Pa^{-1} at vapour activities of between 0.05 to 0.4. The higher solubility coefficient in KR-10 film found in the current study shows the greater affinity of ethyl acetate for this polymer. In contrast, Neilsen and Giacin (1994), reported considerably higher solubility coefficients for ethyl acetate in orientated polypropylene (OPP) at 22°C. Values ranged from 3.1 to 3.5 x10^{-3} kg m^3 Pa^{-1} at vapour activities of between 0.04 to 0.56, these values are approximately 100 times greater than those found for KR-10 and 1000 times greater than values reported for the PE films, indicating an extremely high solubility of ethyl acetate in OPP.

The effect of temperature was found to be statistically significant. Figure 15 shows the temperature dependence of the solubility coefficient which decreases with increasing temperature at the three vapour activities studied. The heat of solution (ΔH_s) for ethyl acetate, calculated from the slope of the

curve of the Arrhenius plot using Equation (12), is 38kJ.mol^{-1} (9 kcalmol^{-1}), this is approximately half the value calculated for d-limonene.

The heat of solution indicates the extent of solubility of a compound in a polymer, a higher ΔH_s value indicates that solubility is favoured. D-limonene has a higher ΔH_s value and, as expected, has a higher solubility coefficient compared to ethyl acetate. At low vapour concentrations, where interaction between permeant and polymer is negligible, the solubility coefficient is dependent mainly on the permeant boiling point, though a number of polymer/permeant factors including size and shape of the permeant molecule and its solubility parameter will impact to a lesser degree. The physio-chemical properties of the polymer including interchain bonding, polarity and percentage crystallinity also contribute to permeant solubility. As discussed above, the higher boiling point of d-limonene favours its solubility compared to ethyl acetate. The absence of a polar component makes it more compatable with styrene butadiene and will additionally contribute to its higher solubility coefficient.

Table 10. Solubility coefficient values for ethyl acetate determined by the gravimetric method as a function of temperature.

Temperature (°C)	**Solubility coefficient x 10^6 (kg.kg^{-1}Pa^{-1})**
25	21.6
35	11.4
42	9.7

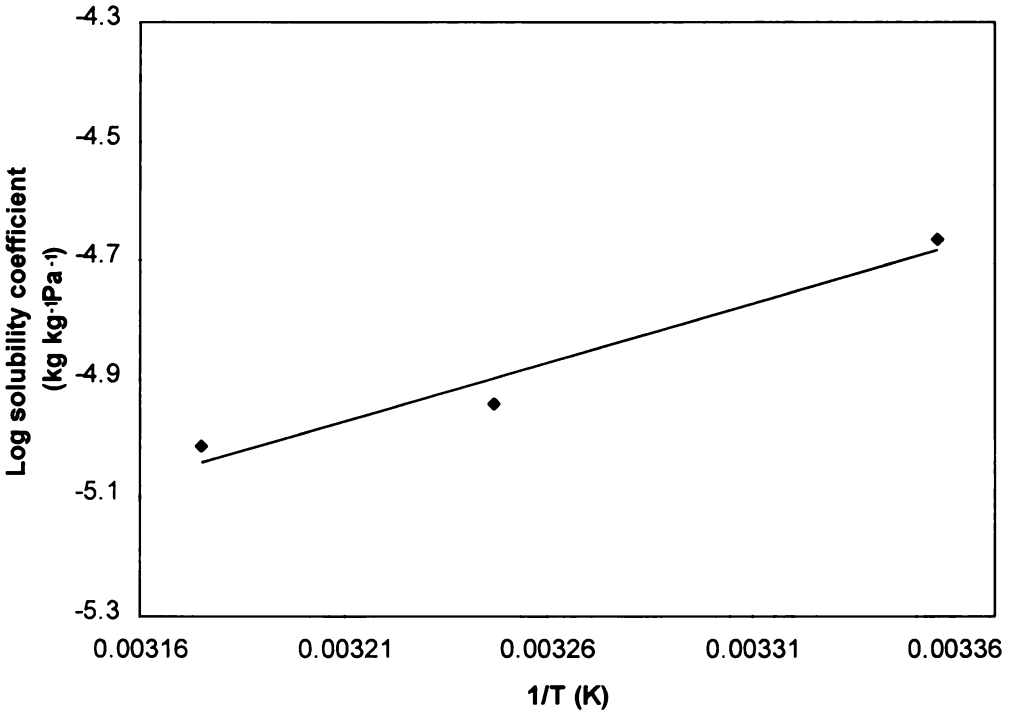

Figure 15. Temperature dependence of the solubility coefficient for ethyl acetate in KR-10 film.

Diffusion coefficient values for ethyl acetate in KR-10 film determined by the gravimetric procedure.

The diffusion coefficient for ethyl acetate was calculated from the half-time equilibrium sorption value using Equation (18). The least sum of squares method was used to determine the best estimate for ethyl acetate diffusion coefficients. A sample sum of squares plot is shown in Figure 16.

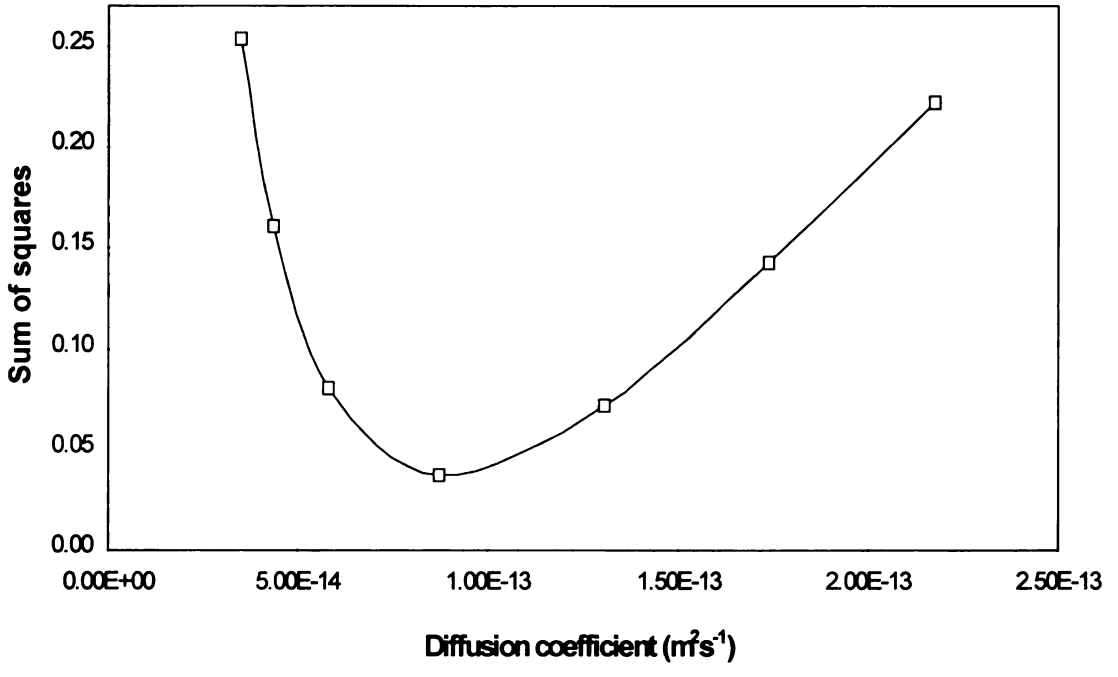

Figure 16. Determination of best fit diffusion coefficient for ethyl acetate in KR-10 film at Av = 0.1 and 42°C.

The half-time (D_s) and best estimate (D_{est}) diffusion coefficients determined at vapour activities of 0.05, 0.1 and 0.2 and at temperatures of 25, 35 and 42°C, are shown in Table 11. Best estimate diffusion coefficients ranged from 3.3 to 8.6 $x10^{-14}$ m^2 sec^{-1} at a vapour activity range of 0.05 to 0.2 and temperatures of 25 to 42°C. Neilsen and Giacin (1994), reported ethyl aceate

diffusion coefficient values of between 1.2 to 3.0 $x10^{-14}$ m^2 s^{-1} in OPP at 22 $\pm$ 1°C at vapour activities of between 0.04 to 0.56. The higher diffusion coefficient in KR-10 film suggests faster permeant transport through this polymer compared to OPP. One contributing factor is the presence of crystalline regions in OPP which inhibits the diffusion of permeants and therefore reduces their diffusion rate through the polymer matrix.

Table 11. Half-time (D_s) and estimated sorption diffusion coefficient (D_{cal}) values obtained by the gravimetric method for ethyl acetate in KR-10.(*)

Temp. (°C)	Vapour activity	Diffusion coefficient $x10^{14}$ (m^2sec^{-1})		
		D_{cal}	Std dev.	D_s
25	**0.05**	5.6	0.08	5.6
25	**0.1**	4.3	0.17	4.9
25	**0.2**	3.3	0.84	3.3
35	**0.05**	7.7	0.36	7.7
35	**0.1**	5.6	1.10	6.6
35	**0.2**	4.9	0.52	4.8
42	**0.05**	8.6	0.30	8.3
42	**0.1**	8.2	0.58	8.1
42	**0.2**	6.3	0.50	6.1

* average of triplicate runs.

Effect of vapour activity on the diffusion coefficient of ethyl acetate in KR-10 film.

The diffusion coefficient values for ethyl acetate plotted as a function of vapour activity at temperatures of 25, 35 and 42°C are shown in Figure 17. The lines of best fit through the data at each temperature show a decreasing diffusion coefficient with increasing vapour activity, at all three temperatures studied and is statistically significant to at least the 5% level.

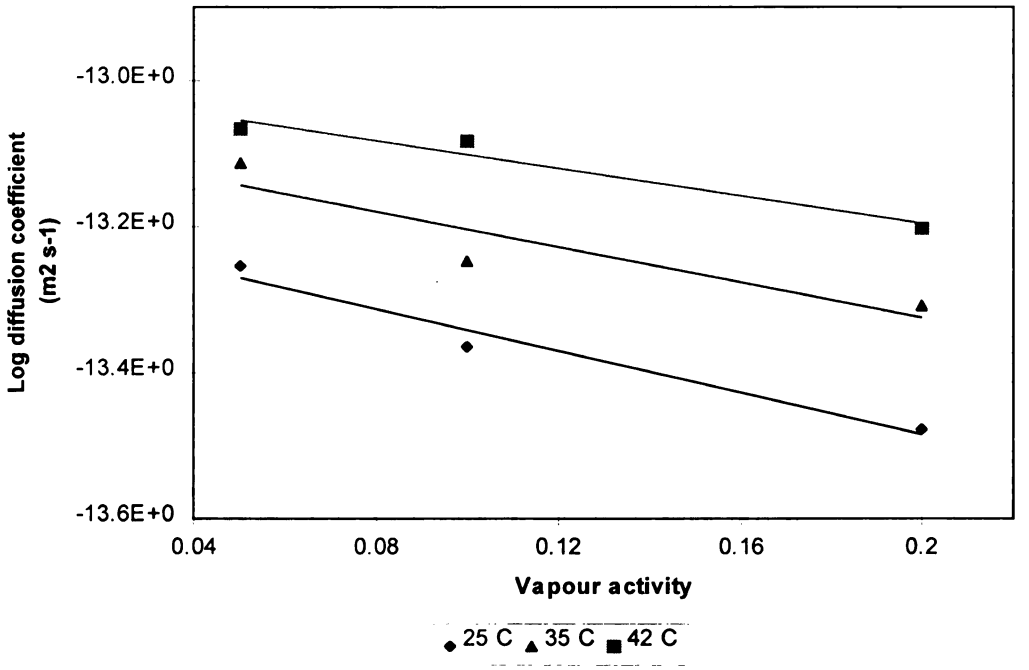

Figure 17. Ethyl acetate diffusion coefficient as a function of vapour activity in KR-10 film at temperatures of 25, 35 and 42°C.

Effect of temperature on the diffusion coefficient of ethyl acetate vapour in KR-10 film.

The effect of temperature on the ethyl acetate diffusion coefficient can be best illustrated by an Arrhenius plot of log diffusion coefficient versus the reciprocal of temperature (°K). The graph in Figure 18 shows the increase in diffusion coefficient with temperature at the three vapour activities studied.

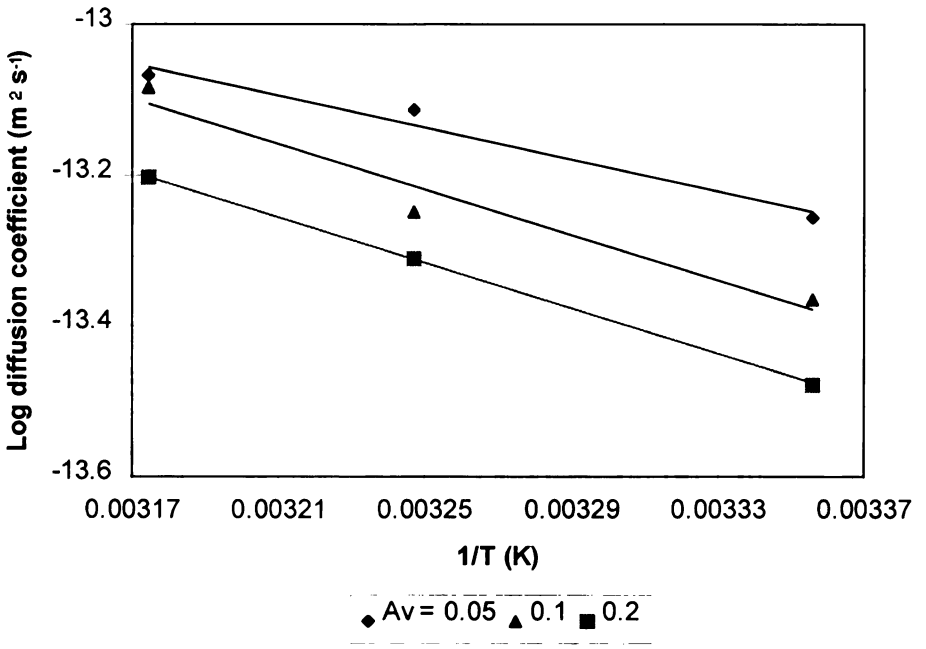

Figure 18. Temperature dependence of the diffusion coefficient for ethyl acetate in KR-10 film at vapour activities of 0.05, 0.1 and 0.2.

The activation energy values for diffusion (E_D) of ethyl acetate in KR-10 film were determined at the three vapour activities from the slope of the curves in the Arrhenius plot.

vapour activity = 0.05: $y = -1063.1x - 9.681$; ($R^2 = 0.9720$)

vapour activity = 0.1: $y = -1515.3X - 8.2942$; ($R^2 = 0.9546$)

vapour activity = 0.2: $y = -1519.3x - 8.3786$; ($R^2 = 0.9999$)

The corresponding activation energies for diffusion (E_D) are:

vapour activity = 0.05: 20 kJ mol^{-1} (4.8 kcal mol^{-1})

0.1: 29 kJ mol^{-1} (6.9 kcal mol^{-1})

0.2: 29 kJ mol^{-1} (6.9 kcal mol^{-1})

The average E_D for ethyl acetate in KR-10 film is 26 $\pm$ 5 kJ mol^{-1} (6.2 $\pm$ 1.2 kcal mol^{-1}). This is approximately half the activation energy value found for d-limonene (60 kJ mol^{-1}).

Ethyl acetate is a smaller molecule (molar volume: 97.8 cm^3 mol^{-1}) therefore the energy required to form holes of sufficient size to enable passage of the permeant molecules would be expected to be less than that for d-limonene. Ethyl acetate will diffuse through the polymer along its long axis and can therefore occupy voids of less diameter than d-limonene, which is a bulkier molecule (molar volume: 162.1 cm^3 mol^{-1}). The latter would require higher energy input to produce voids of sufficient size which will allow its passage through the polymer matrix and therefore will have a lower diffusion coefficient compared to ethyl acetate at the same temperature. Zobel (1985), measured the diffusion coefficient for a number of organic compounds in coextruded polypropylene. The reported diffusion coefficients for d-limonene and ethyl acetate are 0.65 and

15 x 10^{-15} m^2s^{-1} respectively. These results agree with the findings in the current study - with ethyl acetate having the higher diffusion rate through the polymer.

Berens and Hopfenberg, (1982) measured the diffusion coefficients for a number of organic vapours (C_1 to C_6) in polystyrene, at a range of temperatures by a gravimetric procedure using polymer spheres. Diffusion coefficients ranged from 6.3 x10^{-14} m^2s^{-1} (log -14.8 m^2s^{-1}) for ethanol to 1.6 x 10^{-18} m^2s^{-1} (log -17.8 m^2s^{-1}) for carbon tetrachloride. Activation energy for diffusion ranged from 39 kJ mol^{-1} (9.3 kcal.mol^{-1}) to 86 kJ mol^{-1} (20.7 kcal.mol^{-1}) and generally increased with increasing penetrant size. Although the authors did not include d-limonene or ethyl acetate in their studies, the diffusion coefficient values for d-limonene (3.0 to 23.4 x 10^{-15} m^2s^{-1}) partially fall (at the lower values) within the reported range for the organic compounds studied. The diffusion coefficient for ethyl acetate found in the current study (3.3 - 8.6 x10^{-14} m^2s^{-1}) is greater than the reported range. The activation energy for diffusion of ethyl acetate (26 kJ.mol^{-1}), is lower than the range of values reported by Berens and Hopfenberg. This would comply with the larger diffusion coefficient value. The activated energy of diffusion for d-limonene (60 kJ.mol^{-1}) falls within the reported range. The structure of styrene butadiene block copolymer may better facilitate diffusion compared to PS and therefore require lower energy input to open the structure, allowing passage of permeant molecules.

Water vapour permeability in KR-10 film

Water vapour transmission rate of KR-10 film was measured at 15, 25 and 35°C and at 40, 70 and 90% RH using a MOCON Permatran-W. Experiments were conducted in triplicate for each treatment. Permeability coefficients, calculated from the WVTR values, are shown in Table 12, with corresponding mean values and standard deviations for each treatment. Mean values obtained in this study ranged from 3.4 $kg.m.m^{-2}.s^{-1}$ Pa^{-1} $x10^{-15}$ at 15°C/40% RH to 4.5 at 35°C/90%RH. Phillips (1996) reported a WVTR value of 105g m^{-2} day^{-1} for 1 mil KR-10 film measured by ASTM-E96 (25$\pm$ 0.5°C and 95 $\pm$ 2% RH). The WVTR in the present study ranged from 8.1 to 77.4 g m^{-2} day^{-1}) for 1 mil KR-10 film. The experimental results are therefore close, if slightly less than, the reported value.

Robertson (1993), reports water vapour transmission rates for a number of polymers at 38°C and 95%RH. Transmission rate (thickness normalised) averages range from 0.12 g mm m^{-2} day^{-1} for polypropylene (PP) to 5.46 g mm m^{-2} day^{-1} for ethylene-vinyl alcohol copolymer (EVOH). In the present study, KR-10 at 35°C and 90% RH, has a value of 2.0 g mm m^{-2} day^{-1} and is comparable to Robertson's reported value of 3.4 g mm m^{-2} day^{-1} for PS. The similar WVTR values of PS and KR-10 are expected since both have the same non-polar functional and side chain groups. Highly polar polymers are generally poor water barriers, which can be further reduced due to the plasticising effect of water, as in the case of certain moisture sensitive nylons. Non-polar hydocarbon polymers, such as polyethylene possess excellent water barrier properties.

Table 12. Water vapour permeability coefficient of KR-10 film measured by MOCON Permatran at 40, 70, 90% RH and 15, 25 and 35°C.

Temperature (°C)	Permeability coefficient ($kg.m.m^{-2}.s^{-1}\ Pa^{-1}\ x10^{15}$)		
	RH 40%	**RH 70%**	**RH 90%**
15	3.53	3.32	3.59
	3.41	3.69	3.70
	3.13	3.83	3.53
Average	**3.4**	**3.6**	**3.61**
Std. dev.	0.2	0.3	0.08
%SE	5.9	8.3	2.2
25	3.71	3.69	3.99
	3.79	3.80	3.90
	3.70	3.94	3.93
Average	**3.73**	**3.81**	**3.94**
Std. dev.	0.05	0.12	0.04
%SE	1.3	3.2	1.0
35	4.47	4.28	4.52
	4.40	4.60	4.52
	4.34	4.55	4.53
Average	**4.40**	**4.5**	**4.52**
Std. dev.	0.01	0.2	0.01
%SE	0.2	4.4	0.2

The effect of relative humidity on water vapour permeability coefficient

Water vapour permeability coefficient values plotted as a function of relative humidity and at temperatures of 15, 25 and 35°C are shown in Figure 19. Statistical analysis suggests that relative humidity has no significant effect on permeability coefficient over the RH range studied. Water vapour will not have a plasticising effect on the structure of styrene butadiene copolymer and therefore an increase in the permeability coefficient with increasing RH would not be expected. In comparison, moisture sensitive polymers such as ethylene vinyl alcohol will show an increasing permeability to moisture (and gases) with increasing relative humidity, due to hydrogen bond formation between water molecules and the polar groups on the polymer chains which disrupts interchain bonds.

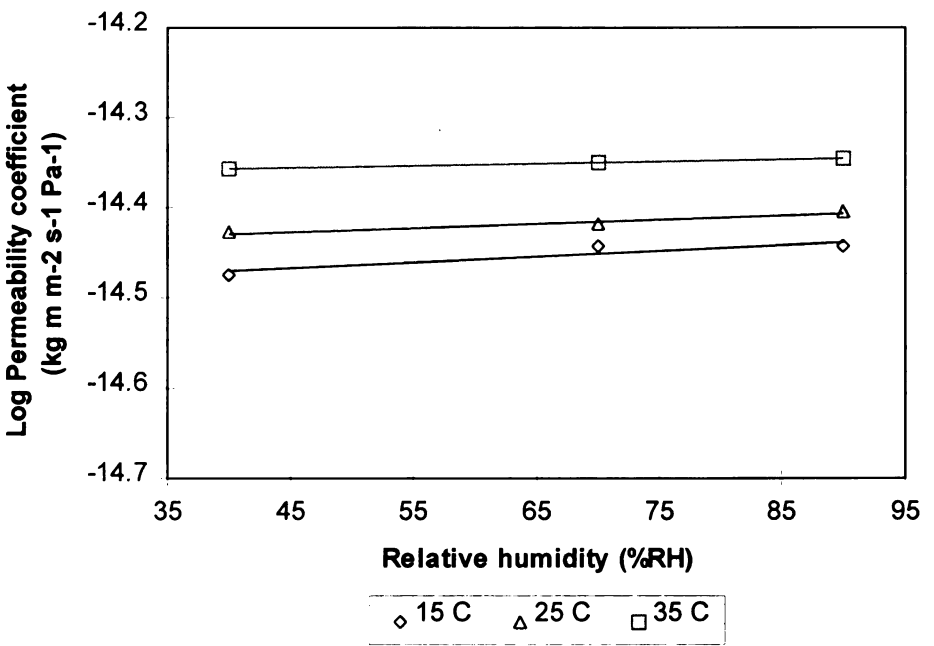

Figure 19. Water vapour permeability dependence of KR-10 film on the relative humidity at temperatures of 15, 25 and 35°C.

Temperature dependence of the water vapour permeability coefficient

Permeability coefficient increases with temperature at all three relative humidities studied. Figures 20 to 22 show the Arrhenius plots of log permeability coefficient as a function of the reciprocal of temperature (°K) at 40, 70 and 90%RH respectively.

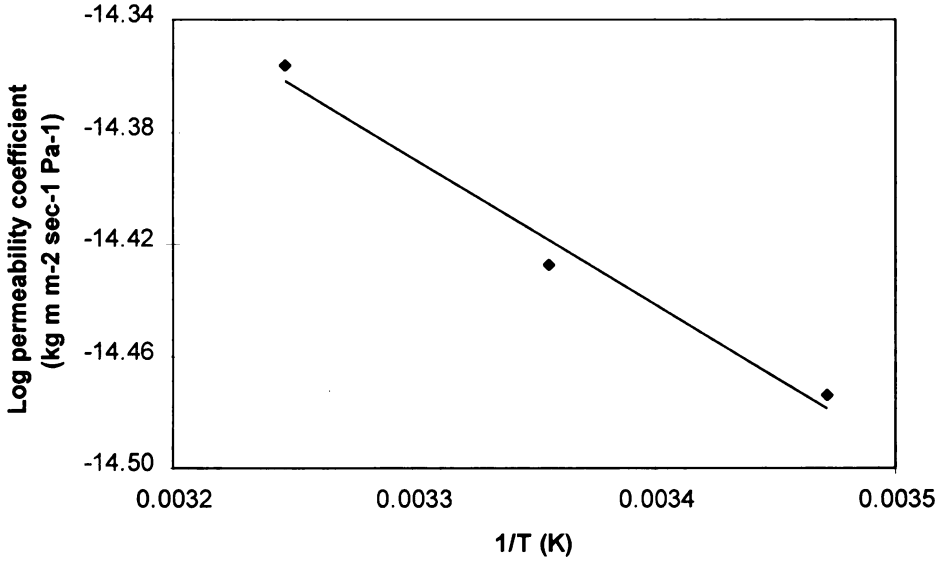

Figure 20. Temperature dependence of water vapour permeability coefficient at 40% RH in KR-10 film.

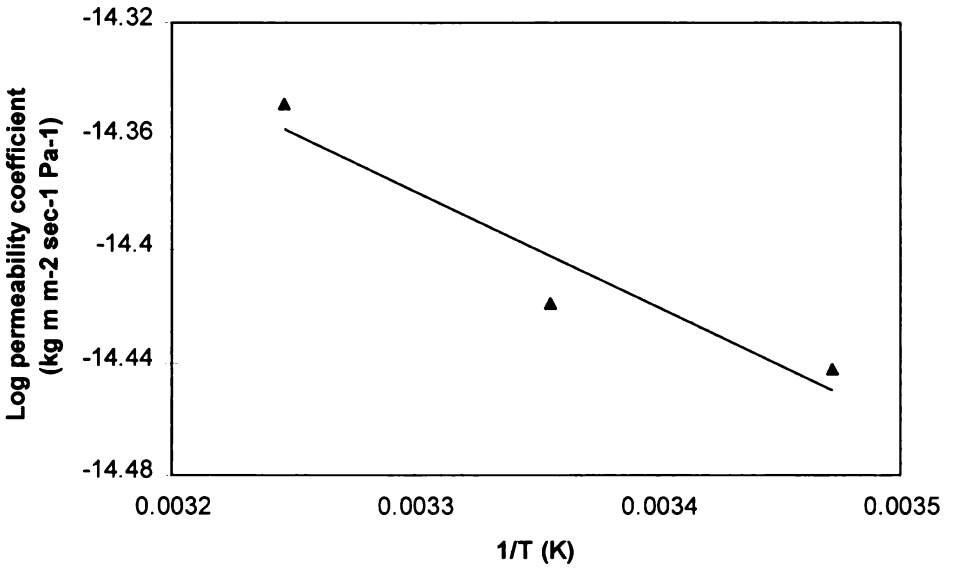

Figure 21. Temperature dependence of water vapour permeability coefficient at 70% RH in KR-10 film.

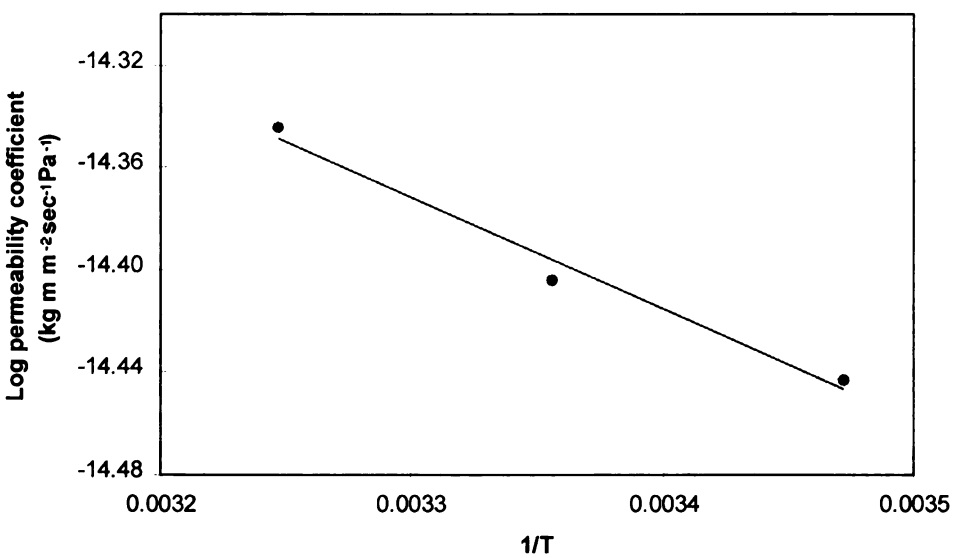

Figure 22. Temperature dependence of water vapour permeability coefficient at 90% RH in KR-10 film.

The activation energy for water vapour permeability at 40, 70 and 90%RH can be determined from the slope of the permeability coefficient versus 1/T graphs. The equations and associated R^2 values for the Arrhenius plots are as follows:

RH = 40%: $y = -519.51x - 12.675$; ($R^2 = 0.9800$)

RH = 70%: $y = -411.20x - 13.022$; ($R^2 = 0.9128$)

RH = 90%: $y = -434.58x - 12.938$; ($R^2 = 0.9798$)

the corresponding activation energies for permeation at the three relative humidities are:

RH = 40%: 9.9 kJ mol^{-1} (2.4 kcal mol^{-1})

RH = 70%: 7.9 kJ mol^{-1} (1.9 kcal mol^{-1})

RH = 90%: 8.3 kJ mol^{-1} (2.0 kcal mol^{-1})

which give a mean activation energy for water permeation through KR-10 film of 8.7 ± 1.1 kJ mol^{-1} (2.1 ± 0.26 kcal mol^{-1}).

For comparative purposes, Table 13 gives water vapour permeability coefficients of KR-10 and other polymers at 25°C and 90%RH. From these values, KR-10 shows a relatively high permeability coefficient, compared to the hydrocarbon polymers. The polybutadiene content of KR-10 appears to offer some degree of water vapour barrier, since the value for PS is over 100 percent larger. Notably nylon-6, at this high relative humidity, is becoming plasticised and its permeability to water vapour is therefore relatively high.

Table 13. Water vapour permeability for KR-10 and other polymers (from Robertson, 1993).

Polymer	Permeability coefficient $x10^{16}$ ($kg.m.m^{-2}.s^{-1}\ Pa^{-1}$)
Polyvinylidene chloride	0.1
High density polyethylene	1.0
Polypropylene	5.1
Low density polyethylene	6.0
KR-10	39.4
Nylon-6	52.5
Polystyrene	90.0

Oxygen permeability coefficient and diffusion coefficient

Oxygen transmission rate studies were determined on a MOCON Ox-tran Twin at 30, 35 and 42°C with triplicate runs. Trial tests demonstrated a high oxygen transmission rate of KR-10, therefore compressed air (21% oxygen) was used in place of pure oxygen and the surface area of the film sample was reduced from 50 to 5 cm^2 using an aluminium foil mask. The modifications were taken into account when determining transmission rates. The Ox-tran Twin prints transmission rate values at two minute intervals on a data logger. This information was used to determine $t_{0.5}$ from which diffusion coefficients were calculated using Equation 24.

Oxygen transmission rate and permeability coefficient

The oxygen permeability coefficient values, determined from the transmission rate data, are shown in Table 14. Phillips (1996), report an oxygen transmission rate of 0.09 $cm^3\,m^{-2}\,s^{-1}$ (500 $cm^3.100in^{-2}\,day^{-1}$) for 1 mil KR-10 film at 23°C. The transmission rate determined in this study at 30°C for 1mil KR-10 film is 0.11 $cm^3\,m^{-2}\,s^{-1}$ (617 cm^3 mil.$100in^{-2}\,day^{-1}$), which although slightly higher than the reported value, would be expected of the higher test temperature. The transmission rate at 23°C was determined using the equation for the Arrhenius relationship from Figure 23. The permeability coefficient for KR-10 at 23°C is 2.2 $m^3\,m\,m^{-2}\,s^{-1}\,Pa^{-1}$ equivalent to a transmission rate of 0.089 $cm^3\,m^{-2}\,s^{-1}$, which is the same as the value reported by Phillips.

Table 14. Permeability coefficient values for oxygen in KR-10 film at 30, 35 and 42°C.

Run	Temperature (°C)	Transmission rate $x10^{-1}$ ($cm^3m^{-2}s^{-1}$)	Permeability coefficient x 10^{17} (m^3 m m^{-2} s^{-1} Pa^{-1})
1		1.142	2.8629
2	**30**	1.143	2.8643
3		1.149	2.8795
Mean		**1.144**	**2.8689**
Std dev		**0.004**	**0.0091**
%SE		**0.35**	**0.32**
1		1.390	3.4844
2	**35**	1.351	3.3877
3		1.347	3.3767
Mean		**1.363**	**3.4167**
Std dev		**0.024**	**0.0592**
%SE		**1.76**	**1.73**
1		1.751	4.3890
2	**42**	1.724	4.3213
3		1.703	4.2702
Mean		**1.726**	**4.3268**
Std dev		**0.024**	**0.0595**
%SE		**1.39**	**1.38**

Temperature has a highly significant effect on the oxygen permeability. P values range from 2.9 x 10^{-17} m^3 m m^{-2} s^{-1} Pa^{-1} at 30°C to 4.3 x 10^{-17} m^3 m m^{-2} s^{-1} Pa^{-1} at 42°C. The present study found that the oxygen diffusion coefficient increased with temperature and the solubility coefficient, though not measured, can be assumed to increase with temperature (as ideal gases, unlike organic vapours, have a positive heat of solution and their solubility increases

Figure 23. shows the temperature dependence of the permeability coefficient. The activation energy for oxygen permeability in KR-10 film, calculated from the slope of the Arrhenius plot, is 27.1 kJ mol^{-1}.

The structure of styrene butadiene would suggest it to offer a relatively high permeability to oxygen, accounting for the requirement to use compressed air as the test gas (rather than oxygen) and to mask the sample film, to avoid exposing the coulometric sensor to excessive levels of oxygen which could result in sensor damage.

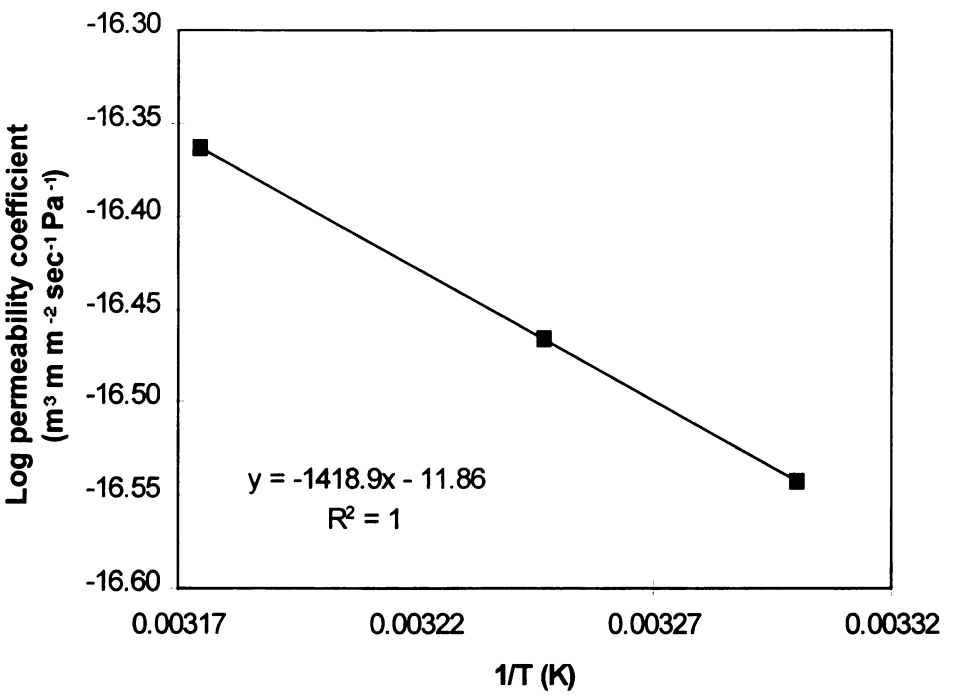

Figure 23. Temperature dependence of the oxygen permeability coefficient for KR-10 film.

Oxygen diffusion

The diffusion coefficient was determined from the transmission rate data using the half-time method. An example of an oxygen transmission rate profile for 1.0 mil KR-10 film at 30°C is shown in Figure 24. Values for $t_{0.5}$ and corresponding diffusion coefficients are presented in table 15.

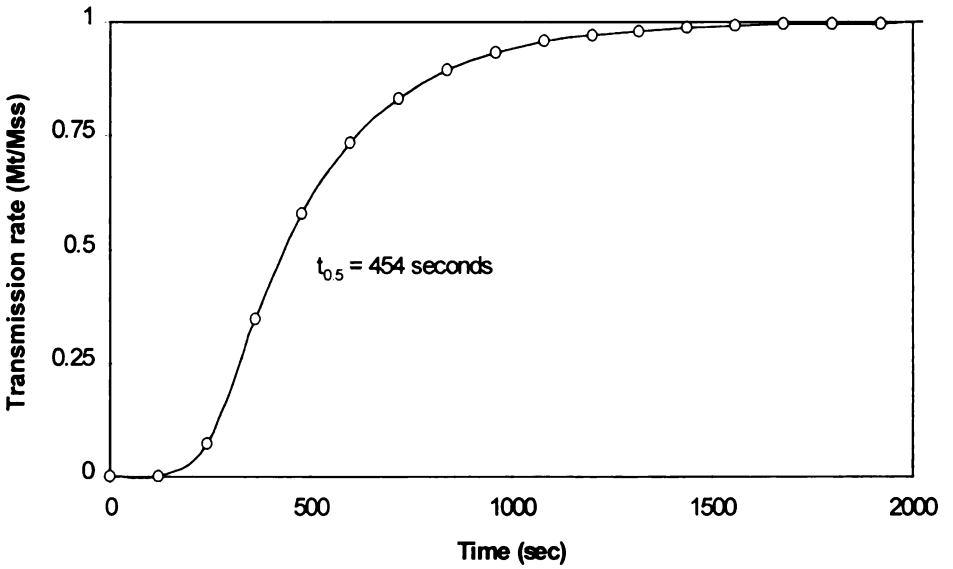

Figure 24. Oxygen transmission rate profile at 30°C, measured by the MOCON Ox-tran Twin.

Table 15. Diffusion coefficient values for oxygen at 30, 35 and 42°C, measured by the MOCON Ox-tran Twin.

Run	Temperature (°C)	$t_{0.5}$ (s)	Diffusion coefficient x 10^{13} (m^2s^{-1})
1		482	1.85
2	**30**	486	1.84
3		454	1.97
Mean		**474**	**1.89**
Std dev			**0.07**
%SE			**3.7**
1		486	1.84
2	**35**	468	1.92
3		400	2.22
Mean		**451**	**1.99**
Std dev			**0.20**
%SE			**10.0**
1		474	1.89
2	**42**	466	1.88
3		396	2.26
Mean		**445**	**2.01**
Std dev			**0.22**
%SE			**11.0**

Effect of temperature on the oxygen diffusion rate in KR-10 film

Increasing temperature resulted in a small decrease in $t_{0.5}$ values and a very small increase in oxygen diffusion coefficient values, from a mean value of 1.89×10^{-13} m^2 s^{-1} at 30°C, to a mean value of 2.01×10^{-13} m^2 s^{-1} at 42°C. Van Krevelen and Hoftyzer (1976), report an oxygen diffusion coefficient in

polystyrene at 298°K (25°C) of 1.1 x 10^{-11} m^2 s^{-1}. This value is considerably higher than that found in the present study for KR-10, possibly the effect of polybutadiene reduces the diffusion of oxygen through the polymer.

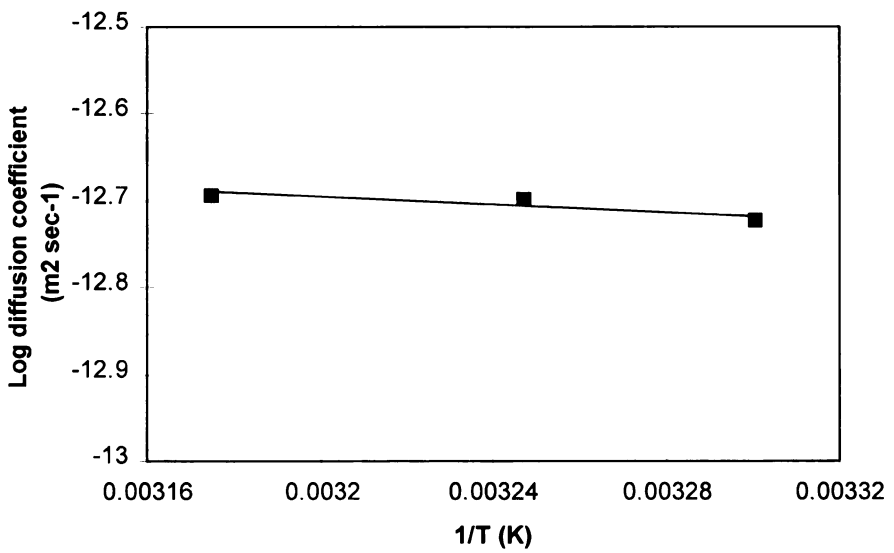

Figure 25. Temperature dependence of the oxygen diffusion coefficient for KR-10 film.

The activation energy (E_D) for oxygen diffusion through KR-10 film was calculated from the slope of the Arrhenius plot. The value for E_D is 4.3 kJ mol^{-1}. Together with the low PO_2,the low E_D value may suggest that styrene butadiene has a free volume value higher than, for instance, LDPE. This may result in the observation that increasing temperature, in the range studied, has not affected to a high degree, the diffusion of oxygen. Ethyl acetate and d-limonene have significantly larger E_D values of 26 kJ $mol^{-1}$and 60 kJ mol^{-1} respectively,

determined by the gravimetric procedure. The lower activation energy for oxygen diffusion is expected since oxygen has a lower molar volume, compared to d-limonene and ethyl acetate. Oxygen activation energy will be higher for more effective oxygen barriers. Weinkauf and Paul (1990), report an activation energy for oxygen diffusion in PET (amorphous volume fraction of 0.58) of 46.1 $kJ.mol^{-1}$ (11.0 $kcal.mol^{-1}$). This is considerably higher than the activation energy for oxygen diffusion in KR-10.

Carbon dioxide transmission rate and permeability in KR-10 film.

The carbon dioxide transmission rate was determined by the MOCON Permatran CIV at ambient temperature (26 $\pm$ 1°C) and 0% RH, using duplicate film samples by the continuous method of testing. The transmission rate was determined to be 1.1 $x10^{-6}$ m^3 m^{-2} s^{-1} (95,680 cm^3 m^{-2} day^{-1}), equivalent to a permeability coefficient of 2.8 $x10^{-16}$ m^3 m m^{-2} s^{-1} Pa^{-1}. Phillips (1996), reported a transmission rate of 2170 cm^3 $100in^{-2}$ day^{-1} (35,000 cm^3 m^{-2} day^{-1}). This is approximately 35% of the transmission rate value found in the present study.

The oxygen permeability coefficient in KR-10 film was 2.7 $x10^{-17}$ m^3 m m^{-2} s^{-1} Pa^{-1}. The carbon dioxide permeability coefficient is significantly larger, by a factor of approximately 10. This is slightly higher than the Pco_2/Po_2 ratio of 8 for polystyrene reported by Robertson (1993), and also calculated from data reported by Nielsen (1994). The larger P value for carbon dioxide is likely to be due to its greater solubility in the polymer, rather than a larger diffusivity. Carbon dioxide is a larger molecule than oxygen and therefore would be expected to have a lower diffusion coefficient. Table 16 compares the carbon dioxide permeability coefficient values for a range of polymers.

Table 16. Carbon dioxide permeability coefficient values for a range of polymers, measured at STP, with the exception of KR-10, measured at 26°C. (from Robertson, 1993).

Polymer	Permeability coefficient x10^{17} ($m^3.m.m^{-2}.s^{-1}$ Pa^{-1})	Pco_2/Po_2
Polyvinylidene chloride	0.02	5.5
Polyethylene terephthalate	0.1	7.0
Nylon-6	1.2	4.2
High density polyethylene	2.6	3.3
Polystyrene	6.6	8.0
Polypropylene	6.9	4.0
Low density polyethylene	26	6.4
KR-10	27	10

The styrene butadiene copolymer has a relatively high carbon dioxide permeability coefficient. This is approximately four times higher than the value reported for polystyrene and very similar to that reported for LDPE (Robertson, 1993). The transmission rate value reported by Phillips, (1996), when converted to a permeability coefficient (10 x10^{17} $m^3.m.m^{-2}.s^{-1}$ Pa^{-1}), compares favourably with the value reported by Robertson, (1993), and gives a Pco_2/Po_2 ratio of 3.7.

Polyvinylidene chloride, a polymer used in apllications where a high barrier is required, has a permeabililty coefficient three orders of magnitude lower than KR-10. The carbon dioxide barrier property of the latter combined with its high oxygen permeability would suggest that it may have potential for

use in CAP of respiring vegetable products. This application requires carbon dioxide removal from the pack and its replacement with oxygen, to maintain a controlled respiration rate and enhancement of product shelf life.

Determination of ethyl acetate solubility, diffusion and permeability coefficients by the MOCON Aromatran

For comparative purposes, the Aromatran 1A was used to determine the solubility, diffusion and permeability coefficients for ethyl acetate in KR-10 film at 25, 30 and 35°C and at vapour pressures of 24, 32 and 43 mmHg. The analysis was conducted in tripicate at each temperature/vapour pressure treatment, using fresh film samples for each test run. Upon completion of the test, the Aromatran reports a result for the solubility coefficient, the diffusion coefficient and the permeability coefficient. These are the data reported in this study.

Ethyl acetate solubility coefficient

Solubility coefficient values for ethyl acetate are shown in Table 17. and plotted as a function of vapour pressure in Figure 26. Values ranged from 2.80 to 9.00 x 10^{-5} $Kg.kg^{-1}$ Pa^{-1} and in some treatments the variance was high; standard deviations ranged from 0.5 to 6.8 x 10^{-5}. The solubility coefficients decreased with increasing temperature, which would be expected. The effect of vapour pressure did not appear to follow a particular trend and is statistically not significant. Therefore ethyl acetate solubility follows Henry's law at the range of vapour pressures studied.

Table 17. Solubility coefficient values for ethyl acetate in KR-10 film with standard deviation values in parenthesis.

	Solubility coefficient x 10^5 ($Kg.kg^{-1}$ Pa^{-1}) Vapour pressure (mmHg)		
Temperature (°C)	**24**	**32**	**43**
25	7.75 (2.6)	4.75 (0.6)	9.00 (6.8)
30	4.55 (1.7)	4.62 (0.6)	6.32 (2.9)
35	2.80 (0.5)	2.80 (1.82)	2.90 (1.5)

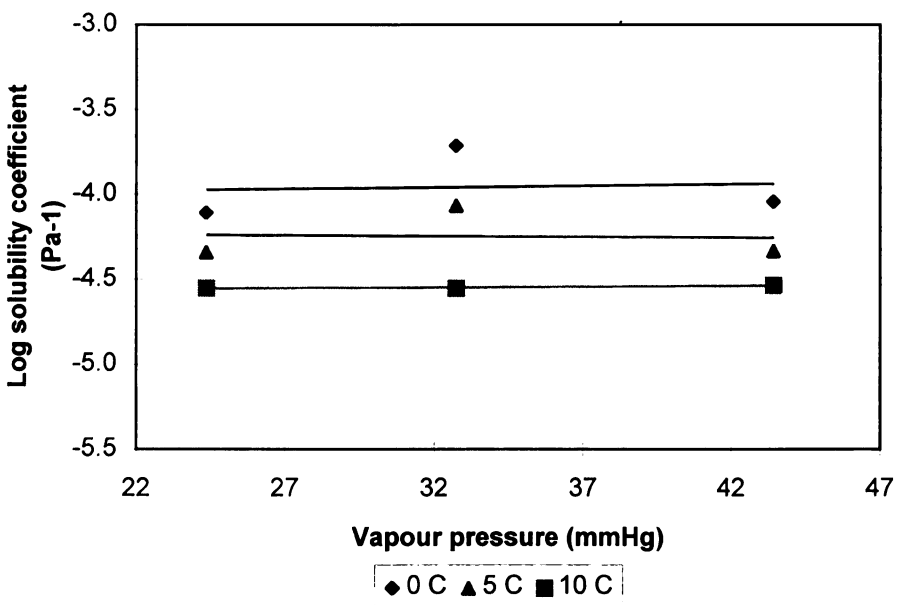

Figure 26. Ethyl acetate solubility coefficient as a function of vapour pressure at temperatures of 25, 30 and 35°C.

The solubility coefficient values determined by the Aromatran are higher than those determined by gravimetric analysis, by a factor of approximately four. Solubility coefficient values determined by gravimetry ranged from 0.7 to 2.3 x 10^{-5} kg kg^{-1} Pa^{-1}.

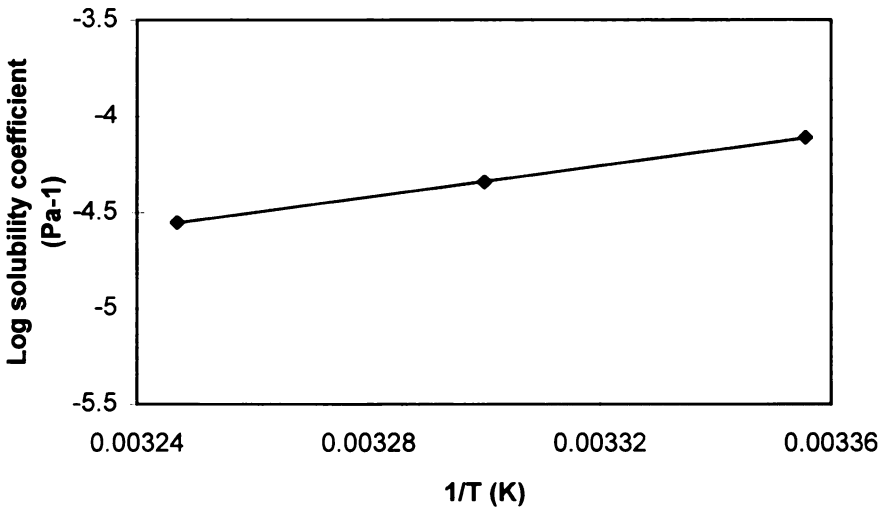

Figure 27. Temperature dependence of ethyl acetate solubility coefficient in KR-10 film at vapour pressure of 24 mm Hg.

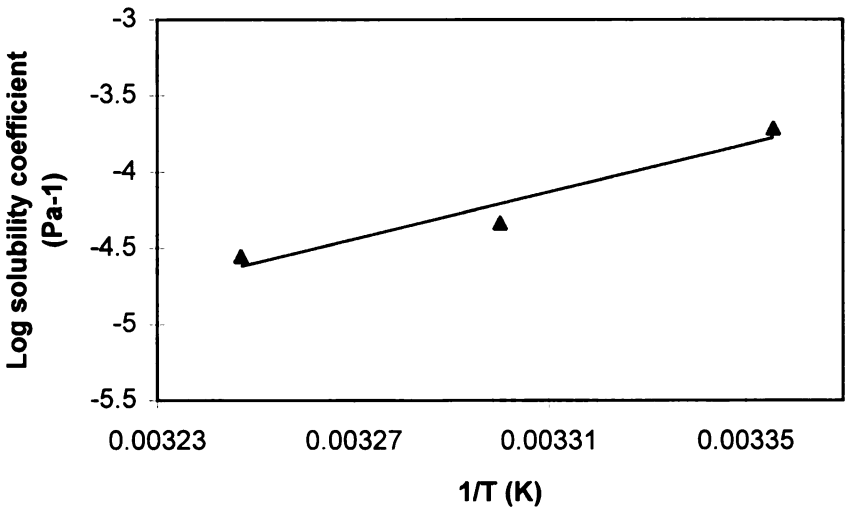

Figure 28. Temperature dependence of ethyl acetate solubility coefficient in KR-10 film at vapour pressure of 32 mm Hg.

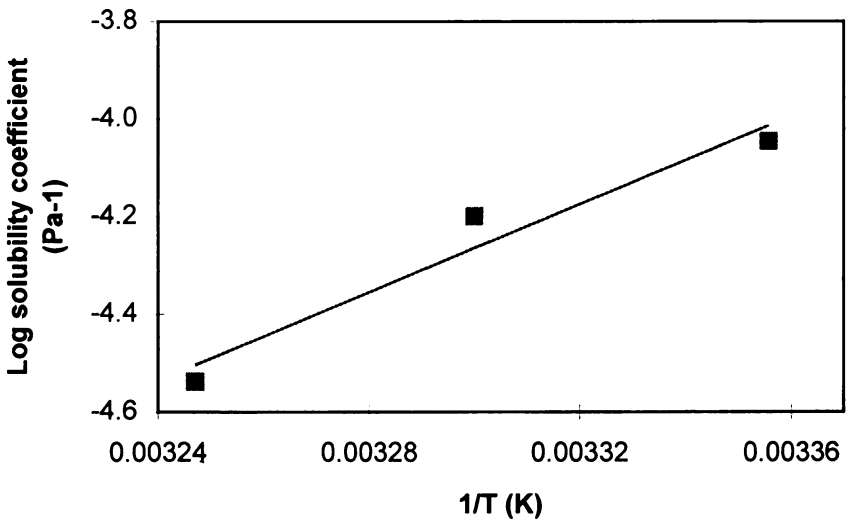

Figure 29. Temperature dependence of ethyl acetate solubility coefficient in KR-10 film at vapour pressure of 43 mm Hg.

The equations for the relationship between log solubility coefficient as a function of the reciprocal of temperature (°K) at each of the vapour pressures are as follows:

vapour pressure 24: $y = 4058.8x - 17.73$ $R^2 = 0.9997$

32: $y = 7714.8x - 29.67$ $R^2 = 0.9332$

43: $y = 4054.6x - 19.13$ $R^2 = 0.951$

the average heat of solution, calculated from each of the plots, is -101 kJ. mol^{-1} (24 $kcal.mol^{-1}$) This is greater than that determined by the gravimetric procedure, where the heat of solution was found to be -37.1 kJ mol^{-1} (24 kcal mol^{-1}). Although the Arrhenius plots of the average solubility coefficient values, determined by the Aromatran have good linear fits (R^2 values range from 0.9332 to 0.9997), there was high variability between the individual results for each treatment, which must lead to significant inaccuracies.

Ethyl acetate diffusion coefficient

The diffusion coefficient values for ethyl acetate are shown in Table 18. Values ranged from 8.6 to 42.9 x 10^{-14} m^2 s^{-1}. In comparison, the best estimate diffusion coefficients, determined by the gravimetric procedure at vapour activities of 0.05, 0.1 and 0.2 ranged from 3.3 to 8.6 x 10^{-14} m^2 s^{-1}, and were therefore lower by a factor of five.

Table 18. Diffusion coefficient values for ethyl acetate in KR-10 film determined by the MOCON Aromatran 1A.

	Diffusion coefficient x 10^{14} (m^2s^{-1}) **Vapour pressure (mmHg)**		
Temperature (°C)	**24**	**32**	**43**
25	8.6 (3.1)	9.3 (1.8)	9.7 (5.4)
30	14.9 (4.6)	11.5 (1.1)	13.3 (4.9)
35	23.1 (3.0)	14.5 (4.1)	26.4 (8.5)

The activation energy for diffusion of ethyl acetate in KR-10 was determined from the Arrhenius plot of diffusion coefficient against 1/T at a vapour pressure of 32 mmHg, as this gave the best linear fit. E_D was determined to be 34 kJ.mol^{-1}. This value was slightly higher, though compared favourably with the activation energy for diffusion for ethyl acetate obtained by the gravimetric method; 26.1 kJ.mol^{-1}.

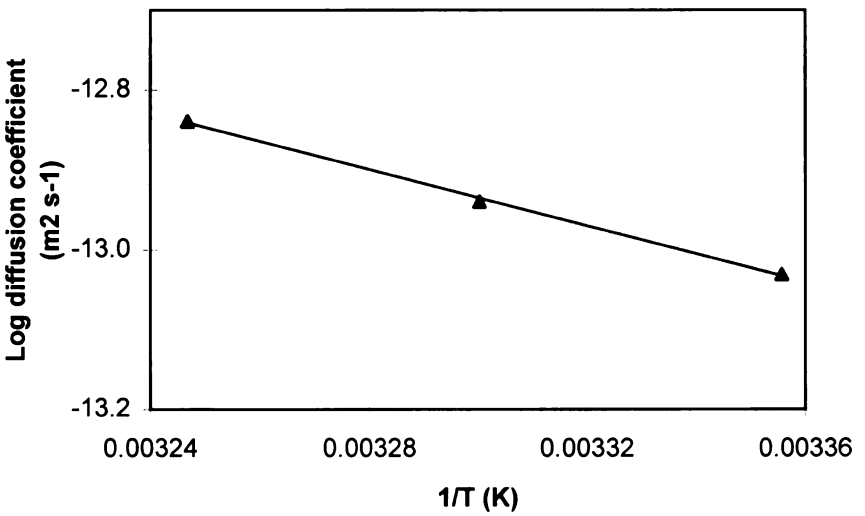

Figure 30. Temperature dependence of ethyl acetate diffusion coefficient in KR-10 film at vapour pressure of 32 mm Hg.

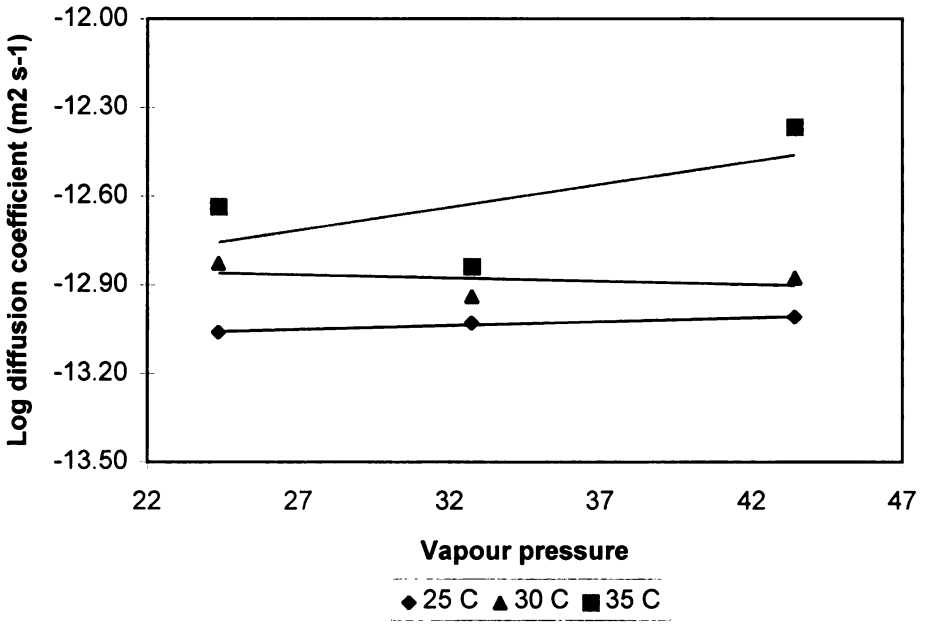

Figure 32. Ethyl acetate diffusion coefficient as a function of temperature at 25, 30 and 35°C.

Ethyl acetate permeability coefficient in KR-10 film

Permeability coefficient values are shown in Table 19. Values ranged from 6.29 to 7.46 $x10^{-16}$ m^3 m m^{-2} s^{-1} Pa^{-1}. Permeability coefficient as a function of vapour pressure is shown in Figure 32. The effect of vapour pressure on the permeability coefficient is not statistically significant, therefore permeability is constant over the ethyl acetate pressure studied.

Table 19. Permeability coefficient of ethyl acetate with standard deviation values in parenthesis.

	Permeability coefficient x 10^{16} (m^3 m m^{-2} s^{-1} Pa^{-1}) Vapour pressure		
Temperature (°C)	**24**	**32**	**43**
25	6.29 (0.8)	6.30 (1.0)	6.40 (0.5)
30	6.33 (0.1)	6.96 (0.2)	7.46 (0.1)
35	6.40 (0.3)	7.04 (0.1)	7.14 (0.6)

The Arrhenius plots of P as a function of 1/T are shown in figures 33 to 35. The effect of temperature on the permeability coefficient is variable and not statistically significant at the vapour activities studied.

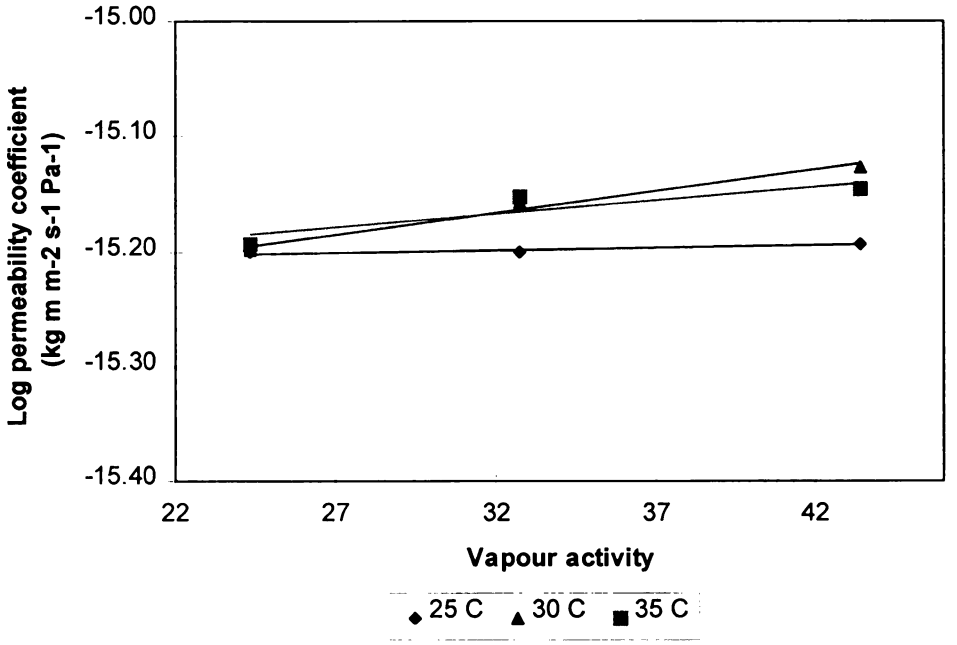

Figure 32. Ethyl acetate permeability coefficient as a function of vapour activity at 25, 30 and 35°C.

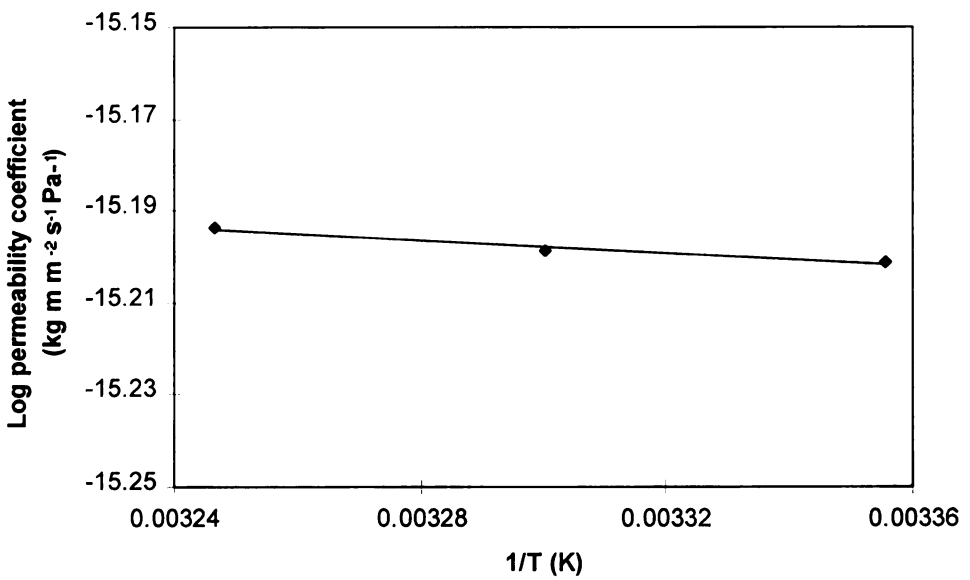

Figure 33. Temperature dependence of ethyl acetate permeability coefficient in KR-10 film at vapour pressure of 24mm Hg.

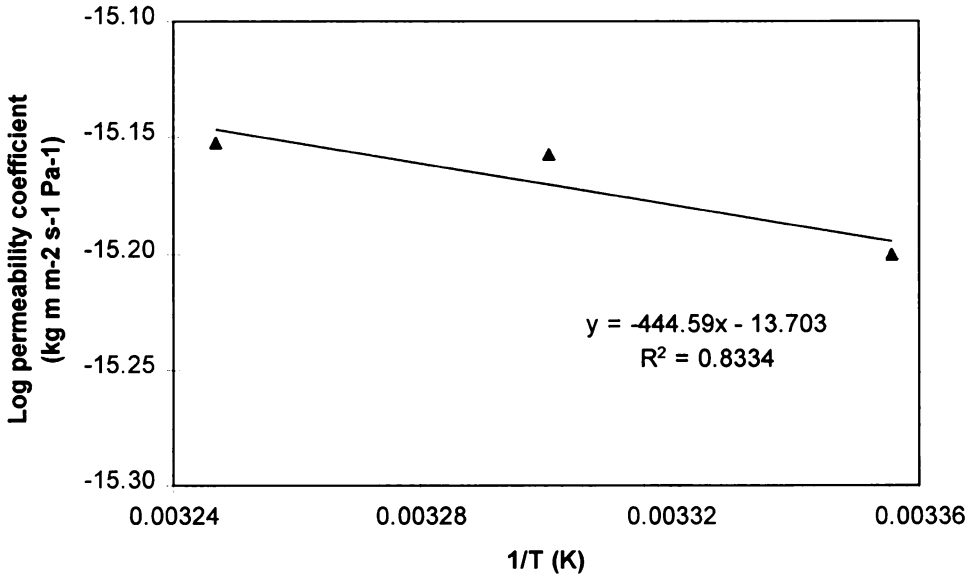

Figure 34. Temperature dependence of ethyl acetate permeability coefficient in KR-10 film at vapour pressure of 32mm Hg.

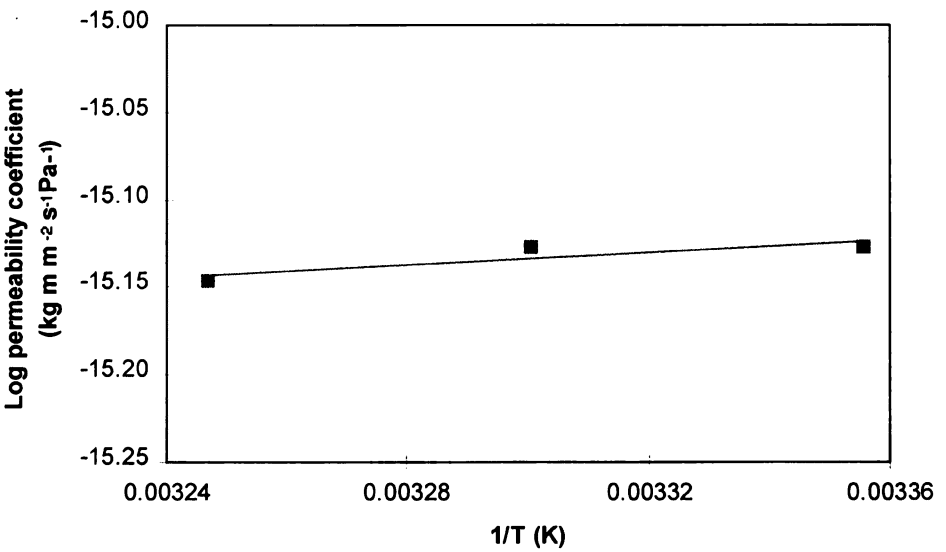

Figure 35. Temperature dependence of ethyl acetate permeability coefficient in KR-10 film at vapour pressure of 43mm Hg.

Conclusions

The results of this study showed temperature dependencies for solubility and diffusion coefficients of d-limonene and ethyl acetate through styrene butadiene copolymer (KR-10) film over the temperature range studied. The sorption of d-limonene and ethyl acetate followed Henry's law sorption and the solubility coefficient was independent of vapour activity over the range investigated. Diffusion coefficients of the organic vapours appeared to decrease with increasing vapour activity, but due to insufficient data, it was concluded that diffusion was independent of concentration. Experimental sorption curves for d-limonene and ethyl acetate were generally fitted well by the theoretical equation, though some curves showed deviation from this. However, experimental (D_s) and best estimated (D_{cal}) diffusion coefficients were similar.

Comparison of solubility and diffusion coefficients for ethyl acetate determined by the gravimetric and isostatic procedures, gave higher values by a factor of four for coefficients determined by the isostatic method. The latter also produced high variability of results within treatment runs.

The diffusion and permeability coefficients for oxygen showed temperature dependency, as did the water vapour permeability coefficient in

KR-10 film. Relative humidity had no effect on the water vapour permeability coefficient.

In terms of practical importance, the study provided a better understanding of the mass transport of d-limonene and ethyl acetate in styrene butadiene copolymer film, and the gas barrier properties of the polymer. The study also provided data for determining certain mass transfer properties for KR-10 film at lower temperatures, by extrapolation of the Arrhenius plots.

Appendix A

Procedure for constructing standard calibration curve

Standard curves of area response versus penetrant concentration were constructed for ethy acetate and d-limonene.

A series of four standard solutions were prepared for ethyl acetate dissolved in acrylonitrile. Aliquots of 1μl were injected into the GC and area response was recorded. This was conducted in triplicate for each standard solution of ethyl acetate. The calibration curve was constructed by plotting 'quantity injected' against the average 'area reponse'.

A calibration curve for d-limonene was constructed using d-limonene vapour standards. The samples were prepared by incubating d-limonene in sealed vials at known temperatures and allowing the liquid/vapour system to reach equilibrium. The saturated vapour pressure for d-limonene was used to determine quantity injected, and the calibration curve was constructed as above.

Calibration curves for d-limonene and ethyl acetate are shown in Figures 36 and 37 respectively.

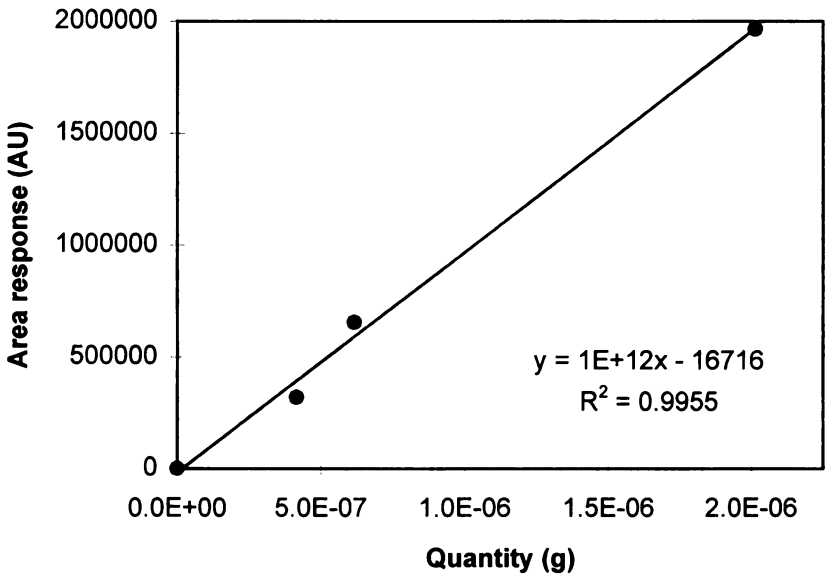

Figure 36. d-limonene calibration curve.

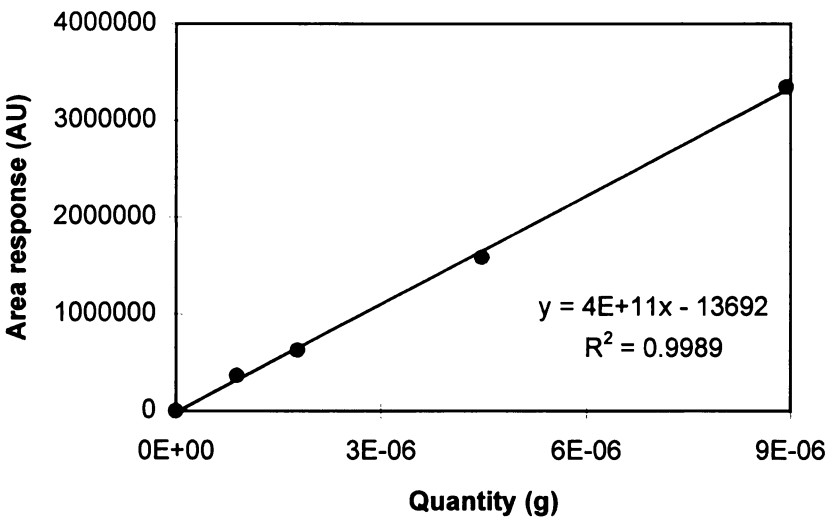

Figure 37. Ethyl acetate calibration curve.

Appendix B

The following charts are plots of the weight gain of styrene butadiene copolymer film samples as a function of time, measured by the electrobalance. The weight gain is a result of organic vapour sorption by the polymer sample. The experimental curves were fitted with a theoretical equation, as discussed in the literature review. This equation was used to determine the best estimated diffusion coefficient. Equilibrium solubility and solubility coefficients were also determined from the sorption data, as described in the literature review.

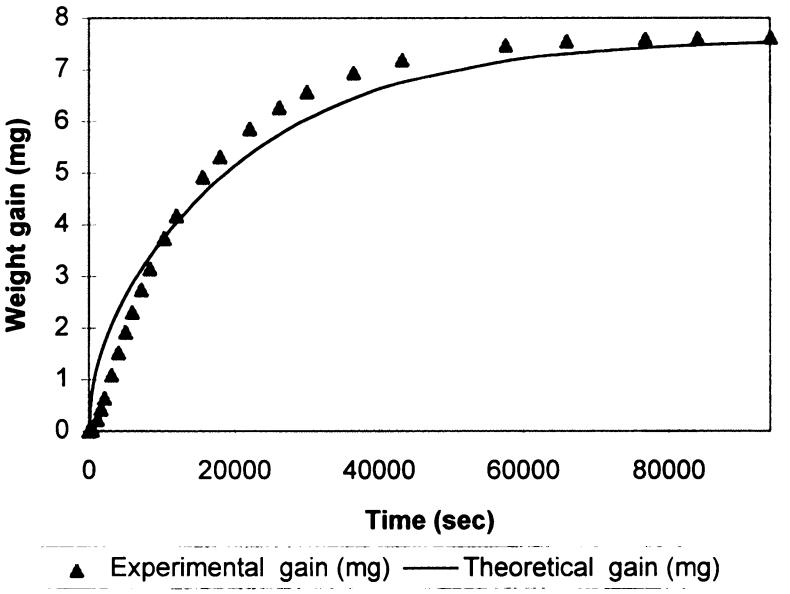

Figure 38. d-limonene sorption curve @ 25°C, Av = 0.1, run 1.

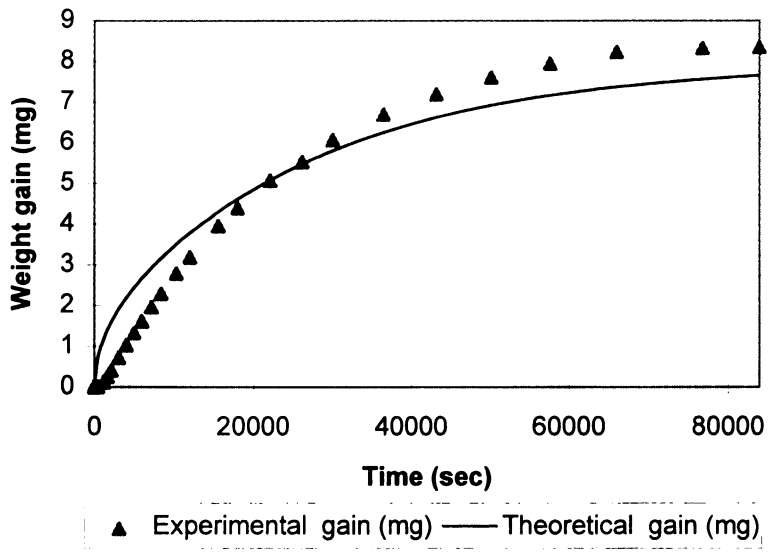

Figure 39. d-limonene sorption curve @ 25°C, Av = 0.1, run 2.

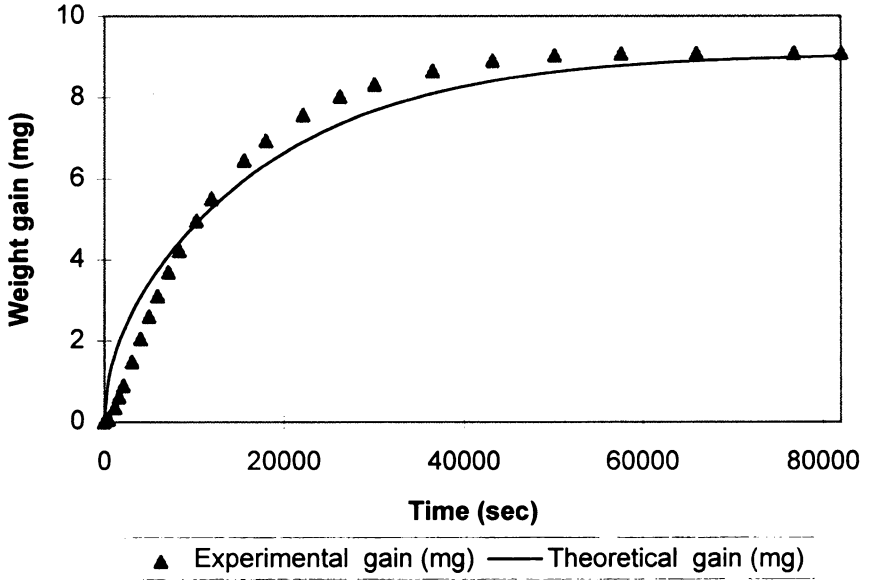

Figure 40. d-limonene sorption curve @ 25°C, Av = 0.1, run 3.

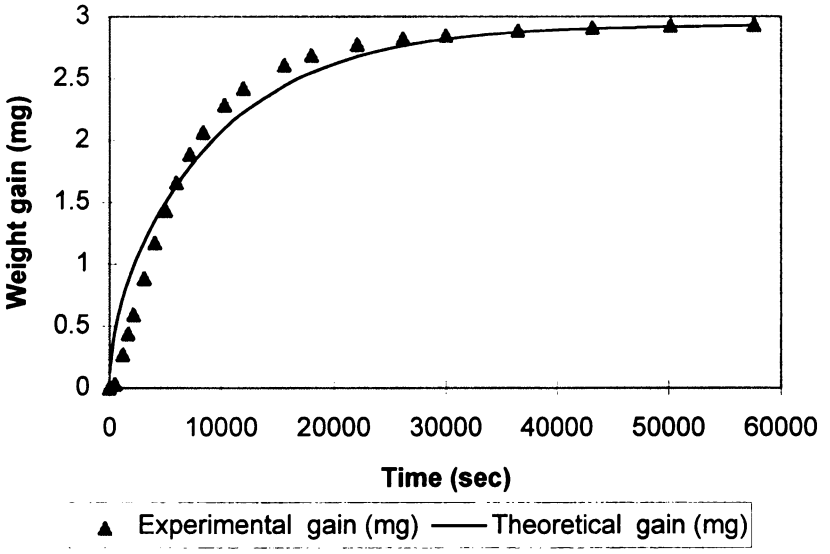

Figure 41. D-limonene sorption curve @ 35°C, Av = 0.1, run 1.

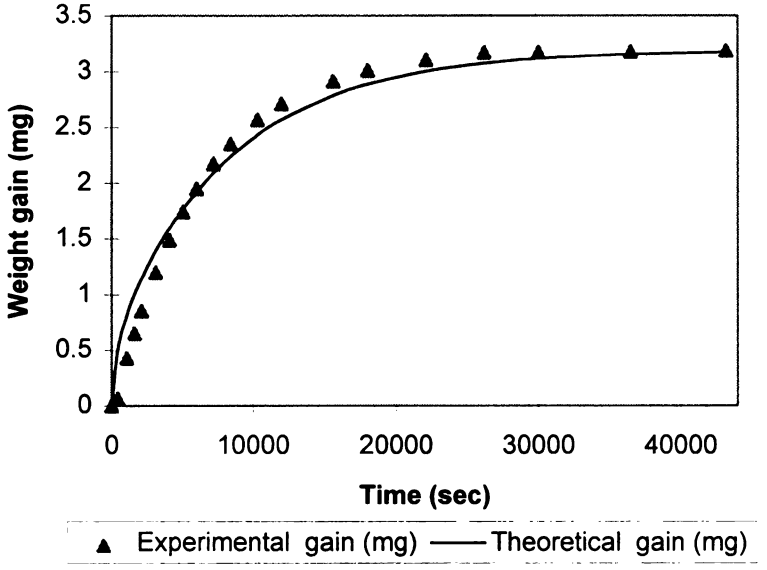

Figure 42. d-limonene sorption curve @ 35°C, Av = 0.1, run 2.

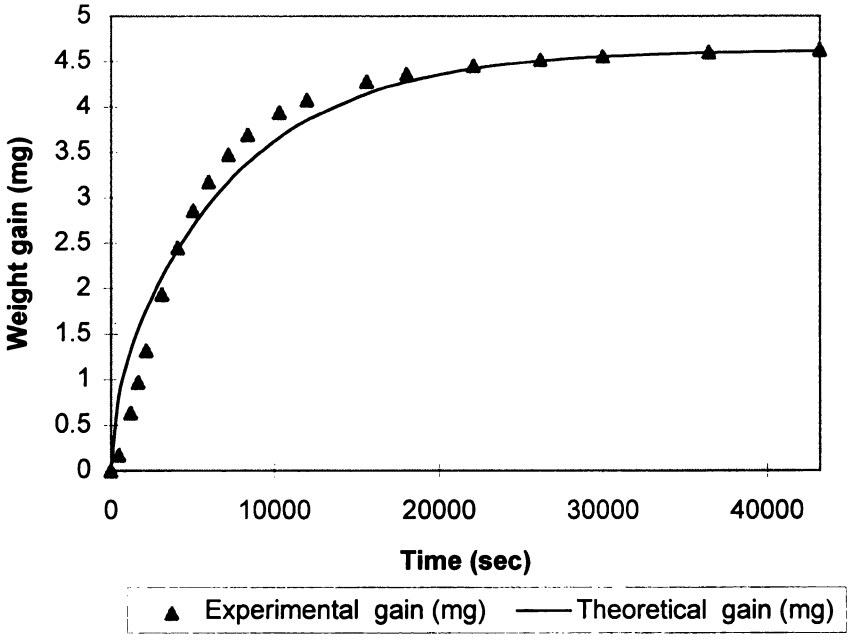

Figure 43. D-limonene sorption curve @ 35°C, Av = 0.1, run 3.

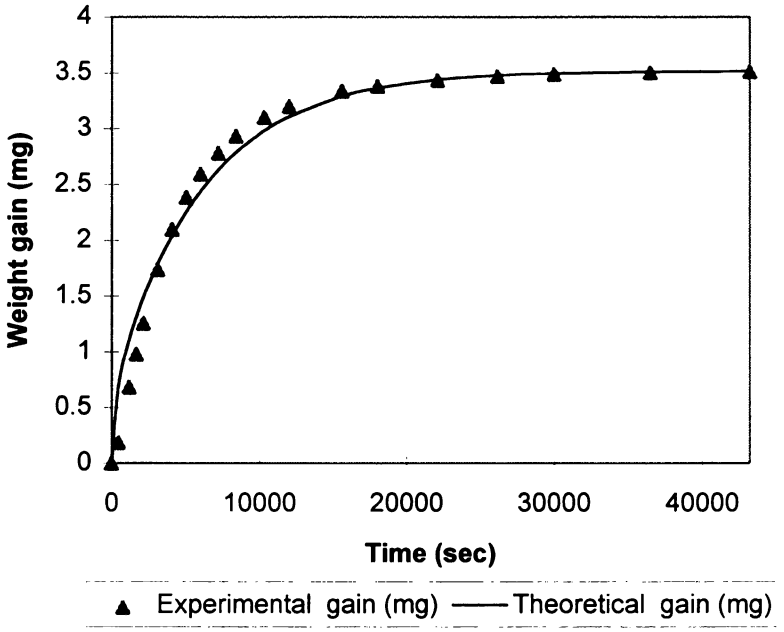

Figure 44. d-limonene sorption curve @ 42°C, Av = 0.2, run 1.

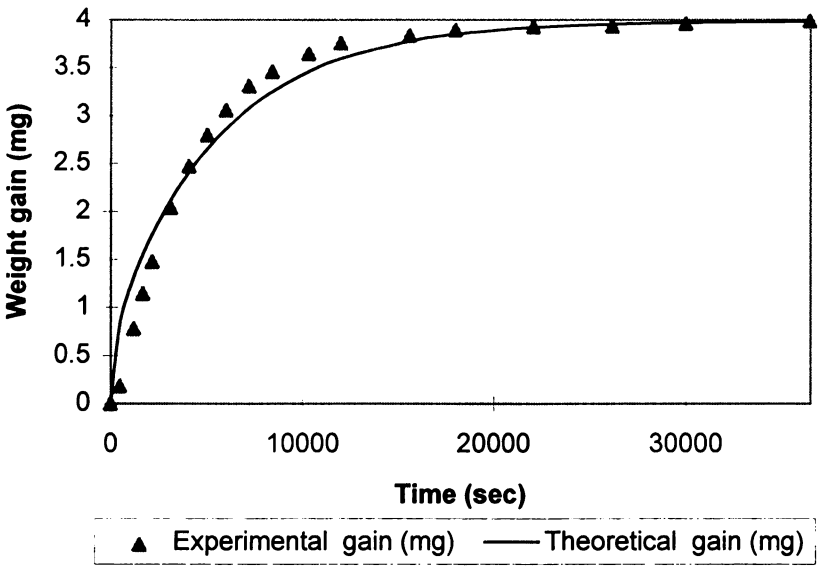

Figure 45. d-limonene sorption curve @ 42°C, Av = 0.2, run 2.

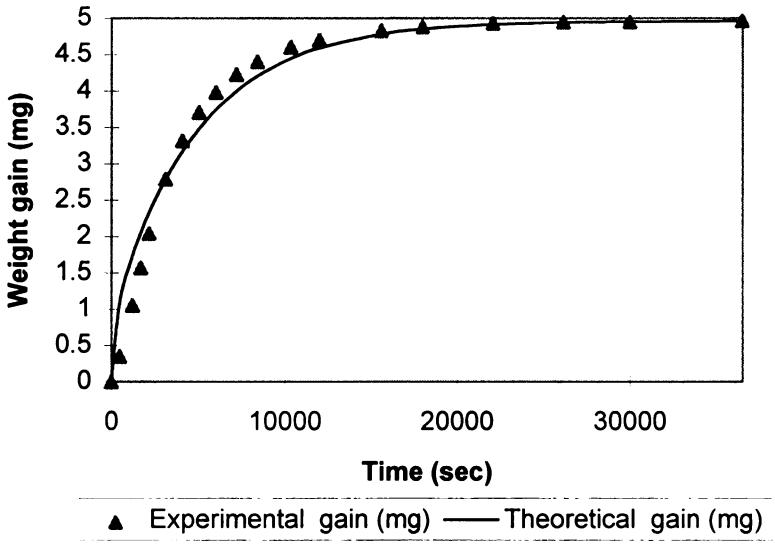

Figure 46. d-limonene sorption curve @ 42°C, Av = 0.1, run 3.

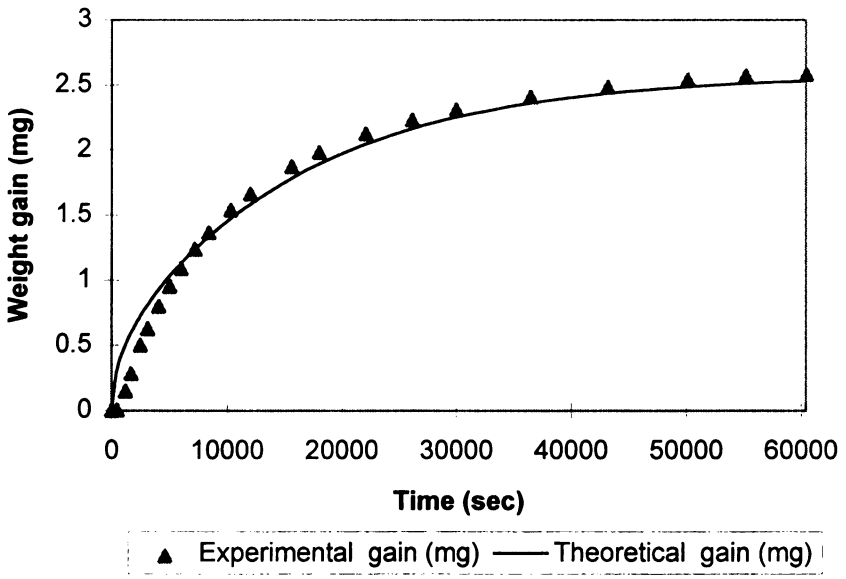

Figure 47. d-limonene sorption curve @ 25°C, Av = 0.2, run 1.

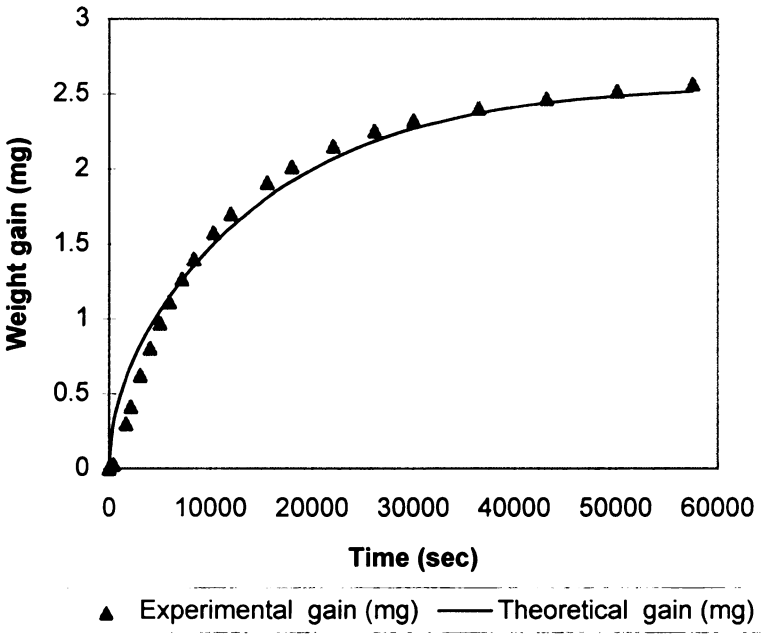

Figure 48. d-limonene sorption curve @ 25°C, Av = 0.2, run 2.

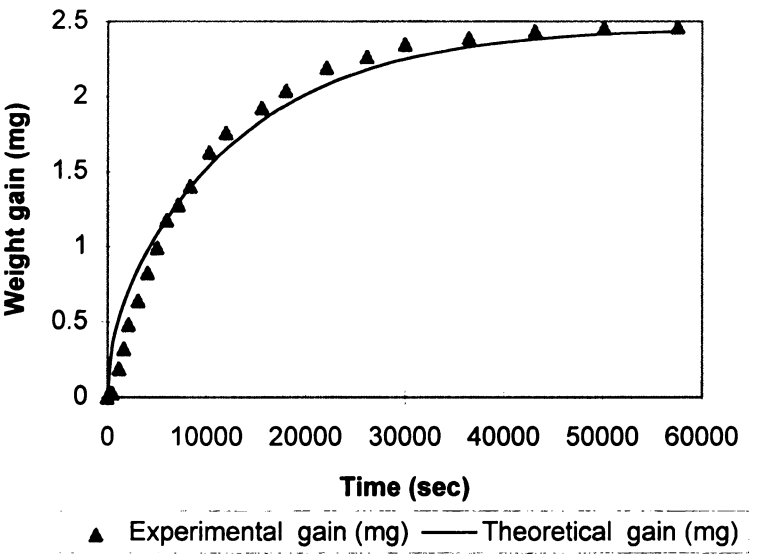

Figure 49. d-limonene sorption curve @ 25°C, Av = 0.2, run 3.

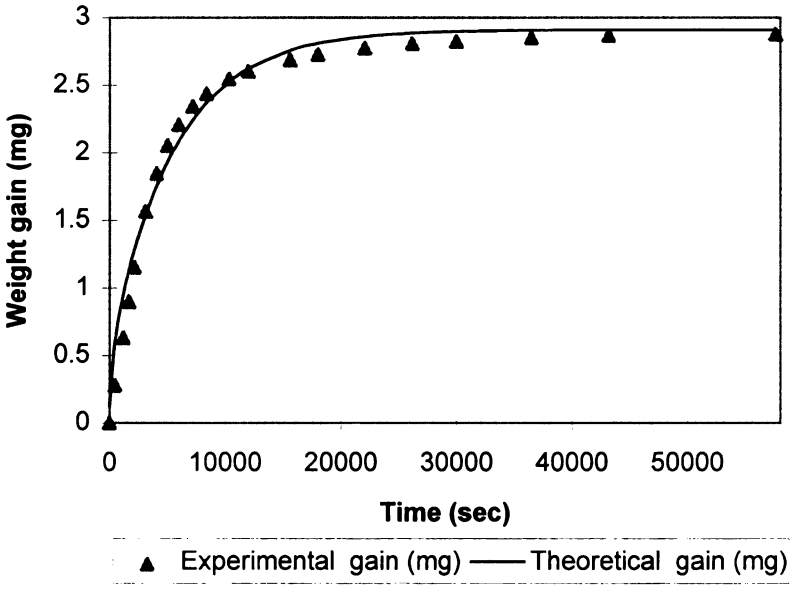

Figure 50. d-limonene sorption curve @ 35°C, Av = 0.2, run 1.

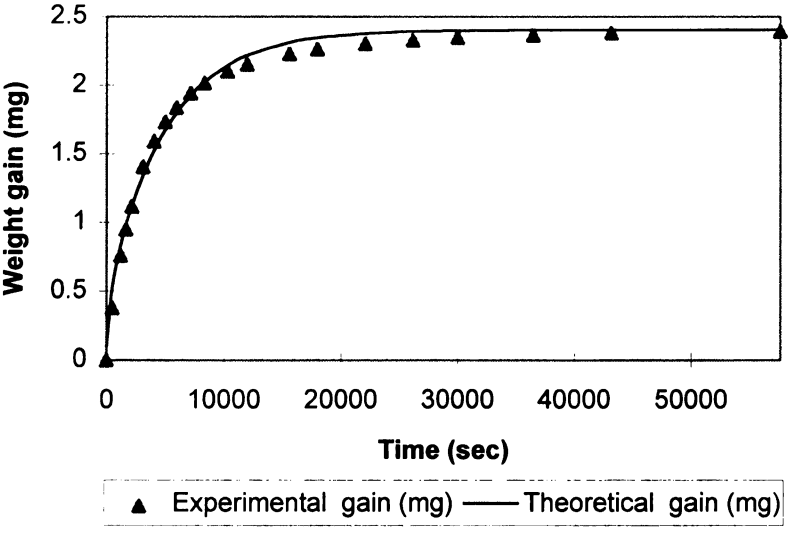

Figure 51. d-limonene sorption curve @ 35°C, Av = 0.2, run 2.

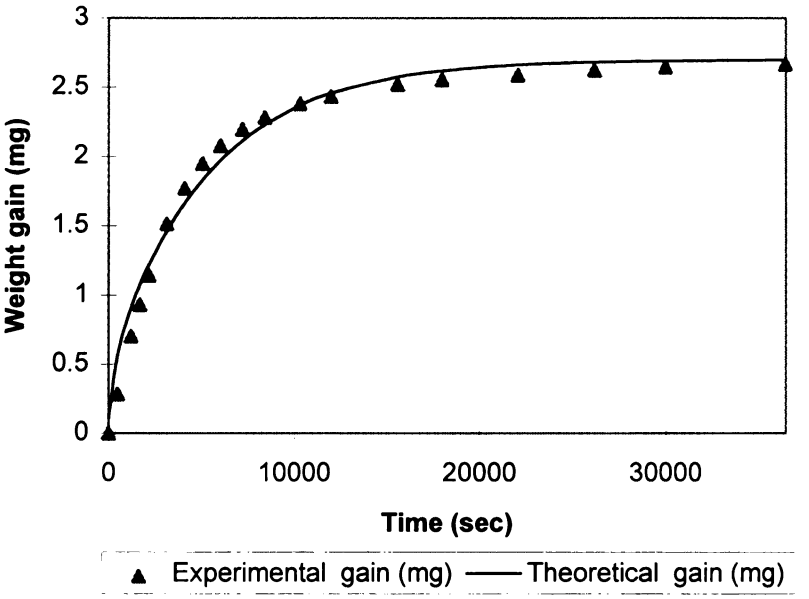

Figure 52. d-limonene sorption curve @ 35°C, Av = 0.3, run 3.

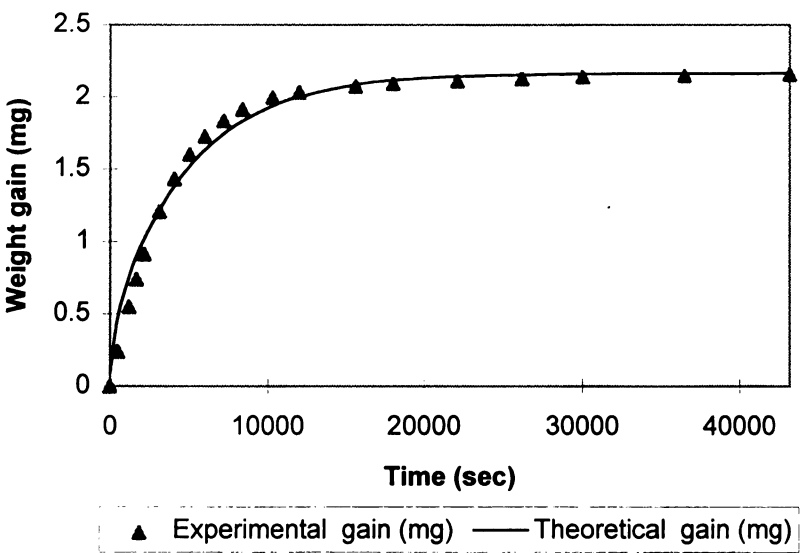

Figure 53. D-limonene sorption curve @ 42°C, Av = 0.3, run 1.

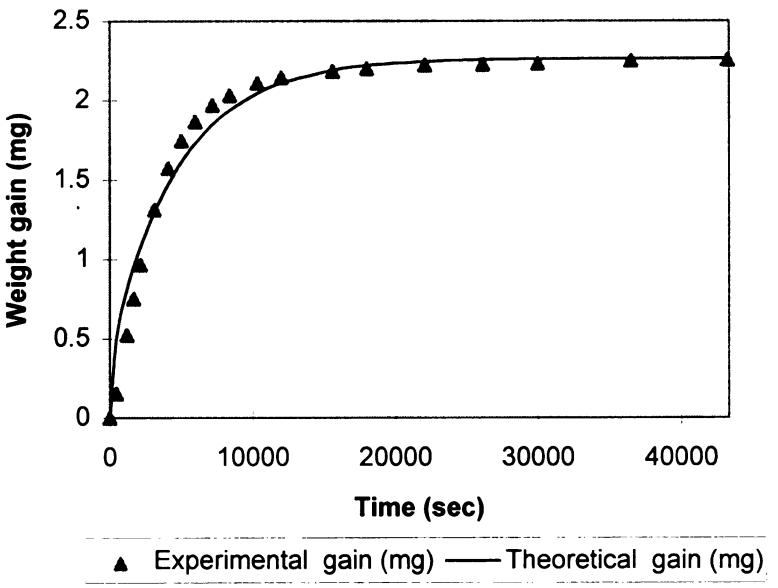

Figure 54. d-limonene sorption curve @ 42°C, Av = 0.2, run 2.

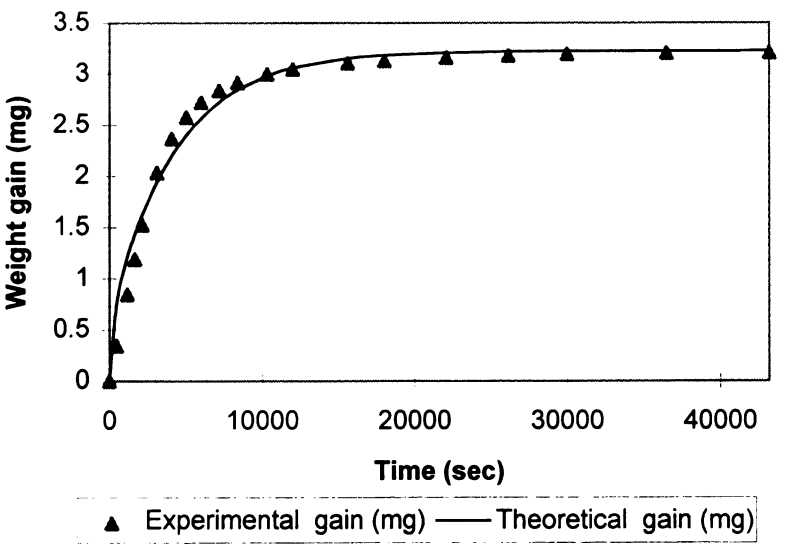

Figure 55. d-limonene sorption curve @ 42°C, Av = 0.2, run 3.

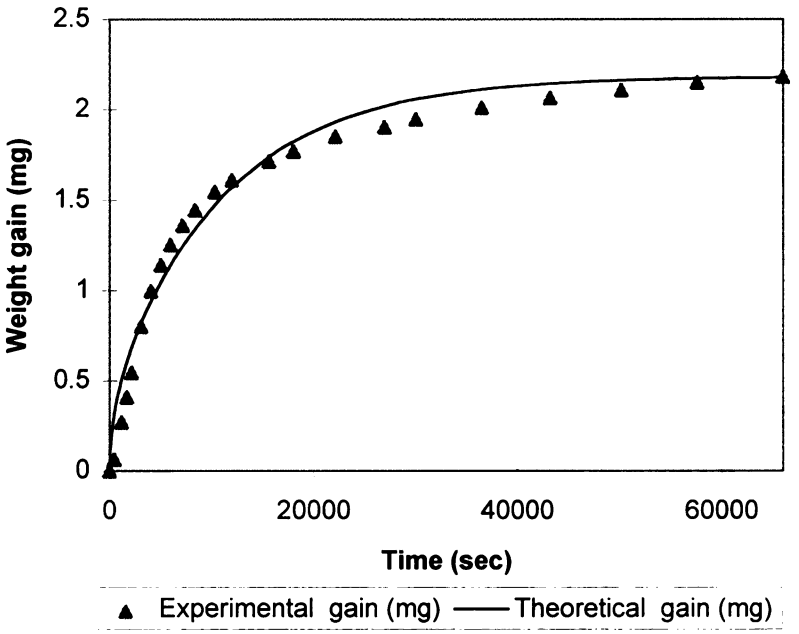

Figure 56. d-limonene sorption curve @ 25°C, Av = 0.3, run 1.

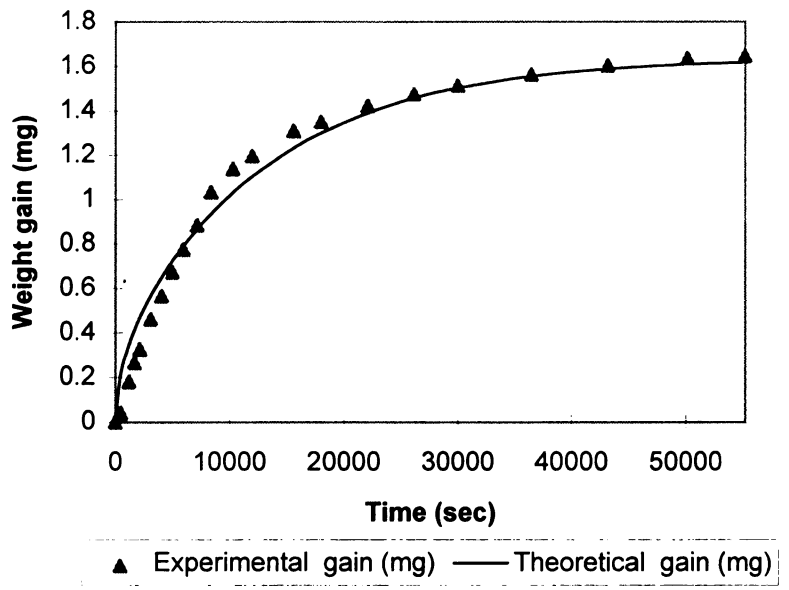

Figure 57. d-limonene sorption curve @ 25°C, Av = 0.3, run 2.

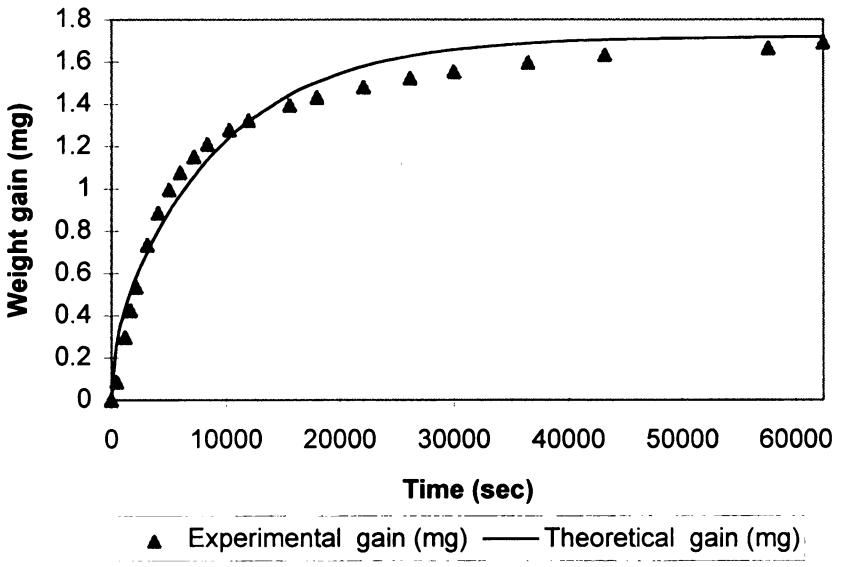

Figure 58. d-limonene sorption curve @ 25°C, Av = 0.3, run 3.

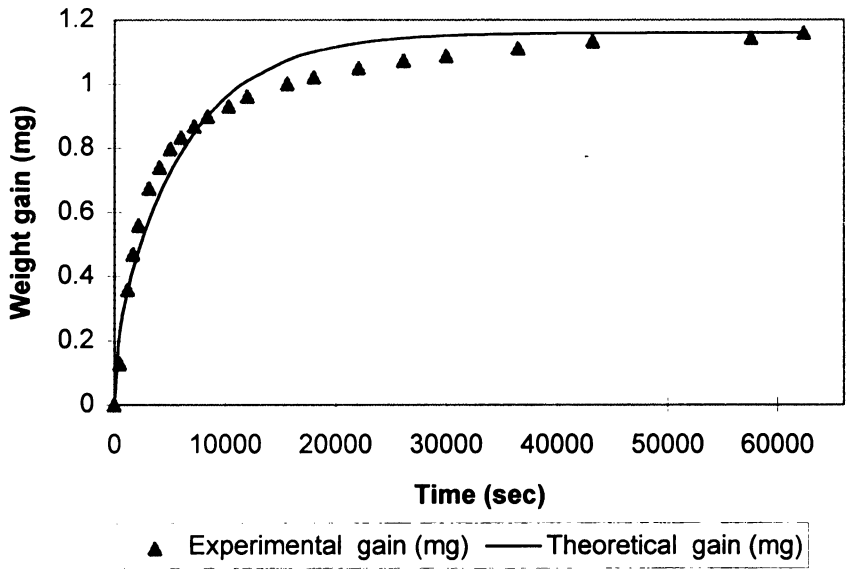

Figure 59. d-limonene sorption curve @ 35°C, Av = 0.3, run 1.

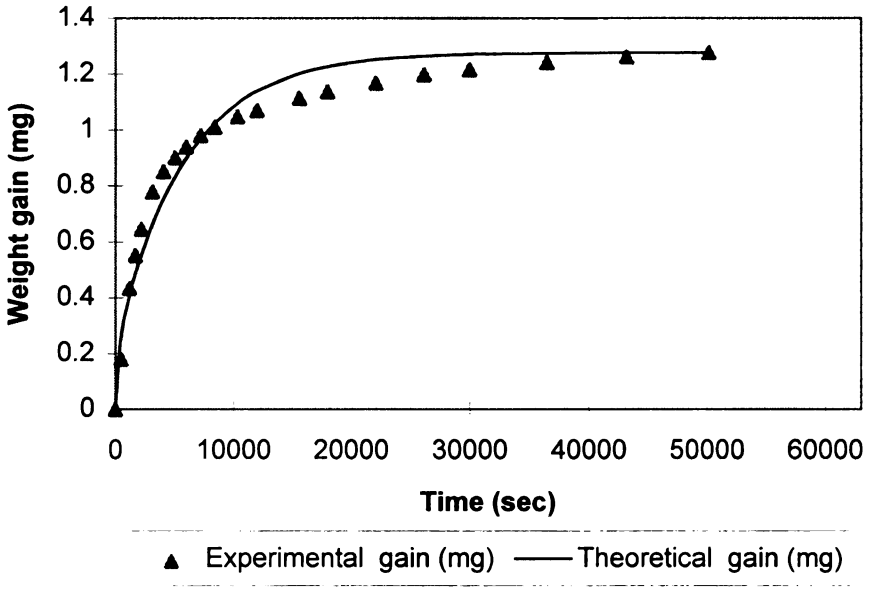

Figure 60. d-limonene sorption @ 35°C, Av = 0.3, run 2.

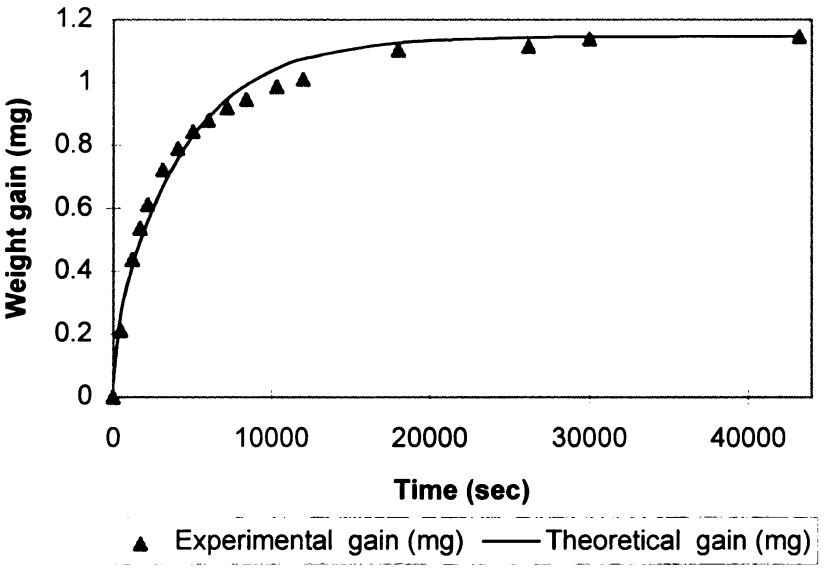

Figure 61. D-limonene sorption @ 35°C, Av = 0.3, run 3.

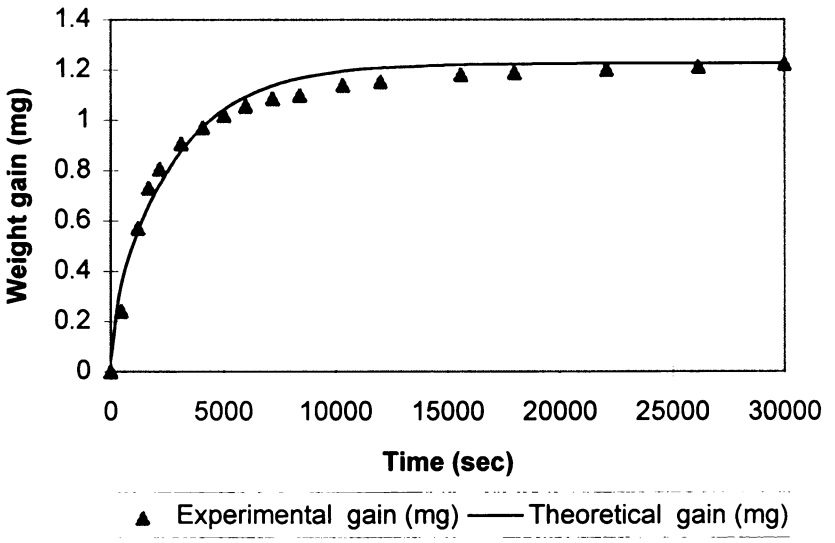

Figure 62. d-limonene sorption curve @ 42°C, Av = 0.3, run 1.

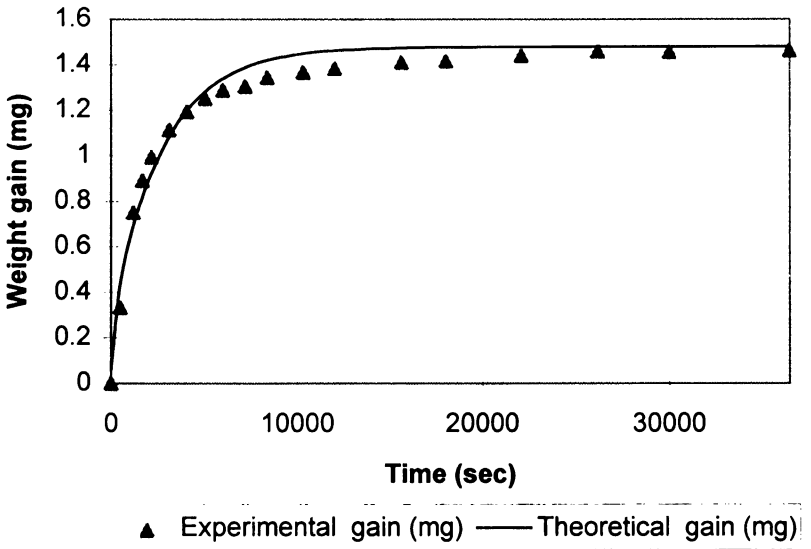

Figure 63. D-limonene sorption curve @ 42°C, Av = 0.3, run 2.

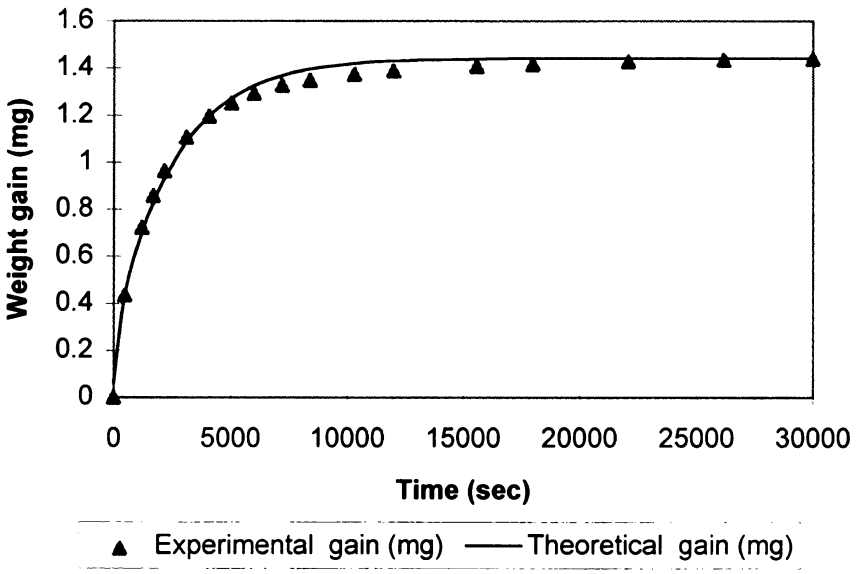

Figure 64. d-limonene sorption curve @ 42°C, Av = 0.3, run 3.

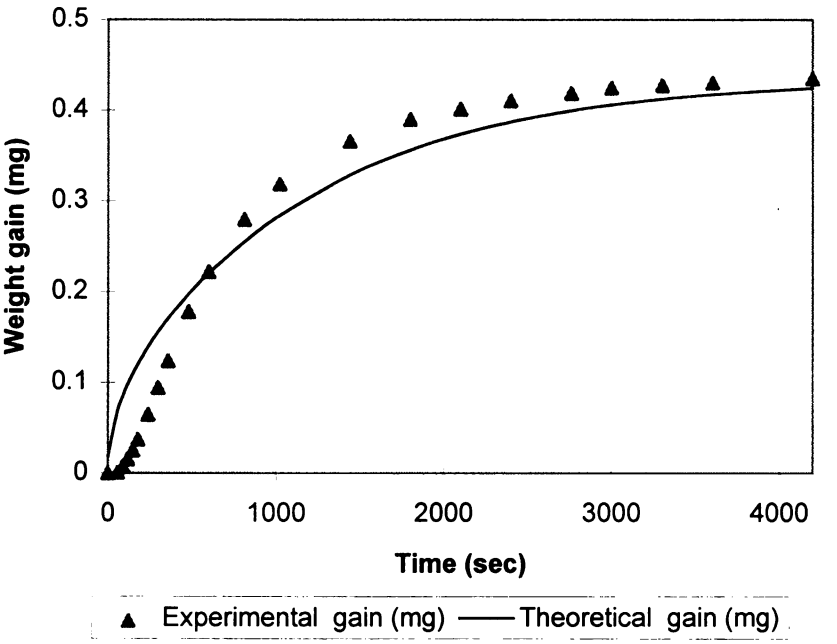

Figure 65. Ethyl acetate sorption curve @ 25°C, Av = 0.05, run 1.

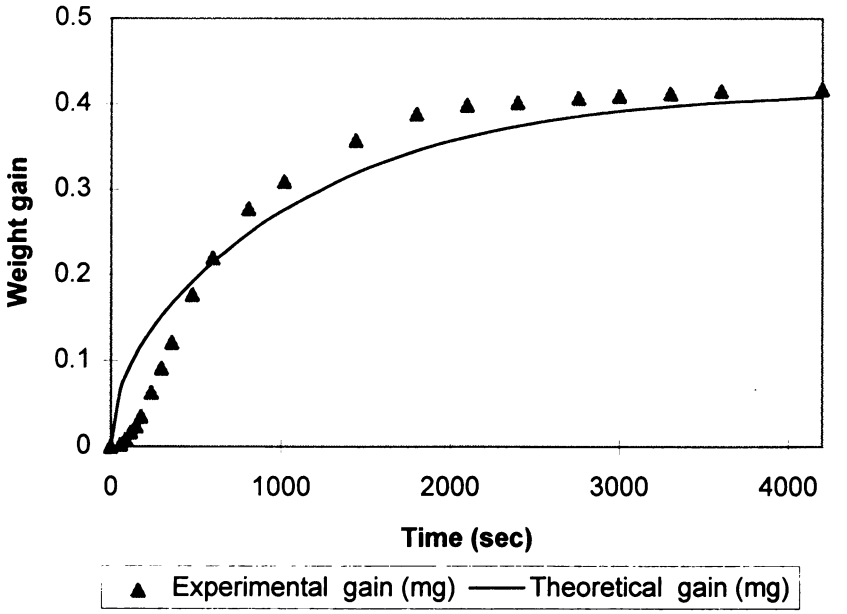

Figure 66. Ethyl acetate sorption curve @ 25°C, Av = 0.05, run 2.

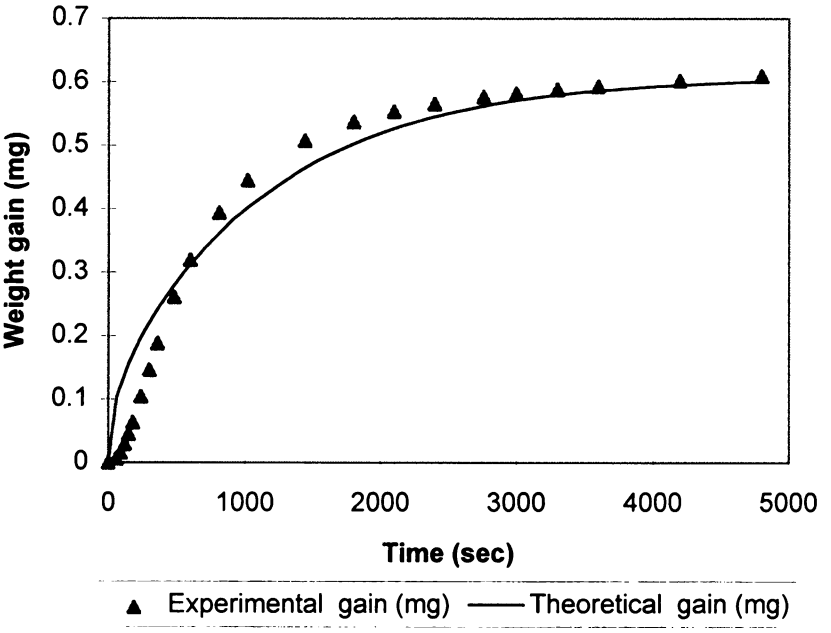

Figure 67. Ethyl acetate sorption @ 25°C, Av = 0.05, run 3.

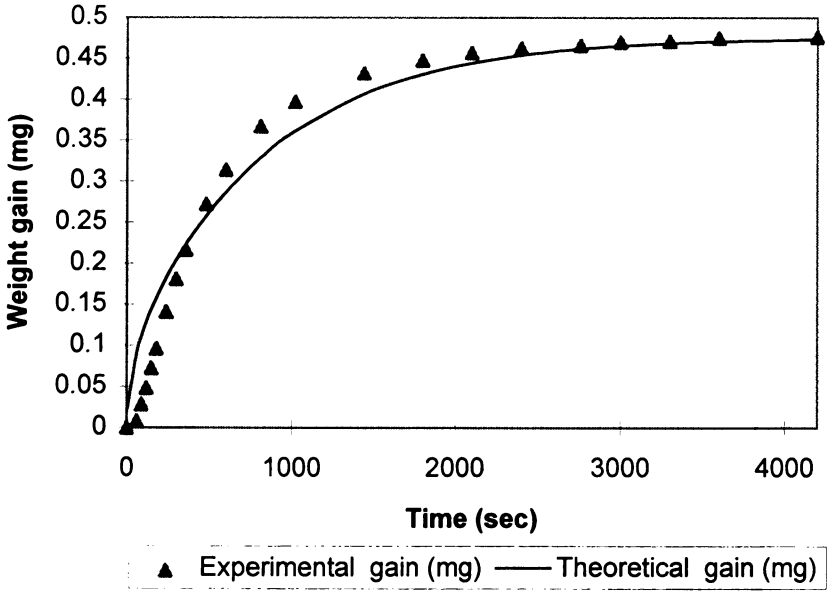

Figure 68. Ethyl acetate sorption @ 35°C, Av = 0.05, run 1.

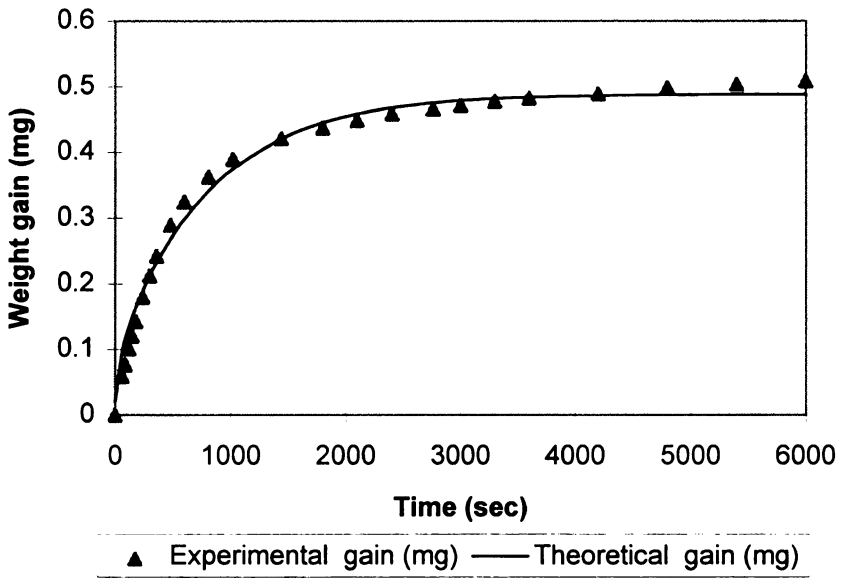

Figure 69. Ethyl acetate sorption curve @ 35°C, Av = 0.05, run 2.

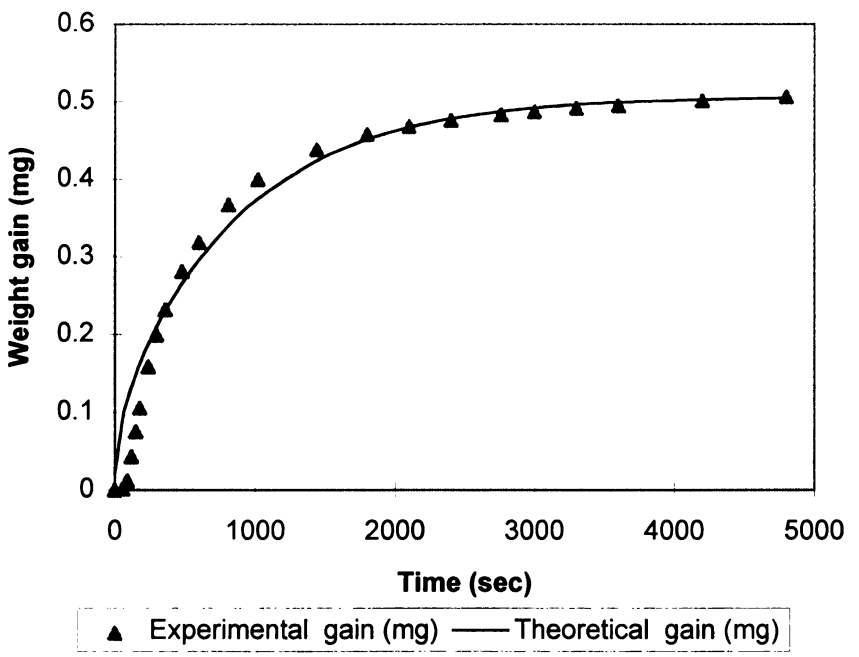

Figure 70. Ethyl acetate sorption curve @ 35°C, Av = 0.05, run 3.

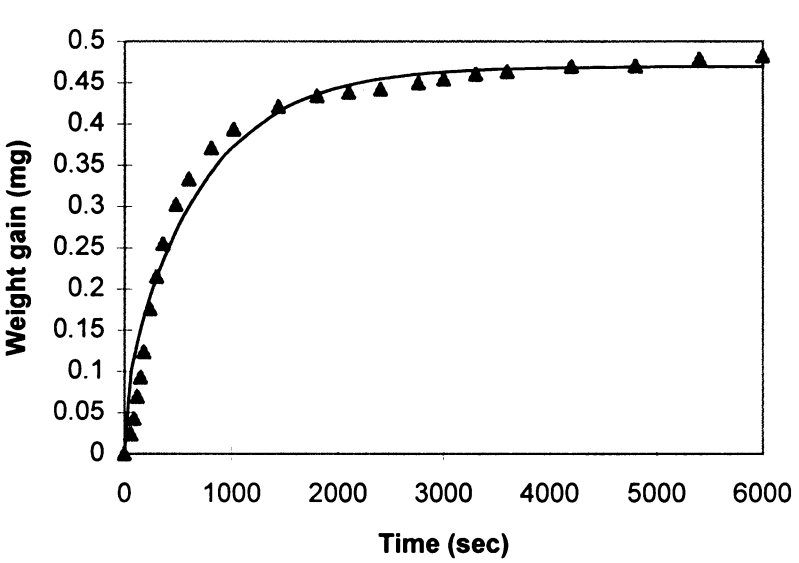

Figure 71. Ethyl acetate sorption curve @ 42°C, Av = 0.05, run 1.

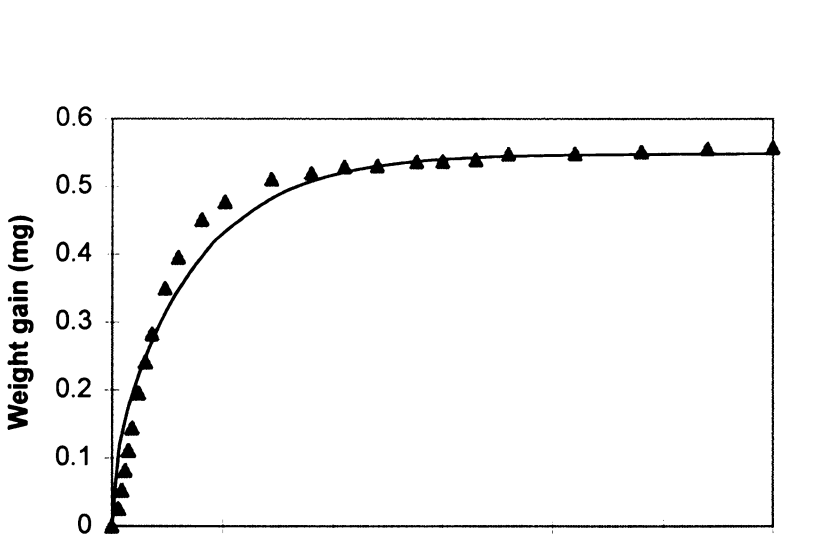

Figure 72. Ethyl acetate sorption curve @ 42°C, Av = 0.05, run 2.

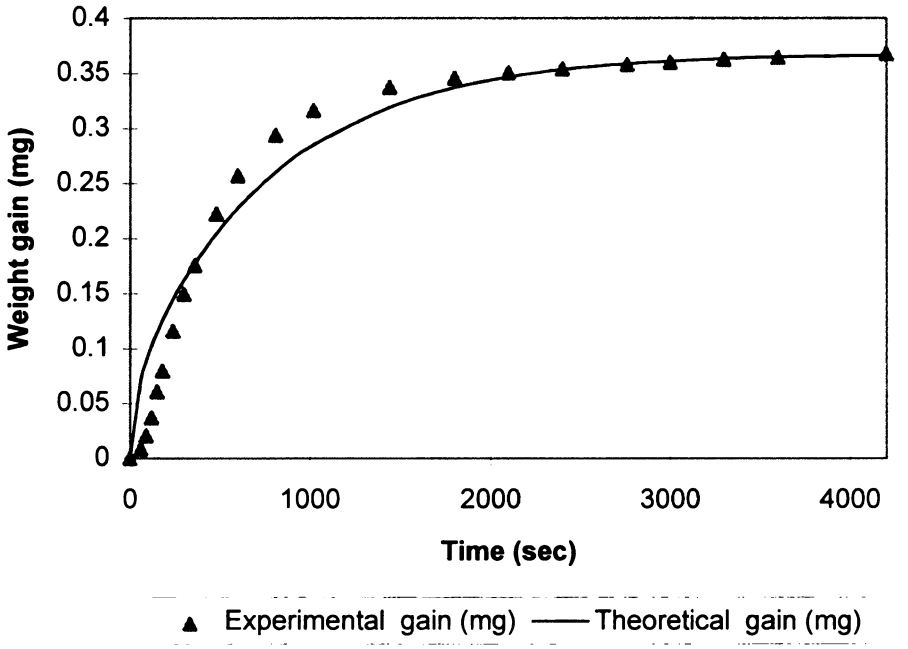

Figure 73. Ethyl acetate sorption curve @ 42°C, Av = 0.05, run 3.

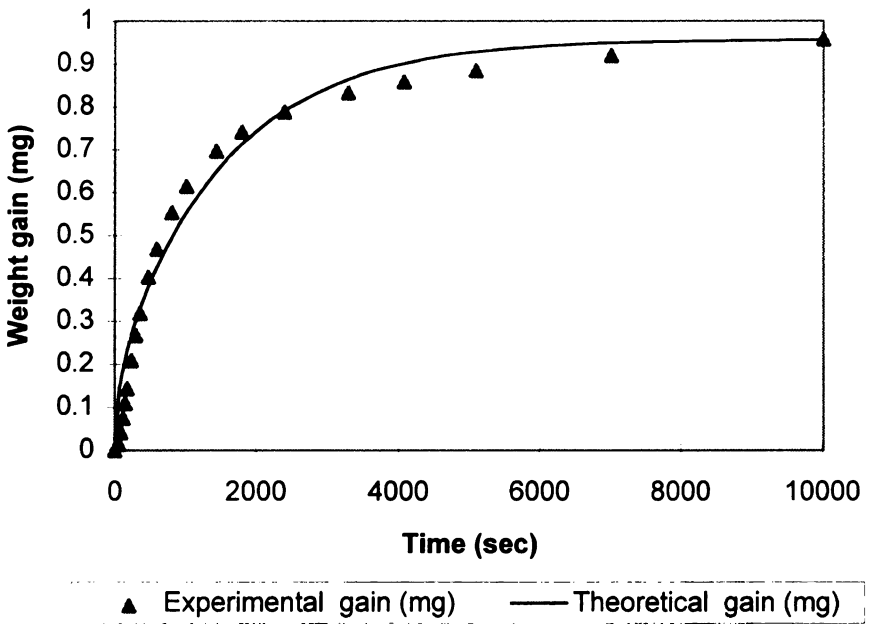

Figure 74. Ethyl acetate sorption curve @ 25°C, Av = 0.1, run 1.

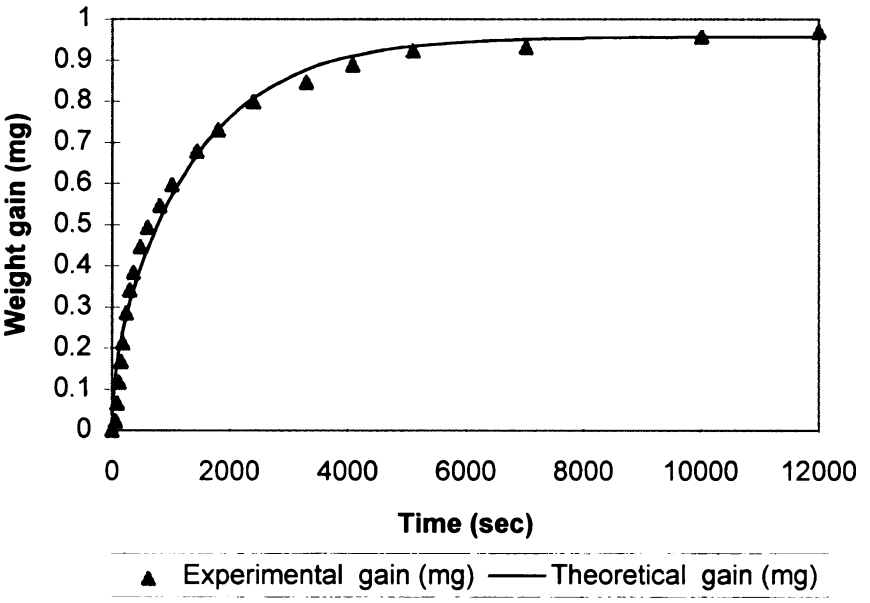

Figure 75. Ethyl acetate sorption curve @ 25°C, Av = 0.1, run 2.

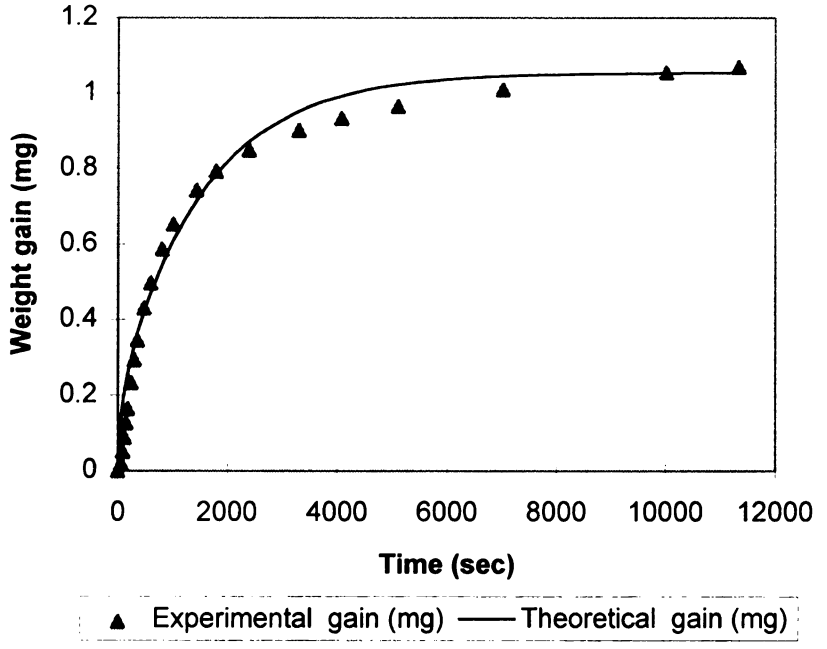

Figure 76. Ethyl acetate sorption curve @ 25°C, Av = 0.1, run 3.

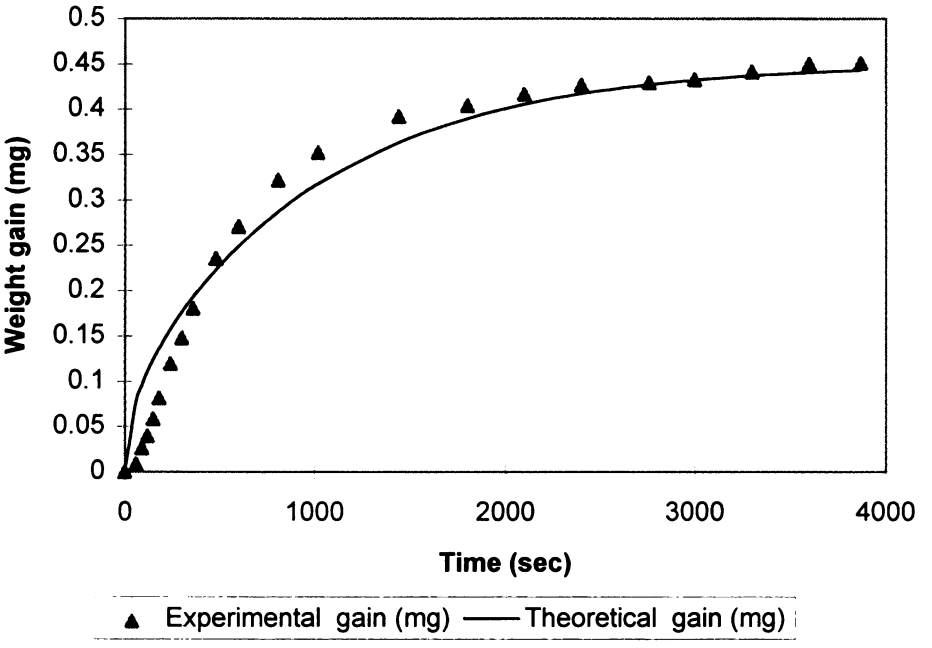

Figure 77. Ethyl acetate sorption @ 35°C, Av = 0.1, run 1

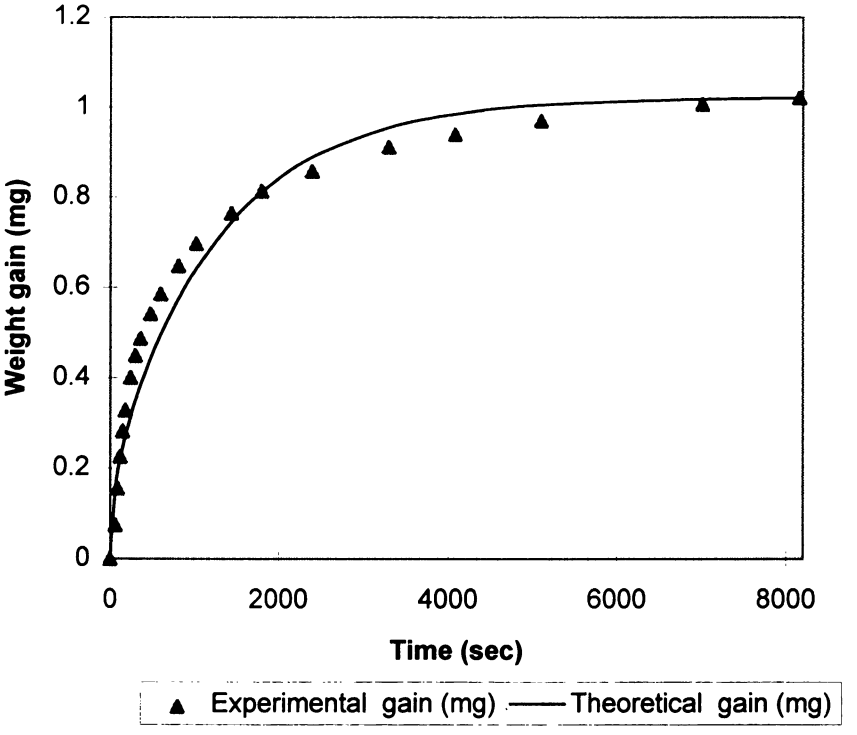

Figure 78. Ethyl acetate sorption @ 35°C, Av = 0.1, run 2.

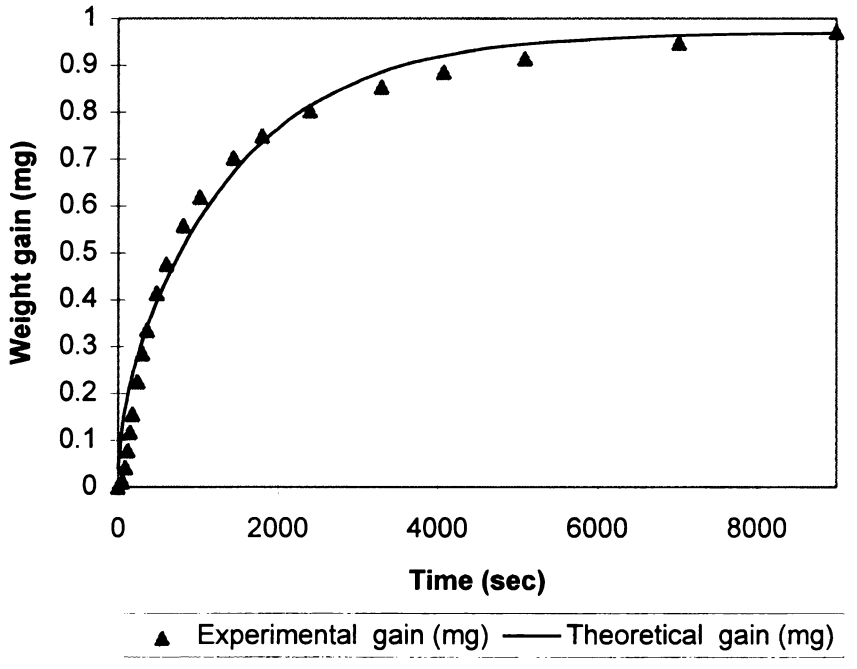

Figure 79. Ethyl acetate sorption curve @ 35°C, Av = 0.1, run 3.

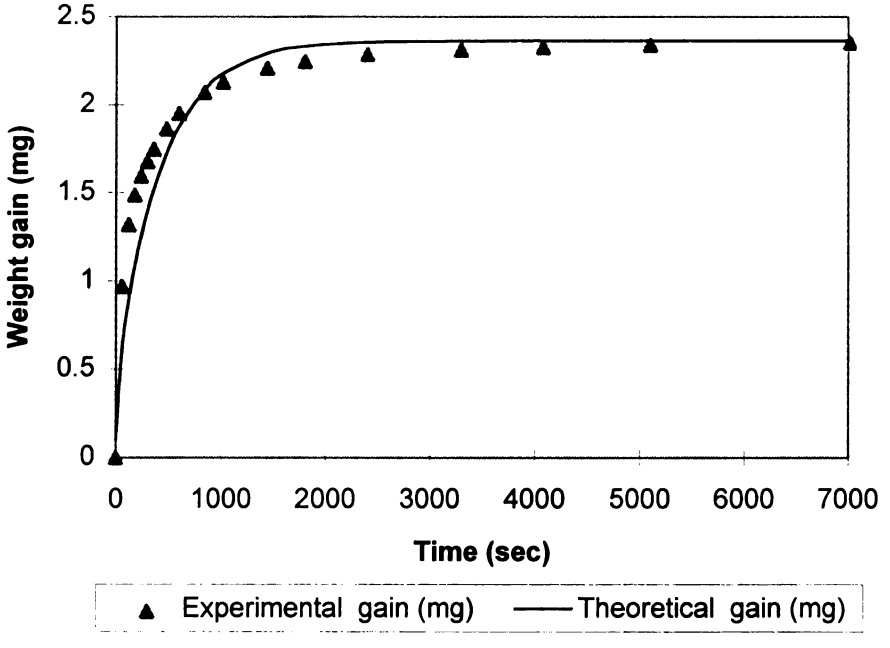

Figure 80. Ethyl acetate sorption curve @ 42°C, Av = 0.1, run 1.

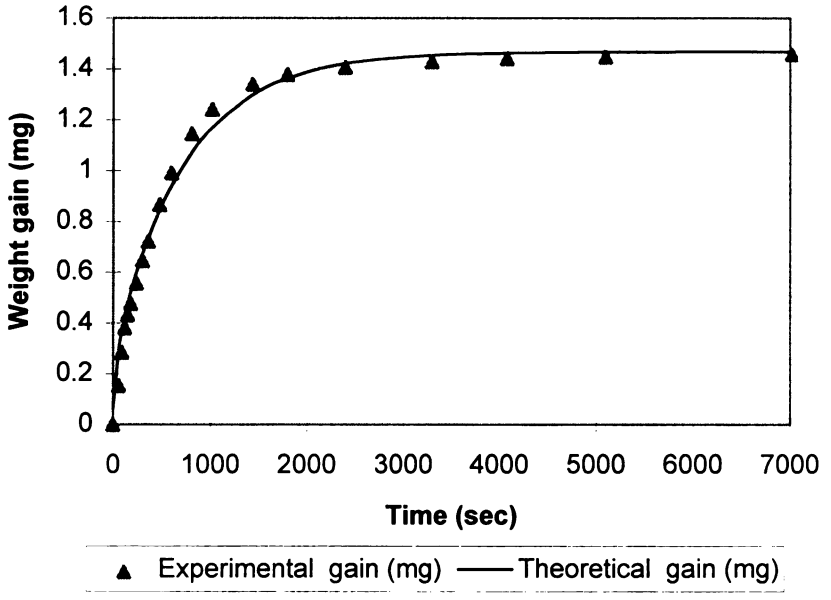

Figure 81. Ethyl acetate sorption curve @ 42°C, Av = 0.1, run 2.

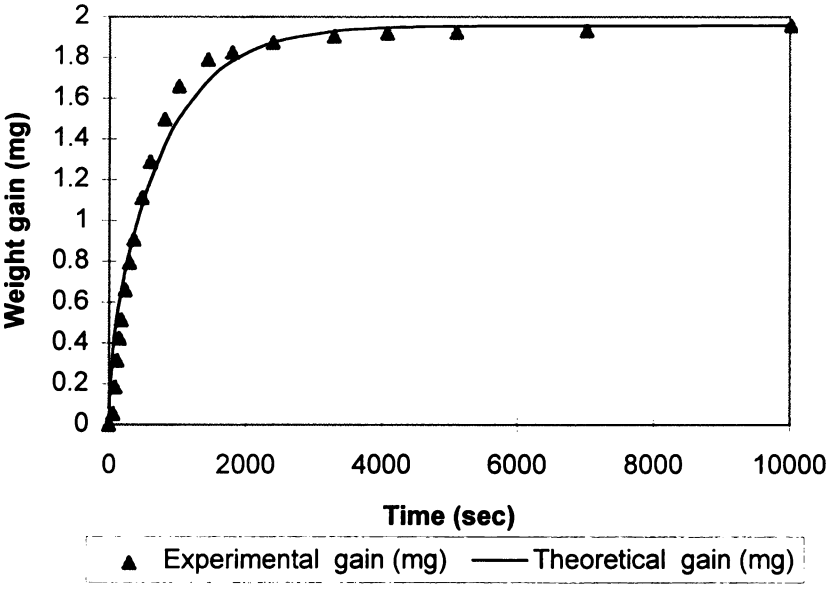

Figure 82. Ethyl acetate sorption curve @ 42°C, Av = 0.1, run 3.

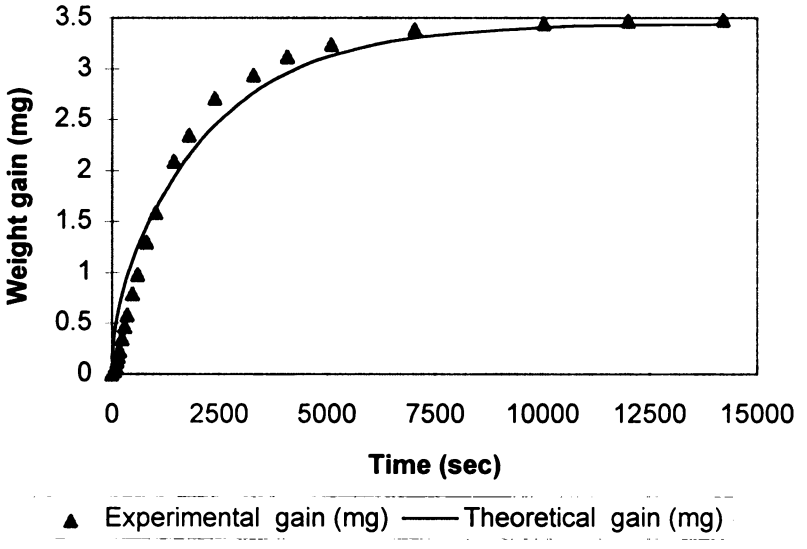

Figure 83. Ethyl acetate sorption curve @ 25°C, Av = 0.2, run 1.

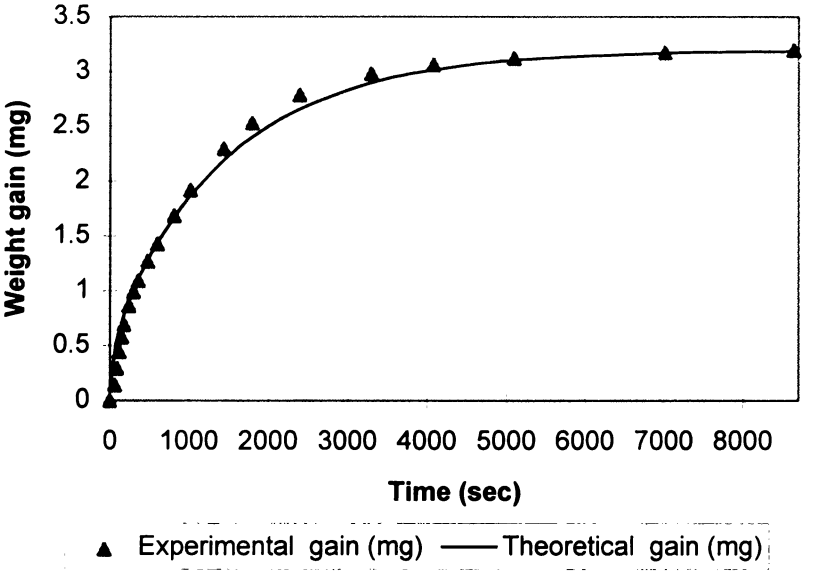

Figure 84. Ethyl acetate sorption curve @ 25°C, Av = 0.2, run 2.

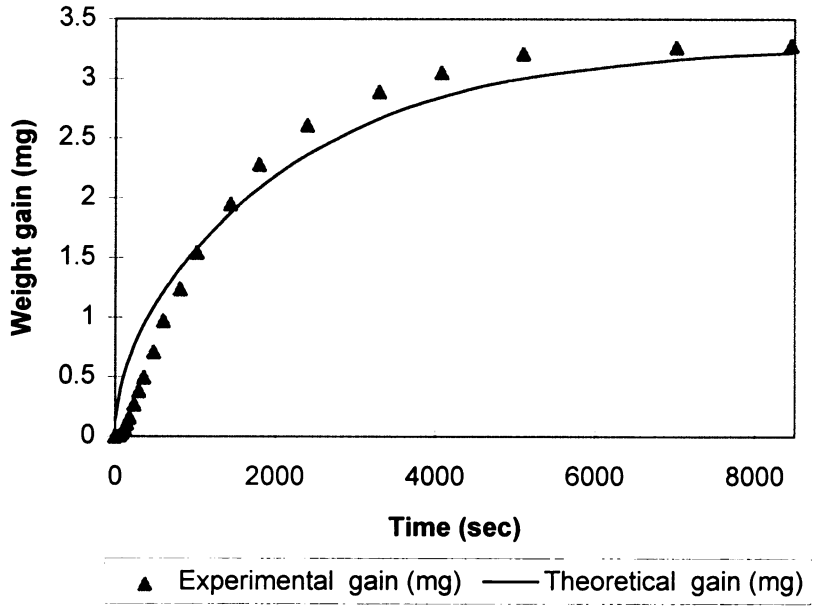

Figure 85. Ethyl acetate sorption curve @ 25°C, Av = 0.2, run 3.

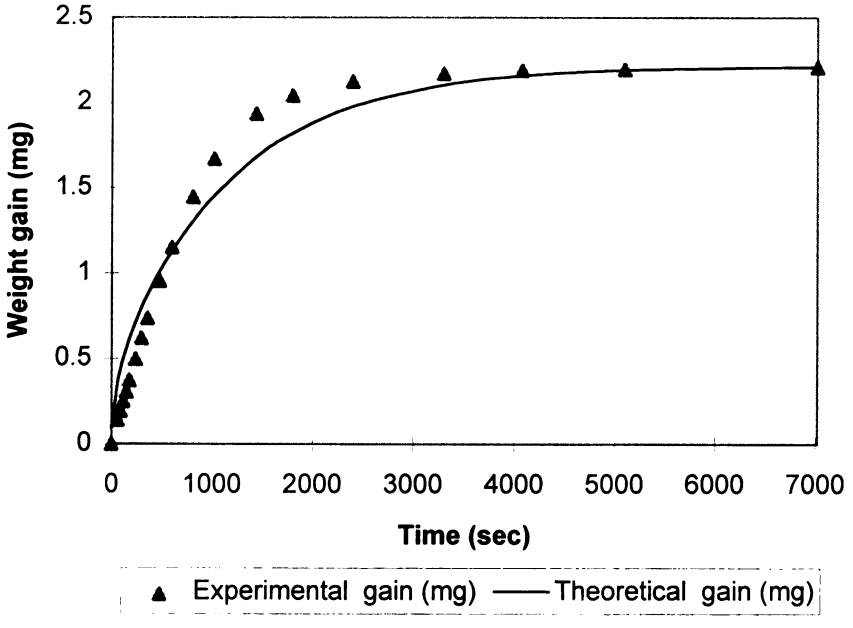

Figure 86. Ethyl acetate sorption curve @ 35°C, Av = 0.2, run 1

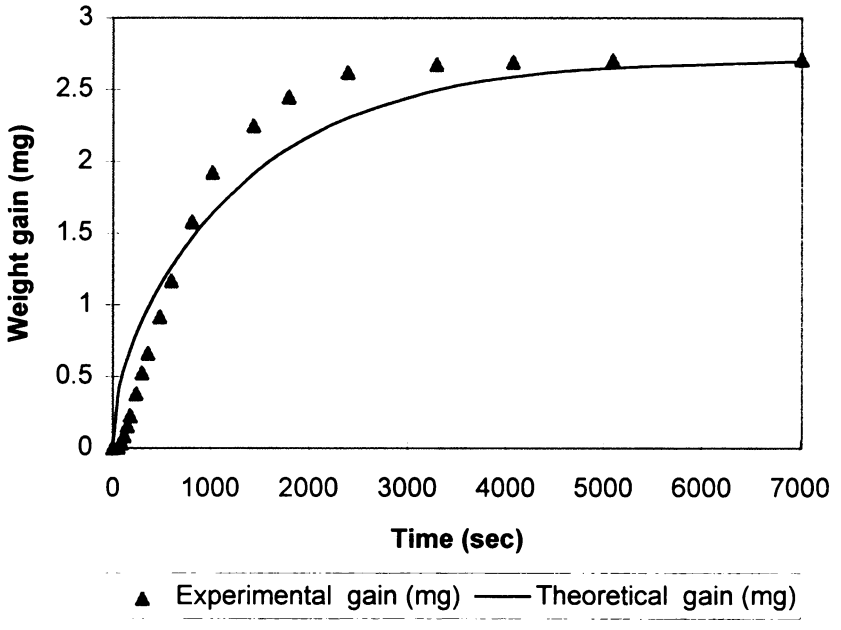

Figure 87. Ethyl acetate sorption curve @ 35°C, Av = 0.2, run 2.

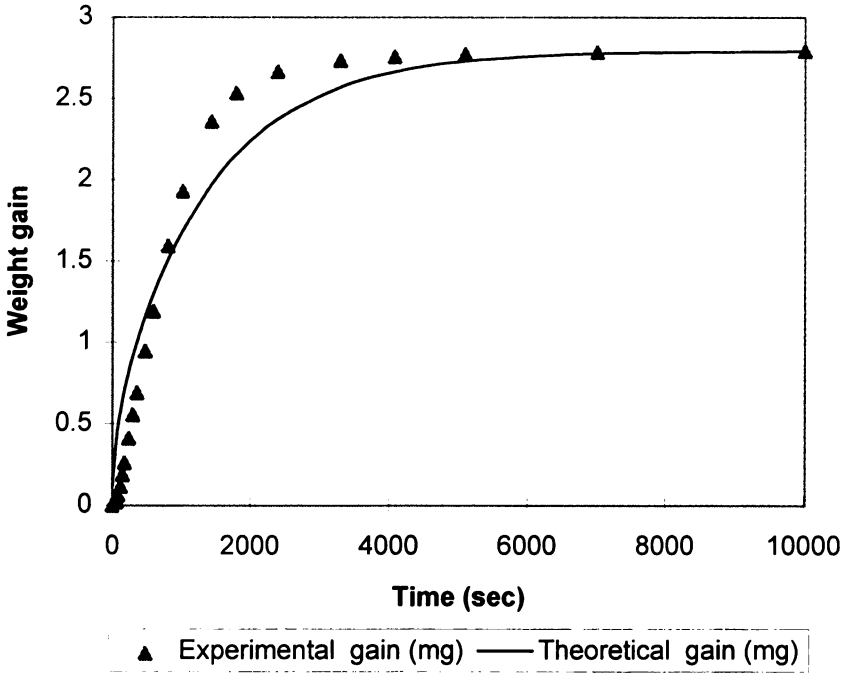

Figure 88. Ethyl acetate sorption curve @ 35°C, Av = 0.2, run 3.

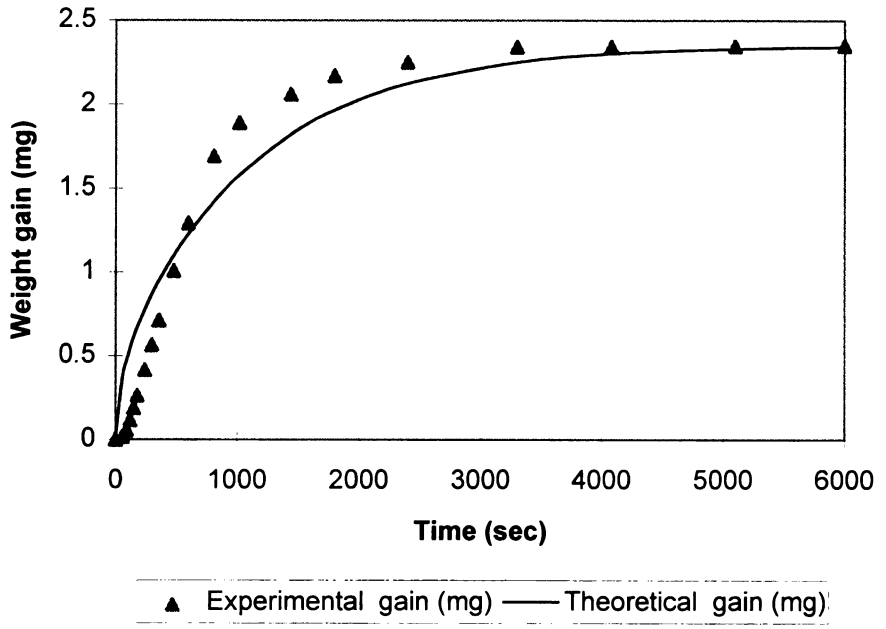

Figure 89. Ethyl acetate sorption curve @ 42°C, Av = 0.2, run 1.

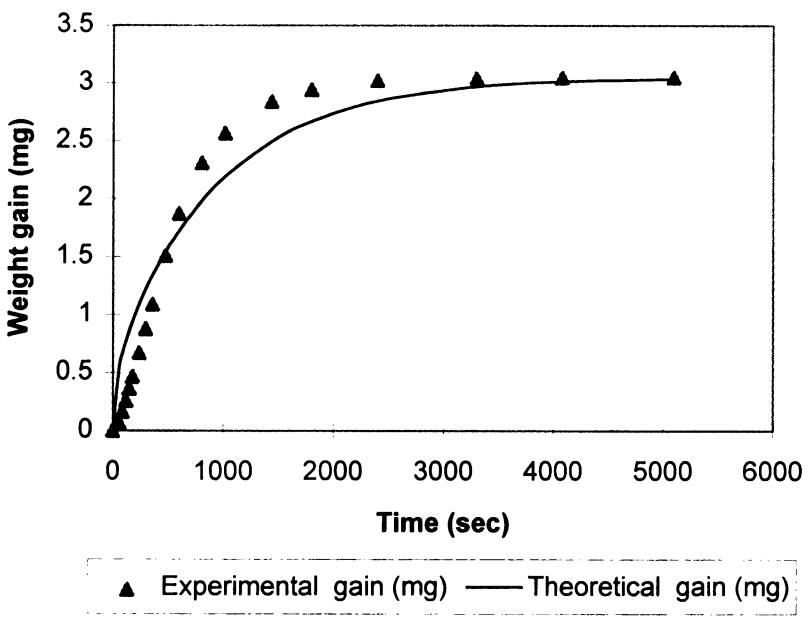

Figure 90. Ethyl acetate sorption curve @ 42°C, Av = 0.2, run 2.

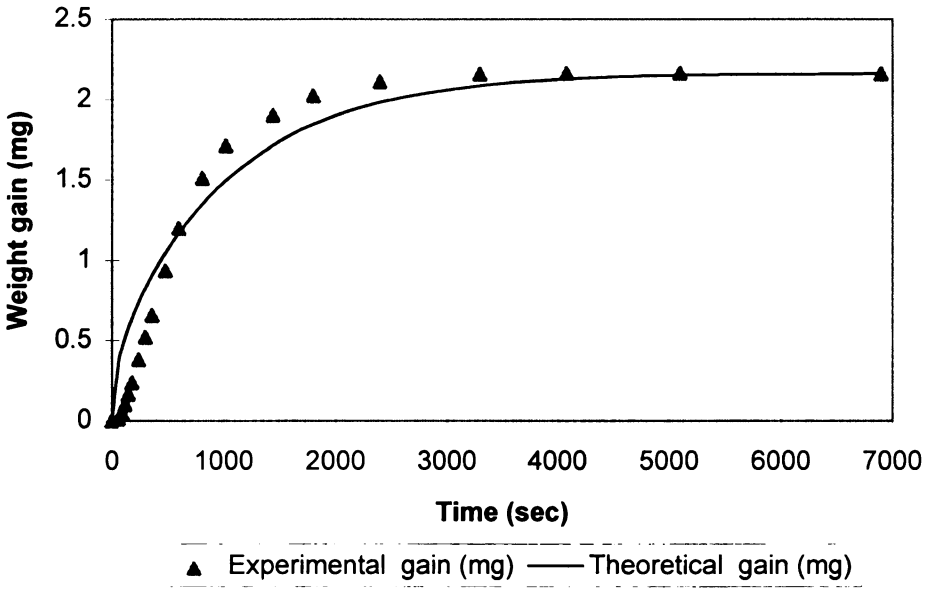

Figure 91. Ethyl acetate sorption curve @ 42°C, Av = 0.2, run 3.

Appendix C

Verification of the structure of styrene butadiene copolymer from infrared analysis

Table 20. Peak absorbance frequencies from infrared analysis of KR-10 film.

Peak frequency (cm^{-1})	**Absorbance (%)**	**Identification**
3060	65	=CH in aromatic and unsaturated hydrocarbons
3025	85	=CH in aromatic and unsaturated hydrocarbons
2922	98	$-CH_3$ and $-CH_2$ in aliphatic compounds
2849	83	$-CH_3$ and $-CH_2$ in aliphatic compounds
1601	50	benzene ring in aromatic compounds
1493	65	benzene ring in aromatic compounds
1448	84	$-CH_2$ in aliphatic compounds
967	75	$-CH=CH_2$ in trans distributed alkanes
910	50	$-CH=CH_2$ in vinyl compounds
756	88	*o*-disubstituted benzenes
699	92	-CH=CH- in cis disubstituted alkenes
542	65	$=CH_2$ in vinyl compounds

Bibliography

Ashley, R.J. 1985. Permeability and Plastics Packaging in Polymer Permeability. Edited by J. Comyn. Elsevier Applied Science Publishers, London.

ASTM D 3985-81, Standard Test Method for Oxygen Gas Transmission Rate Through Plastic Film and Sheeting Using a Coulometric Sensor. Annual Book of American Society for Testing and Materials Standards, Philadelphia, Pa.

ASTM D F 1249-90. 1992. Standard Test Method for Water Vapour Transmission Rate Through Plastic Film and Sheeting Using a Modulated Infrared Sensor. Annual Book of American Society for Testing and Materials Standards, Philadelphia, Pa.

Axelson-Larsson, L., 1992. Oxygen Permeabilities at High Temperatures and Relative Humidities. Packaging Technology and Science, 5, 297-306.

Baner, A.L. 1987. The measurement and analysis of the diffusion of toluene in polymeric films. M.S. thesis, Michigan State University, East Lansing, MI.

Barr, C.D. 1997. A Comparison of Solubility Coefficient Values Determined by Gravimetric and Isostatic Permeability Techniques. M.S. thesis, Michigan State University, East Lansing, MI.

Barrie, J.A., Williams, M.J.L. and Munday,K. 1980. Sorption and Diffusion of Hydrocarbon Vapors in Glassy Polymers. Polym. Eng. & Sci. 20(1), 20-29.

Berens, A.R. and Hopfenberg, H.B. 1982. Diffusion of Organic Vapors at Low Concentrations in Glassy PVC, Polystyrene and PMMA. J. Memb. Sci., 10 283-303.

Birley, A.W., Haworth, B. and Batchelor, J. 1992. Physics of Plastics: Processing, Properties and Materials Engineering, Hanser.

Brandt, W.W. 1985. J. Phys. Chem., 63, 1080.

Brunauer, S. 1944. The adsorption of gases and Vapours - Physical Adsorption. Oxford University Press.

Brydson, J.A. 1991. In Plastics Materials, Butterworth-Heinemann Ltd., Oxford. p 421 - 422,

Cahn, 1987. C2000 electrobalance instruction manual, Cahn Instruments Inc., Cerritos, CA.

Chen, S.P. and Edin, A.D. 1980. Fickian Diffusion of Alkanes in Glassy Polymers., Polym. Eng. & Sci., 20, 40-49.

Crank, J. 1956 Mathematics of Diffusion. Clarendon Press, Oxford.

Comyn, J. 1985. Introduction to Polymer Permeability and the Mathematics of Diffusion, Chapter 1 in: Polymer Permeability. Elsevier Applied Science Publishers, London.

Demorest, R.L. 1995 Measurement of Water Vapour Permeability: Recent Developments and New Standards. Presented at Packforst Symposium, Stockholm, Sweden.

DiBenedetto, A.T. and Paul, D.R. 1964. J. Polym. Sci., A-2, 1001.

Fishman, D. 1995. Barrier structures for food packaging. Plastics World 55, 67-74.

Franz, R. 1993. Permeation of Organic Compounds Across Polymer Films. Pack. Tech. Sci., 6, 91-102.

Frish, H. L. 1980. Sorption and Transport in Glassy Polymers - A Review. Polym. Eng. & Sci., 20, 2-13.

Fujita, H. and Kisimoto, A. 1961. J. Chem. Phys., 34, 343.

Giacin, J.R. 1996. Polymeric Packaging Materials (PKG 825), Course pack, School of Packaging, MSU, MI.

Giacin, J.R. 1996. Instrumental Analysis of Packaging Materials (PKG 817), Course pack, School of Packaging, MSU, MI.

Giacin, J.R. and Hernandez, R.H. 1996 Permeability of Aromas and Solvents in Polymeric Packaging Materials. Wiley Encyclopedia of Packaging, X Edition

Gu, J. 1997. The Barrier Characteristics of Clay/Polyimide Nanocomposites. M.S. thesis, Michigan State University, MI.

Hansen, A.P. and Arora, D.K. 1985. Loss of Flavour Compounds from Aseptically Processed Food Products Packaged in Aseptic Containers, in: Polymer Permeability., Elsevier Applied Science Publishers.

Hernandez, R.H. 1996. Plastics in Packaging, Chapter 8 in Handbook of Plastics, Elastomers, and Composites, third edition. McGraw-Hill, New York.

Hernandez, R.H. and Gavara, R. 1994. Sorption and Transport of Water in Nylon-6 Films. J. Polymer Science, Part B, 32, 2367 - 2374.

Hernandez, R.H., Giacin, J.R., and Baner, A. L. 1986 Journal of Plastic Sheeting, 2,

Holland, R.V., Rooney, M.L., and Santangelo, B. 1980. Angew. Makromol. Chem., 88, 209.

Holland, T. 1995. Current trend creates the right atmosphere, Packag. Week., 11(11), 37-38.

Hotchner, S.J. 1981.Container Shelf Life Methodology. In Shelf-Life: A Key to Shapening Your Competitive Edge. Proceedings, Food Processors Institute, Washington D.C.

Johansson, F. and Leufvén, A. 1994. Food packaging polymer films as aroma vapor barriers at different relative humidities. J. Food Sci., 59(6), 1328.

Karel, M. 1975. Protective Packaging of Foods, Chapter 12 - Principles of Food Science, Part II. Physical Principals of Food Preservation. M. Dekker, Inc.

Lau, O. and Wong, S. 1996. The Migration of Plasticisers from Cling Film into Food during Microwave Heating - Effect of Fat Content and Contact Time. Pack. Tech. & Sci., 9, 19-27.

Liu, K.J., Giacin, J.R., and Hernandez, R.J. 1988. The effect of relative himidity on the permeability of toluene vapour through a multi-layer coextruded film containing hydrophilic layers. Packag. Tech. Sci. 1, 57.

Mannheim, C. H., Miltz, J. and Letzter, J. 1987. J. Food Sci., 52(3), 737-740.

Marsh, K. N., Wilhoit, R. C. and Yin, D. 1995. TRC Data Bases for Chemistry and Engineering Vapor Pressure, Version 2.3P, July 1995. Thermodynamics Research Centre, Texas.

Meares, P. 1954. J. Am. Chem. Soc., 76, 3415.

Marshall, M. R., Nagy, S. and Rouseff, R. 1986, Dev. Food. Sci., 12, 237-254.

Michaels, A.S., Veith, W.R. and Barrie, J.A. 1963. J. Appl. Phys., 34, 1.

Moshonas, M. G., and Shaw, P. E. 1989. J. Food Sci., 54(1), 82-85.

MOCON. 1983. Operating Manual for PERMATRAN C-IV. Modern Controls Inc., Minneapolis, MN.

Neilsen, T. J. 1994. Aroma Sorption by Food Packaging Polymers studied with SFE-GC and other Methods. Thesis, Department of Applied Nutrition & Food Chemistry, Lund Institute of Technology, University of Lund, Sweden.

Neilsen, T. J. and Giacin, J.R. 1994. The sorption of Limonene/Ethyl Acetate Binary Vapour Mixtures by a Biaxially Orientated Polypropylene Film. Pack. Technol. Sci., 7, 247-258.

Olafsson, G., Jägerstad, I. M., Öste, R., and Wesslén B. 1993. J. Food Sci. 58(1), 215-219.

Page, D. B. and Lacroix, G. M. 1992. Studies into the transfer and migration of phthalate esters from aluminium foil-paper laminates to butter and margarine. Food Additives and Contaminants, 9(3), 197-212.

Peiper, G., Borgudd, L., Ackermann, P. and Fellers, P. 1992. J. Food Sci., 57(6), 1408-1411.

Phillips. 1996. K-Resin Technical Data Sheet, 1833-96 K01.

Pieper, G., and Petersén, K. 1995. J. Food Sci., 60(5), 1088-1090.

Robertson, G.L. 1993. Shelf Life of Foods. In Food Packaging Principals and Practice. M Dekker, Inc.

Rogers, C.E. 1985. Permeation of Gases and Vapours in Polymers, Chapter 2 in: Polymer Permeability., Elsevier Applied Science Publishers.

Rogers, C.E., and Machin D. 1972. The Concentration Dependence of Diffusion Coefficients in Polymer-Penetrant Systems. Critical Reviews in Macromolecular Sciences, The Chemical Rubber Co.

Shimoda, M., Matsui, T. and Osajima, Y. 1987. Nippon Shokuhin Kogyo Gakkaishi, 34(6), 402-406.

Shimoda, M., Ikegami, T. and Osajima, Y. 1988. J Sci. Food Agri., 42, 157-163.

Stern, S.A., and Trohalaki, S. 1990. Fundamentals of Gas Diffusion in Rubbery and Glassy Polymers, Chapter 2: Barrier Polymers and Structures. American Chemical Society.
Theodorou, E. and Paik, J.S. 1992. Effect of Organic Vapour Interaction on Permeation Rate Through Polymer Films. Pack. Technol. Sci., 5, 21-25.

Van Krevelen, D.W. and Hoftyzer, P.J. 1976. Properties of Polymers. Elsevier Scientific Publishing Company, Amsterdam.

Vieth, W. and Wuerth, W.F. 1979. J. Appl. Polym. Sci., 13, 685.

Yamada, K., Mita, K., Yoshida, K. and Ishitani, T. 1992. A study of the absorption of fruit juice volatiles by the sealant layer in flexible packaging containers. Pack. Tech. & Sci., 5, 41-47.

Weinkauf, D.H. and Paul D.R. 1990. Effects of Structural Order on Barrier Properties, in Barrier Properties and Structures. American Chemical Society, 61 - 91,

Wessling, M.H.V., Mulder, A., Bos, A., van der Linden, M. and
van der Linden. W.E. 1994. Modelling the Permeability of Polymers: a neural network approach. J. Memb. Sci., 86, 193-198.

Zobel, M.G.R. 1985. The Odour Permeability of Packaging Film. Polym. Test. 5, 153 -165.